DISSERTATION

Protection against severe malaria by hemoglobin S and C: A quantitative understanding of the cytoadhesion behavior of *Plasmodium falciparum* infected erythrocytes

submitted to the

Combined Faculties for the Natural Sciences and for Mathematics

of the Ruperto-Carola University of Heidelberg, Germany

for the degree of Doctor of Natural Sciences

presented by

Christine Lansche (M. Sc.)

Heidelberg 2018

Dissertation

submitted to the

Combined Faculties for the Natural Sciences and for Mathematics

of the Ruperto-Carola University of Heidelberg, Germany

for the degree of

Doctor of Natural Sciences

presented by

Christine Lansche (M. Sc.)

born in Heredia, Costa Rica

Date of oral examination: _____

Protection against severe malaria by hemoglobin S and C: A quantitative understanding of the cytoadhesion behavior of *Plasmodium falciparum* infected erythrocytes

Referees: Prof. Dr. Michael Lanzer

Dr. Ann-Kristin Müller

Hiermit erkläre ich, dass ich die vorliegende Arbeit von May 2014 bis May 2018 unter Anleitung von Prof. Dr. Michael Lanzer selbst durchgeführt habe und schriftlich ausgearbeitet habe. Ich habe mich keiner anderen Hilfsmittel und Quellen bedient als den hier ausdrücklich erwähnten

…… …….

Datum Christine Lansche

Table of Contents

List of Abbreviations

Abbreviations

AFM	Atomic force microscopy
AP	Alkaline phosphatase
ATS	Acidic terminal segment
BSA	Bovine serum albumin
BSS	Balanced salt solution
CD	Cluster of differentiation
cDNA	Complementary DNA
CIDR	Cysteine-rich interdomain region
CO_2	Carbon dioxide
CR1	Complement receptor 1
CSA	Chondroitin-4-Sulfat A
C-terminal	Carboxy terminal
DBL	Duffy-binding like
ddH_2O	Double distilled water
DIC	Differential interference contrast
DNA	Deoxyribonucleic acid
DNase	Deoxyribonuclease
dNTP	Deoxyribonucleoside triphosphate
dsDNA	Double stranded DNA
DV	Digestive vacuole
EC	Endothelial cell
EDTA	Ethylenediaminetetraacetic acid
ELISA	Enzyme linked immunosorbent assay
Em	Emission
EPCR	Endothelial protein C receptor
EPM	Erythrocyte plasma membrane
Ex	Excitation
FACS	Fluorescence activated cell sorter
FCR3	*P. falciparum* adapted Lab strain
FCS	Fetal calf serum
gDNA	Genomic DNA

HA	Hyaluronic acid
Hb	Hemoglobin
HBSS	Hank's Balanced Salt Solution
HDMEC	Human dermal microvascular endothelial cells
HEPES	2-[4-(2-hydroxyethyl)piperazin-1-yl] ethanesulfonic acid
hpi	Hours post invasion
HRP	Horseradish peroxidase
HUVEC	Human umbilical vein endothelial cells
ICAM	Intercellular adhesion molecule
IF	Immunofluorescence
IFN	Interferon
Ig	Immunoglobulin
IL	Interleukin
iRBC	Infected red blood cell
KAHRP	Knob Associated Histidine Rich Protein
KO	Knock out
LFA-1	Lymphocyte-associated function antigen -1
Mac-1	Macrophage antigen-1
MACS	Magnetic activated cell sorter
MHC	Major histocompatibility complex
mRNA	Messenger RNA
NF-κB	Nuclear factor kappa B
NLI	Nuclear labeling index
NO	Nitric oxide
NPP	New permeation pathways
N-terminus	Amino-terminus
NTS	N-terminal sequence
O_2	Oxygen
OD	Optical density
P.	Plasmodium
PBS	Phosphate buffered saline
PCA	Principal component analysis
PCR	Polymerase chain reaction
PE	Phycoerythrin
PECAM	Platelet endothelial cell adhesion molecule

PFA	Paraformaldehyde
PfEMP	*Plasmodium falciparum* erythrocyte membrane protein
pH	Power of hydrogen
PSGL-1	P-selectin glycoprotein ligand-1
PV	Parasitophorous vacuole
PVM	Parasitophorous vacuolar membrane
RBC	Red blood cell
RNA	Ribonucleic acid
rpm	Revolutions per minute
RPMI	Roswell Park Memorial Institute
RT	Room temperature
SCFS	Single cell force spectroscopy
SD	Standard deviation
SDS	Sodium dodecyl sulfate
SEM	Standard error of the mean or scanning electron microscopy
TAE	Tris-acetate-EDTA
Taq	Thermus aquaticus
TM	Transmembrane
TNF-α	Tumor necrosis factor alpha
Tris	Tris(hydroxymethyl)-aminomethan
Ups	Upstream promoter sequence
uRBC	Uninfected red blood cell
UV	Ultra violet
v/v	Volume-volume
VCAM-1	Vascular cell adhesion molecule 1
w/v	Weight-volume
WBC	White blood cells
WHO	World Health Organization

Measuring units and symbols

%	Percent
°C	Degree Celsius
∞	Infinite

A	Ampere or Absorbance
au	Arbitrary units
cm	Centimeter
Da	Dalton
g	Gramm
hr	Hour
k	Kilo
Kb	Kilobasepare
l	Liter
M	Molar
m	Meter or milli
min	Minute
mol	Mol
n	Nano
N	Newton
p	Pico
Pa	Pascal
s	Second
U	Unit(s)
V	Volt
x g	Times gravitational force
α	Alpha - anti
β	Beta
Δ	Delta, difference, change
κ	kappa
µ	Micro
τ	Tau, shear stress

List of Figures and Tables

Summary

To avoid clearance by the spleen, *P. falciparum*-infected erythrocytes adhere to the microvascular endothelial cells lining the blood vessels and sequester in the microvasculature of vital organs. Cytoadhesion results in reduced blood perfusion and inflammatory endothelial cell activation. While the parasite matures during the intraerythrocytic cycle, the infected erythrocyte undergoes a series of modifications including altered morphology, reduced deformability and increased adhesiveness. These properties govern the cytoadherence process and determine the dynamic adhesion behavior under physiological flow conditions. Several red blood cell polymorphisms, including sickle hemoglobin and hemoglobin C, have been associated with protection against severe malaria and malaria-related death. The mechanisms underlying this protection are poorly understood but it might be conferred, in part, by the reduced binding capability of infected erythrocytes to microvascular endothelial cells. Here, we quantitatively compared the adhesion dynamics of infected wild-type and sickle cell trait erythrocytes, at different parasite developmental stages, using flow chamber assays. Differences in the dynamic adhesion behavior were observed for trophozoite and schizont-stages. While a discoid shape in early stage caused flipping of the infected cell, an almost spherical cell at the late stage of the intraerythrocytic cycle results in a regular rolling motion. We further showed that changes in mechanical and adhesive properties of infected sickle cell trait erythrocytes resulted in substantial differences in the flipping and rolling dynamics, relative to infected wild-type erythrocytes, which led to a reduced contact time and predicted contact area to the endothelial cells as well as a reduced firm adherence. As a consequence of the differential firm and dynamic adhesion behavior, infected sickle trait-erythrocytes were less likely to activate microvascular endothelial cells, which in turn, might reduce the pathology observed in sickle cell trait individuals infected with *P. falciparum*. Overall, our findings improve the understanding of the protection mechanism against severe malaria conferred by sickle hemoglobin.

Zusammenfassung

P. falciparum infizierte Erythrozyten adhärieren an mikrovaskuläre Endothelzellen an der Innenseite von Blutgefäßen und sequestrieren in die Kapillarsysteme lebenswichtiger Organe, um ihrer Aussonderung in der Milz zu entgehen. Die Zytoadhärenz reduziert die Blut Perfusion und ruft inflammatorische Endothelzellaktivierung hervor. Das intraerythrozytische Reifen des Parasiten führt zu einer Reihe von Veränderung des infizierten Erythrozyten dazu zählen eine veränderte Morphologie, eine reduzierte Verformbarkeit und verstärkte Zelladhärenz. Diese Eigenschaften bestimmen den Prozess der Zelladhäsion und das dynamische Adhäsionsverhalten unter physiologischen Flussbedingungen. Mehrere Polymorphismen roter Blutkörperchen, wie das Sichelzellhämoglobin oder Hämoglobin C, werden mit dem Schutz vor schweren bis tödlichen Krankheitsverläufen einer Malaria Infektion assoziiert. Der zugrundeliegende Schutzmechanismus ist nur unzureichend verstanden, basiert aber vermutlich auf der verminderten Fähigkeit von infizierten Erythrozyten an mikrovaskuläre Endothelzellen zu binden. In dieser Arbeit wurde das dynamische Adhäsionsverhalten von infizierten Wildtyp-Erythrozyten und Erythrozyten mit heterozygoter Sicherzellanämie mit Hilfe von Durchflusskammer Experimenten für verschiedene Entwicklungsstadien quantifiziert. Dabei konnten für alle intraerythrozytische Entwicklungsstadien Unterschiede im dynamischen Adhäsionsverhalten beobachtet werden. Infizierte Blutzellen führen zu Beginn des Reifezyklus aufgrund der biokonkaven Zell Form eine taumelnde Bewegung aus, was sich in späteren Stadien und der typischen fast sphärische Form zu einer regelmäßigen Rollbewegung wandelt. Änderungen in mechanischen und adhäsiven Eigenschaften infizierter HbAS Erythrozyten resultierten in substanziellen Unterschieden bezüglich der taumelden und rollenden Bewegungsmuster, was zu einer Reduktion der Kontaktzeit, der zu erwartenden Kontaktfläche und der dauerhaften Adhäsion auf Endothelzellen führte. Als Konsequenz aus dem unterschiedlichen dynamischen und beständigen Adhäsionsverhalten haben infizierte Erythrozyten mit heterozygoter Sicherzellanämie eine geringere Wahrscheinlichkeit eine Aktivierung mikrovaskulärer Endothelzellen hervorzurufen, was im Gegenzug den Krankheitsverlauf abmildert, wie es für Patienten mit Sichelzellanämie beobachtet wird. Insgesamt verbessern die Ergebnisse dieser Arbeit das Verständnis des Schutzmechanismus von Sichelzellhämoglobin gegen schwere Formen der Malaria.

1. Introduction

1.1. Blood rheology and hemodynamics

Blood is a biological two-phase suspension composed of red blood cells (RBCs, erythrocytes), white blood cells (WBCs, leukocytes) and platelets suspended in plasma. The cell component comprises about 35-50% of the whole blood volume, where approximately 99% correspond to erythrocytes [1]. Blood is responsible for the transportation of oxygen and nutrients to the cells of the body and for carrying away metabolic waste products [2]. Blood is considered a non-Newtonian fluid as its viscosity changes with varying shear stresses. The non-Newtonian behavior becomes more evident at low shear stresses, when the erythrocytes spontaneously aggregate into linear arranges called rouleaux [2]. The size of the erythrocyte aggregate is inversely proportional to the magnitude of the shear forces [3]. Low shear stresses promote cell to cell encounter, supporting erythrocyte aggregation. As a consequence, the blood viscosity increases. On the contrary, high shear stresses causes the disruption of these aggregates up to single cells, leading to a decrease in viscosity [3]. The shear forces encountered in arterioles and capillaries are too high to promote RBCs aggregates, however, their formation is facilitated in axial regions of large vessels and under low shear stress in small vessels [4].

Erythrocytes are highly specialized cells, responsible for transporting oxygen from lungs to the tissue and carbon dioxide from the tissue to the lungs. To perform this function, erythrocytes must be highly deformable in order to squeeze and pass through very narrow capillaries (about 2-3 µm diameter) without damage [5]. The deformability is determined by the red blood cell geometry, viscosity and membrane elasticity [2].

Erythrocytes have a biconcave-discoid shape with an approximate diameter of 6-8 µm and a thickness of 2-3 µm [5][6]. With a mean cell volume of about 90 μm^3 and an approximate mean surface area of 135 μm^2, erythrocytes possess a high surface area to volume ratio, which enables cell shape changes [2][7]. Furthermore, mature mammalian erythrocytes lack a nucleus and other organelles, ensuring full flexibility, as well as providing more space for hemoglobin storage [8]. Consequently, about 95% of the erythrocyte cytosolic protein content corresponds to hemoglobin [9],

giving a low cytoplasmic viscosity [2][7]. The extent of the erythrocyte deformation however, is mainly determined by the membrane elasticity. The erythrocyte membrane consists of a carbohydrate rich glycocalyx on the outer surface, a 4-5 nm tick phospholipid bilayer and the underlying two-dimensional membrane skeleton. The latter, is responsible for the maintenance of the biconcave-discoid shape and is composed of a protein network, where spectrin and actin are the main components [2].

Several genetic or acquired pathological conditions like sickle cell disease [10] or malaria [11], can drastically affect the erythrocytes deformability and fluidity, leading to impairments of the blood flow and significantly affecting tissue perfusion. During an episode of *Plasmodium falciparum*-malaria, two major rheological abnormalities impair the infected red blood cells (iRBCs) ability to circulate. Firstly, the cell rigidity increases due to the presence of a large and rigid intracellular parasite and the erythrocyte membrane elasticity decreases as consequence of extensive erythrocyte modifications induced by the parasite [12]. Secondly, *P. falciparum*-infected erythrocytes become adhesive and bind to several host receptors expressed on the microvasculature [12]. These modifications prevent infected erythrocytes from flowing through small vessels and, at the same time, they cause infected erythrocytes to sequester in the deep microvasculature, leading to vascular obstruction, vascular inflammation, ischemia and organ failure [11].

1.2. Background about malaria

Malaria is an infectious disease caused by a protozoan parasite of the genus *Plasmodium*. It is transmitted to the human host through a female anopheles mosquito during blood feeding. Among all *Plasmodium* species *P. falciparum, P. vivax, P. ovale* (*P. ovale curtisi* and *P. ovale wallikeri*), *P. malariae and P. knowlesi* infect humans [13][14][15]. Infection with malaria parasites causes a range of clinical manifestations including fever, headache and chills. If not treated in time, infection can progress to severe disease often leading to death, especially in the case of *P. falciparum* malaria [16]. *P. vivax*, on the other hand, is responsible for a significant world-wide morbidity, being the major cause of illness in most parts of the world, nevertheless it is rarely life-threatening [16]. In 2017, the World Health Organization (WHO) reported approximately 216 million clinical cases of malaria and 445 000

deaths [16]. To date, *P. falciparum* is responsible for most malaria-related deaths, especially among non-immune children under the age of five in sub-Saharan Africa [16]. Other groups with high risk of mortality include pregnant women and non-immune travelers [16]. The morbidity and mortality caused by *P. falciparum* is mainly attributed to the resistance of mosquito vector to insecticide, socio-economic factors, resistance of *P. falciparum* to antimalarial drugs and the absence of a vaccine which provides full protection [17].

1.3. *Plasmodium falciparum* biology and pathogenesis

P. falciparum has a complex life cycle involving a human host and a mosquito vector (Figure 1). During a blood meal, an infected mosquito inoculates < 25 sporozoites (motile form) into the host skin [13]. Some will reach the blood stream and travel to the liver, cross the sinusoidal barrier (endothelial cells and Kupffer cells) and invade the hepatocytes. There, parasites multiply asexually to produce approximately 40000 infective daughter cells called merozoites in a period of about 10 days [18][19]. The merozoites are released into the blood circulation and invade erythrocytes in a very fast manner (~2 min).

Once the intraerythrocytic infection is established, the 48 h replicative cycle starts [18]. The parasite develops subsequently from ring stage (up to 16 h post invasion (hpi)) to trophozoite (20 to 36 hpi) and finally to schizont (40 to 48 hpi) [20]. Each schizont divides asexually to produce 16-32 merozoites [19]. Following erythrocyte rupture, merozoites are released and able to infect new red blood cells. Intracellular parasite growth and replication prevents direct parasite exposure to immune cells [21]. Additionally, erythrocytes surface lack MHC class I molecules, preventing the recognition of the infected erythrocytes by CD^{+8} T cells [22][23].

The rupture of schizont infected erythrocytes and the release of their contents is characterized by episodes of fever [24]. The fever is caused by systemic release of pyrogenic cytokines such as tumor necrosis factor alpha (TNF-α), produced by macrophages in response to parasite derived products such as glycosylphosphatidylinositol (GPI) [25][26][27][28].

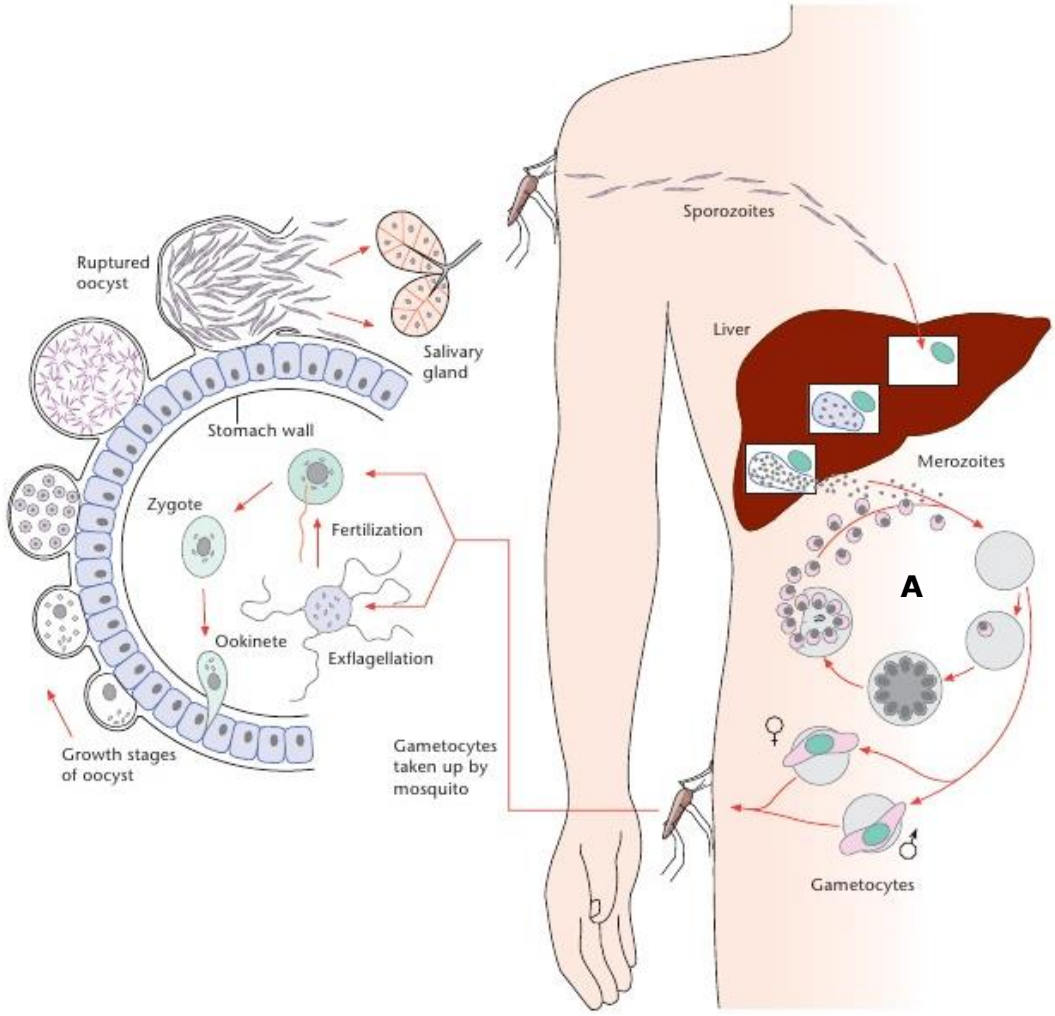

Figure 1 | Life cycle of *Plasmodium falciparum* (adapted from L. Bannister and W. Sherman (2009) [29]). (A) Asexual intra-erythrocytic cycle.

Approximately 10% of intraerythrocytic parasites commit to sexual development and produce sexual forms called gametocytes [30]. Circulating gametocytes can be ingested by a female mosquito, were the parasite sexual replication occurs. Once in the mosquito midgut, the microgametes exflagellate from the male gametocyte and can then swim and fertilize the female gametocyte called macrogamete, to form the zygote [19]. The latest transforms into a motile form called ookinete, which migrates through the mosquito midgut epithelium and encyst to form the oocyst. Through asexual multiplication, thousands of sporozoites are produced and released into the mosquito hemocoel after ~17 days. Resultant sporozoites find their way to the salivary glands, from where they can be transmitted to the human host by a subsequent mosquito bite and initiate a new cycle [19][18].

The intra-erythrocytic stage of infection is responsible for the clinical manifestations of malaria. Malaria disease can range from asymptomatic parasitemia or mild symptomatic malaria (fever) to severe illness and death [31]. The clinical outcome depends on several factors including parasite virulence and drug resistance, host immunity and genetics, mosquito transmission intensity and access to treatment [26]. About 1 to 2% of the malaria cases progress to life-threatening illness [32][33]. The clinical manifestations of severe *P. falciparum* malaria are variable and thus difficult to define. The WHO criteria to define severe malaria include the manifestation of one or various of the following symptoms: (1) cerebral malaria (CM) (coma and seizures), (2) respiratory distress as consequence of lactic acidosis (plasma bicarbonate <15 mmol/l), (3) pulmonary edema (radiologically confirmed), (4) jaundice (plasma bilirubin >3 mg/dl), (5) severe anemia (hemoglobin <5 g/dl), (6) hypoglycemia (blood glucose <40 mg/dl), (7) renal failure (plasma creatinine >3 mg/dl) and (8) hyperparasitaemia (>10%) [16]. CM, is the most common severe complication in children, causing up to 30% of deaths [34][35][36][37] and neurological sequelae in about 9 to 12% of the survivors [34][37].

The most prominent and early observed pathological feature in *severe P. falciparum*-malaria cases is the presence of late stage-infected erythrocytes in capillaries and post-capillary venules of several organs including brain, placenta, heart, eyes, liver, kidneys, intestines and adipose tissue [38][39][33][40][41]. The ability of *P. falciparum* infected erythrocytes to adhere to endothelial cells (EC) and sequester from the circulation, ensures the parasite survival by avoiding passage to the spleen. There, parasitized erythrocytes would be eliminated by splenic clearance mechanisms, which remove old and damaged erythrocytes [42][43][44].

Sequestration not only facilitates dissemination of the parasite in the human host, but also causes severe disease by obstructing the vascular lumen which can lead to low blood perfusion, ischemia, acidosis and organ damage [45]. Increased rigidity of uninfected erythrocytes, possibly as a consequence of membrane oxidation by parasite derived products such as hemozoin (β-haematin) [46][47][47], may act synergistically with sequestered infected erythrocytes in compromising the blood tissue perfusion [48][47]. Oxygen delivery to the affected tissue might be further compromised by anemia, induced as a consequence of elevated hemolysis of

parasitized erythrocytes, accelerated elimination of rigid uninfected erythrocytes and impaired erythropoiesis due to excessive release of proinflammatory cytokines such as TNF-α and IFN-γ [25].

Anemia as well as lactic acid production from the parasite anaerobic glycolysis, contribute to the observed lactic acidosis during severe malaria [49]. However, the main cause of this syndrome is the increase of anaerobic glucose metabolism caused by the generalized microvascular sequestration of infected erythrocytes and the resultant decreased blood flow perfusion into the tissues [50][41]. As result of lactic acidosis, the body will experience respiratory distress when it tries to equilibrate the blood pH by excreting larger amounts of carbon dioxide. At the same time, hypoglycemia might also develop as a consequence of high glucose consumption by the intra-erythrocytic parasite and by the hypermetabolic peripheral tissue [51].

1.4. *Plasmodium falciparum*-infected erythrocytes cytoadherence and antigenic variation

Sequestration of infected erythrocytes on the microvasculature coincides with the erythrocyte surface expression of the major *P. falciparum* adhesin termed *P. falciparum* erythrocyte membrane protein 1 (PfEMP-1) at approximately 16 hpi [52][53], matching with the time of transition from ring to trophozoite. PfEMP-1 proteins are encoded by the *var gene* family and mediate both cytoadherence and antigenic variation [54]. About 60 different copies of *var* genes exist per haploid genome and they are distributed along the parasite 14 chromosomes, predominantly located in clusters at the subtelomeric regions [55][56]. The localization at the subtelomeric regions makes them more susceptible to recombination and likely to undergo frequent sequence alterations, thus diversifying the antigenic repertoire [57]. *Var* genes are not only diverse in sequence polymorphism but also in size, ranging from 3.9 to 13 kb and generating PfEMP-1 proteins with sizes between 200 and 350 kDa [57].

All *var* genes possess conserved features in their structure, consisting of a 5´upstream promoter sequence (Ups) followed by the first exon, an intron and the second exon (Figure 2). The first exon is highly variable in sequence and size

(between 3.5 to 9 kb) and it encodes the extracellular exposed portion of the protein, as well as the transmembrane domain (TM) [13]. The TM anchors the PfEMP-1 to the erythrocyte plasma membrane. Following a relatively conserved intron, the second exon, shorter in sequence (1 to 1.5 kb) and highly conserved. It encodes the cytoplasmic tail which contains the acidic terminal segment (ATS) that anchors PfEMP-1 molecules to the host cell cytoskeleton [13][58].

The extracellular portion of PfEMP-1 is composed of a variable N-terminal segment (NTS), several Duffy-binding like domains (DBL, five distinct sequence classes α-ε) and cysteine-rich interdomain regions (CIDR, three distinct sequence classes α-γ) [59]. The number and types of DBL and CIDR in the polymorphic interdomain region controls the parasite binding phenotype. This determines the infected erythrocytes tissue tropism, thus contributing to the parasite survival, transmission and clinical outcome [59]. PfEMP-1 mediates binding of infected erythrocytes to several host receptors including CD36, intercellular adhesion molecule-1 (ICAM-1/CD54), endothelial protein c receptor (EPCR), thrombospondin (TSP), complement receptor 1 (CR1)/CD35, chondroitin sulphate A (CSA), hyaluronic acid (HA), E-selectin/CD62E, vascular cell adhesion protein 1 (VCAM-1), platelet endothelial cell adhesion molecule (PECAM/CD31) and P-selectin/CD62P [60][61][62][63][64]. The ability of PfEMP-1 molecules to target different host receptors, expressed differently in diverse vascular beds, leads to organ-specific syndrome, such as cerebral malaria or placental malaria [26][40].

Only a single PfEMP-1 variant is exclusively expressed on each infected erythrocyte at a time, while the other members of the family remain silenced [65][66]. This prevents unnecessary exposure of the parasite antigenic repertoire. Successful immune evasion through antigenic variation thus requires the mutual expression of a single *var* gene at the time and slow switching to another variant. *In vitro* the *var* gene switching occurs in a rate of 2% per generation [67]. Antigenic variation is advantageous for the parasite because it prolongs the length of infection within the host and thus increases the chances of transmission to new hosts [68]. The infection would be cleared once the host immune response detects and controls all variants present [69].

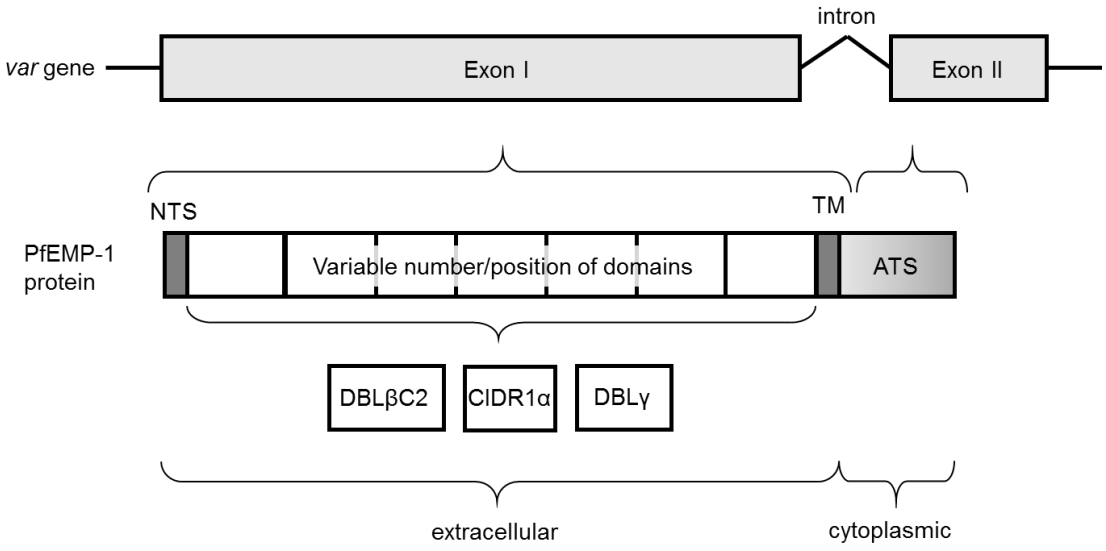

Figure 2 | *Var* gene structure and protein diagram (adapted from I. W. Sherman (2005) [13]). The features of PfEMP-1 structure include the extracellular exposed N-terminal composed of the NTS followed by a variable number of polymorphic DBL domains and CIDR domains, and the TM region, encoded by the highly variable exon I. Adhesion of some DBL and CIDR domains to host receptors such as CD36 by CIDR1α domain [70][71][72][73], ICAM-1 by DBLβC2 [74], CSA by DBLγ [75][76] have been reported. The intron flanked between exon I and II is noncoding. Exon II encodes the semi-conserved ATS.

1.5. Molecular mechanism of infected erythrocytes adherence to host receptors

Three major forms of *P. falciparum* infected erythrocytes adhesion to host receptors have been described. (1) Cytoadhesion to endothelial cells [77] (also includes adhesion to syncytiotrophoblasts in placenta [78]), (2) rosetting to uninfected erythrocytes [79] and (3) auto-agglutination of infected erythrocytes due to binding interactions with platelets (platelet-mediated clumping) [80].

Cytoadhesion via CD36

CD36 is an 88 kDa transmembrane glycoprotein that belongs to the B class scavenger receptor. It is involved in fatty acid metabolism, angiogenesis and phagocytosis [81]. It is expressed on various cells such as vascular endothelial, macrophages, monocytes, dendritic cells, platelets and adipocytes [82][45] and is most abundant in the liver, kidney, lungs and muscle [55]. The CD36 binding pocket of PfEMP-1 resides in amino acids 139-184 [83]. Binding to this receptor is a feature of almost all clinical parasites isolates [84][85]. Several studies associate CD36

binding to severe disease in Asia [85][86] and polymorphisms in this receptor confer protection against severe malaria in Africa [87] and Asia [88].

Cytoadhesion via ICAM-1

ICAM-1, a 80-115 kDa membrane glycoprotein from the immunoglobulin superfamily, is expressed on the surface of endothelial cells and leukocytes [89][45]. It is found in different vascular beds including lungs [90] and brain [91]. Its natural function is to enable adhesion of leukocytes to vascular endothelial cells during immune and inflammatory responses [92]. It contains five immunoglobulin like-domains (D1 to D5) and the binding site for *P. falciparum* infected erythrocytes is localized in the first domain [93]. Adhesion to ICAM-1 has been linked to cerebral malaria (CM) [94][84][95]. The sequestration of infected erythrocytes in the brain of CM post-mortem samples co-localize with ICAM-1 expression [96] and parasitized erythrocytes isolated from CM patients highly bind to ICAM-1 *in vitro* [84].

Cytoadhesion via CSA and HA

CSA and HA are glycosaminoglycan highly expressed on the syncytiotrophoblasts of the placenta intervillous space. CSA serves as major receptor for *P. falciparum* adhesion during pregnancy causing pregnancy-associated malaria (PAM) [40][97]. PAM often leads to premature birth, low-birth weight, stillbirth, maternal anemia and increased maternal and neonatal mortality [98]. Binding to CSA is mediated by a single PfEMP-1 encoded by the distinct highly conserved *var2csa* gene [99][100]. PAM syndrome affects primarily women in their first pregnancy [101]. After first exposure, effective humoral responses against placental binding parasites develop, since antibodies recognize the highly conserved regions of the *var2csa* on different parasite isolates [102]. Some parasitized erythrocytes isolated from infected placentas show binding to HA [103]. Thus, binding to HA might contribute to placental malaria [103].

Other receptors mediating cytoadhesion

Binding of infected erythrocytes to EPCR in the brain has recently been associated with cerebral malaria [63]. Other endothelial cell receptors like P-selectin, E-selectin and VCAM-1, all important for leukocyte trafficking, mediate cytoadhesion of infected

erythrocytes via PfEMP-1 [64][104][105] but no correlation with severity has been found [73][84].

Rosetting

Infected erythrocytes can bind via PfEMP-1 to complement-receptor 1 (CR1) expressed on uninfected erythrocytes [106]. This interaction promotes the binding of uninfected erythrocytes to infected erythrocytes, forming cell clusters termed rosettes [79]. Rosetting contributes to disease severity by increasing vascular obstruction, shielding infected erythrocytes from immune recognition and by facilitating new erythrocytes reinvasion [107]. A common African polymorphism on CR1, which leads to CDR1 deficiency, is associated with reduced rosettes formation [106] and with protection against severe malaria [108].

Platelet-mediated clumping

Adhesion of infected erythrocytes to other infected erythrocytes via platelets can also occur [80]. Infected erythrocytes can bind to the CD36 expressed on activated platelets and auto-agglutinate. This phenomenon strongly correlates with malaria severity [80][109]. Similarly, infected erythrocytes can bind and sequester in the brain via platelets that are simultaneously bound to von Willebrand factor (vWF) strings exposed on the activated endothelium [110].

1.6. Knob formation and its role in cytoadherence

Effective cytoadherence of infected erythrocytes requires the display of PfEMP-1 molecules on the parasite derived knob-like nanoscale protrusions that are located on the erythrocyte plasma membrane [111]. The display and concentration of PfEMP-1 molecules in the knobs is necessary to ensure adherence under physiological flow conditions [111]. Knobs are positively charged, whereas the remaining infected erythrocyte membrane is negatively charged [112]. Concentrating PfEMP-1 molecules at the knobs might be necessary to elevate the positive charged structure for proper adherence to the negatively charged endothelial cell surfaces [113][114]. A mature infected erythrocyte can express as many as 10000 knobs on its surface with height and diameter varying between 2-20 nm and 50-120 nm, respectively [115][116][117].

The transport of PfEMP-1 molecules to the knobs on the erythrocytes plasma membrane is mediated via Maurer´s cleft [118]. These structures are uni-lamellar membrane profiles that function as an intermediate compartment for trafficking of parasite-encoded proteins [119]. It was proposed that the parasite remodels the erythrocyte membrane skeleton to build its own actin network that connects the Maurer's cleft to the knobs at the plasma membrane, where cargo vesicles, carrying e.g. PfEMP-1, move towards the knobs [120][121][122][123].

Knobs are formed by interaction of parasite derived proteins such as knob-associated histidine rich protein (KAHRP), PfEMP-1 and *Plasmodium* helical interspersed subtelomeric proteins (PHIST) with host membrane skeletal proteins such as spectrin, actin, ankyrin R and protein band 4.1 (4.1 R) [124] (Figure 3). KAHRP, the major constituent of knobs [125], is a 85-105 kDa protein expressed during late stages of the intraerythrocytic cycle [126]. Its essential role in knob formation has been demonstrated in several studies [111][114][127], where erythrocytes infected with *kahrp*-deficient *P. falciparum* were unable to produce knobs and to cytoadhere to several host receptors under physiological flow conditions [111][114][127]. PfEMP-1 proteins however, remain at the erythrocyte surface [114][111][128] suggesting that PfEMP-1 display on the knobs is critical for proper cytoadhesive interactions.

KAHRP contains several protein binding domains which distinctly interact with several host and parasite-derived proteins (Figure 3). It binds to both α- and β-spectrin, but preferentially to the β-spectrin. The latest is mediated by electrostatic interactions and partly by sequence specificity [129][130]. Additionally, KAHRP self-associate into clusters and bind to spectrin-actin-protein 4.1 complexes [58]. At the same time, KAHRP binds to ankyrin R, which seems to be essential for KAHRP attachment to the erythrocyte plasma membrane (EPM) [131]. In turn, ankyrin R binds to the cytoplasmic domain of the transmembrane protein band 3, which is found to be attached to the spectrin tetramers [132][133].

The PfEMP-1 cytoplasmic domain binds to spectrin-actin junction and to self-associated KAHRP via a conserved cytoplasmic segment [58][134]. At the same time, PfEMP-1 binds to PHIST [135], which interacts with junctional complexes such as band 3 and α-/β- spectrin [136]. Furthermore, *P. falciparum* histidine rich protein 1

(PfHRP-1) mediate anchoring of the parasite PfEMP-1 to ankyrin R [137]. All these interactions provide the required mechanical support for binding of PfEMP-1 to host receptors under physiological flow conditions [124]. Additional mechanical support could be provided by the conical spiral structure (spiral scaffold) of unknown nature, underlying the knobs [138].

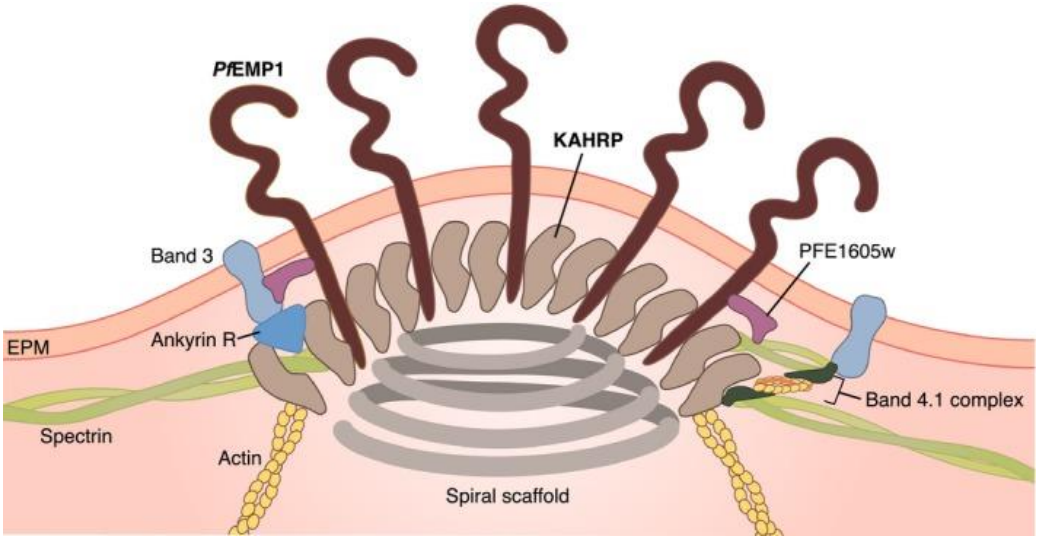

Figure 3 | Schematic representation of the *P. falciparum*-infected erythrocytes knob structure (adapted from Helms *et al.*, (2016) [124]). The different *P. falciparum* and host erythrocyte proteins involved in knob formation at the infected erythrocyte surface are shown. PFE1605w is a member of the PHIST family which links the cytoplasmic tail of the PfEMP-1 molecule to spectrin and band 3 [135].

The role of knobs in the increased rigidity of infected erythrocytes

Theoretical predictions and experimental tests provide fundamental understanding of the stiffening mechanism of *P. falciparum*-infected erythrocytes and indicate that knobs are the main cause of membrane stiffening [139][140][114][141]. Micropipette aspiration measurements show an increase in rigidity of the infected erythrocytes from several knobby parasite lines compared to knobless parasite lines [140]. Additionally, KAHRP, responsible for knob formation, accounts for the 51% of the increased erythrocyte rigidity [114][141]. Other parasite-derived cytoskeleton binding proteins such as PfEMP-3 [141][142] and ring parasite-infected erythrocytes surface antigen (RESA) [143], as well as the spiral scaffold [138], can contribute to the increased cell membrane rigidity observed for infected erythrocytes [144][145].

Rigidity of *P. falciparum* parasitized erythrocytes might be further amplified by oxidative damage of the erythrocyte plasma membrane due to parasite derived products [47]. Moreover, an important contributor to the increased cell rigidity is the presence of a large and stiff intracellular parasite, as well an unfavorable increase in cell sphericity (increase surface area/volume ratio)[146][20].

1.7. Dynamic adherence: a multi-step process

Less deformable and spherical cells such as activated leukocytes are marginated as soon as they enter post-capillary venules, by being pushed away from the aggregated erythrocytes at the center of the blood vessel. This passive rheological mechanism is known as margination [147][148][149]. The overall increase in cell stiffness and change in morphology (biconcave to spherical) of *P. falciparum*-infected erythrocytes causes the infected cell to behave similarly to leukocytes and show margination towards the endothelium [150]. For both, leukocytes and *P. falciparum*-infected erythrocytes, margination is the initial step in the adhesion process to endothelial cells lining the vessels.

Adhesion dynamics of Leukocytes

The dynamic adhesion of leukocytes is a multistep process, where cells are initially captured from flow (tether) and roll on the endothelial cell surface, forming weak interactions that strengthen following leukocyte activation [151]. In detail (Figure 4), leukocytes express at high density L-selectins and P-selectin glycoprotein ligand-1 (PSGL-1) near the tips of microvillus cell surface protrusions [152][124]. At the same time, endothelial cells express P- and E-selectins upon activation by cytokines and other proinflammatory agents. PSGL-1 expressed on leukocytes can weakly bind to endothelial P- and E-selectin, causing the cell to capture from flow and to roll, reducing its velocity [153]. Binding interactions between selectins and their endothelial ligands occur with very fast association and dissociation rates, which allows the fast-flowing leukocytes to initially engage from the blood stream to the endothelium [153]. Further rolling adhesion is provided by L-selectin on leukocyte with endothelial peripheral-node addressin (PNAd) [154][124].

Slow rolling velocities promote the leukocytes to encounter chemokines, such as IL-8, presented on the luminal surface of the inflamed endothelium [155][156]. Chemokines induce inside-out activation via G-protein couple receptors, leading to the upshift in affinity of leukocyte integrins such as LFA-1 ($\alpha_L\beta_2$) and Mac-1 ($\alpha_M\beta_2$) [161][124][157]. These integrins mediate binding to ICAM-1 and ICAM-2, expressed constitutively on the vascular endothelial cells [124][157]. Consequently, leukocytes stop rolling, arrest and initiate transmigration [92][124][158].

Adhesion dynamics of P. falciparum-infected erythrocytes

P. falciparum infected erythrocytes adhere to endothelial cells similarly as leukocytes. An iRBC tether to and roll on the endothelium, reduces its motion velocity and finally adheres [124]. Similar to the microvilli in leukocytes, infected erythrocytes express and elevate their ligands on their knobs, but instead of binding mainly to selectins, infected erythrocytes use a broader range of receptors found along different vascular beds [124]. iRBCs roll on ICAM-1, P-selectin and VCAM-1 [45], while CD36 and CSA provide stable stationary adherence [159]. Moreover, studies show that infected erythrocytes can firmly adhere to ICAM-1 [160] and that this receptor might also act synergistically with CD36 to promote firm adhesion [161]. Infected erythrocytes will not transmigrate but will, however, activate several signaling pathways in endothelial cells, leading to various responses such as actin recruitment and CD36 clustering [162], CD36 ecto-dephosphorylation [163] and $\alpha_5\beta_1$ integrin recruitment [164]. These events result in an increased adhesion strength, which ensures lasting adherence under variable flow conditions.

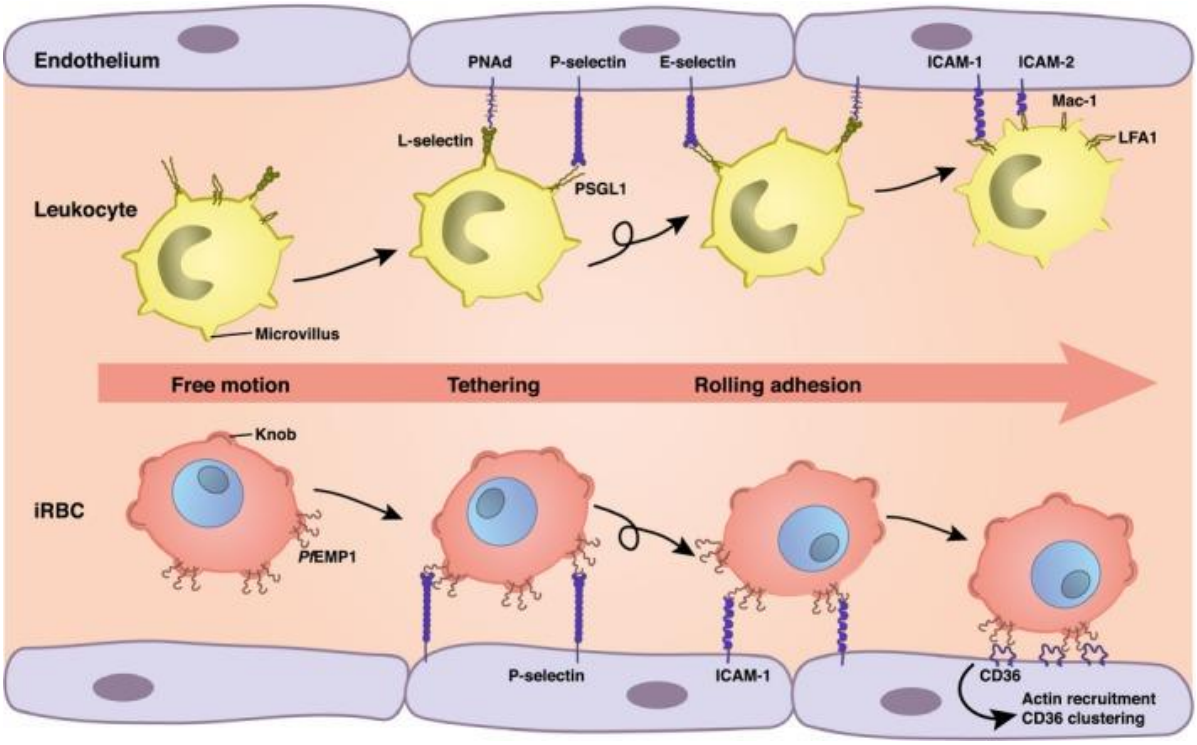

Figure 4 | Schematic illustration of leukocytes and *P. falciparum*-infected erythrocytes dynamic and firm adhesion process (adapted from Helms *et al.*, (2016) [125]). The different receptor-ligand pairs are shown. The adhesive structures correspond to microvilli in leukocytes which expose, concentrate and elevate the adhesion molecules L-selectin, PSGL-1 and integrins, and to knobs in iRBC with similarly expose PfEMP-1. The cell adhesion for leukocytes involves selectin-mediated rolling, chemokine-triggered activation and integrin-dependent arrest, while for iRBC rolling and firm adhesion is mediated by a broader range of receptors, and binding strengthening is followed by endothelial activation.

1.8. Endothelial cells response to infected erythrocytes adherence

Endothelial cell activation is a feature of severe malaria [96]. It potentiates sequestration and vascular obstruction through the upregulation of vascular endothelial receptors and by strengthening the adhesion interaction [96][165][162][163][164]. Furthermore, other signaling pathways involved in vascular dysfunction, vascular leak and apoptosis are initiated in endothelial cells upon infected erythrocytes binding [166][167].

Increased expression of adhesion receptors

Upregulation of ICAM-1, VCAM-1 and E-selectin and their co-localization with parasitized erythrocytes sequestration have been observed in various organs,

including the brain, from malaria fatal cases [96][168]. The upregulation of these vascular receptors can be mediated in endothelial cells by binding of iRBCs *in vitro* [96][165]. Increase of ICAM-1 surface expression by binding of infected erythrocytes is linked to the nuclear translocation of nuclear factor kappa B (NF-κB) [169]. This is a fast response transcription factor present in the cytoplasm in an inactive form [170]. It is involved in immune and inflammatory responses and upon activation, induces the transcription of several genes encoding for cytokines, chemokines and cell adhesion molecules [170]. Its translocation to the nucleus, occurs rapidly, upon *P. falciparum*-infected erythrocytes binding to microvascular brain endothelial cells [169][171].

Adhesion strengthening

Initial attachment to CD36, leads to Scr-familly kinase-dependent dephosphorylation of the CD36 ectodomain (threonine 92 residue) via an ecto-alkaline phosphatase (AP) anchored to the endothelial plasma membrane [163][172]. This event might be critical for firm adhesion under flow conditions, since the removal of the negatively charged phosphate group from the CD36 ecto-domain, leads to greater interactions [162]. Furthermore, AP activity increases by IL-6, which is markedly elevated during malaria infection [173][172]. Moreover, studies showed correlations between IL-6 levels and malaria severe outcome [173][174]. IL-6 is produced by a variety of cells including endothelial cells [175] and *in vitro* studies showed that iRBC binding induced endothelial cells to secrete large amounts of IL-6 [165]. IL-6 expression might as well be induced via NF-κB nuclear translocation [176][165][171].

Activation of the Src-familly kinases followed by CD36 engagement, also triggers rapid CD36 clustering and actin rearrangement via the adaptor protein P130CAS, increasing the adhesion binding strength of iRBCs to microvascular endothelial cells [162]. Moreover, $\alpha_5\beta_1$ integrins, which do not support iRBC binding on their own, are recruited upon CD36 docking, further enhancing the magnitude of adhesion strength [164].

Loss of barrier integrity and vascular leak

Endothelial cells constitute a vascular barrier, with selective permeability, between blood and underlying tissues. This function can be carried out by the connection of

adjacent endothelial cells via tight, gap and adherens junctions [177]. Modulation of endothelial permeability due to pulmonary or cerebral sequestration of iRBC during malaria infection might be implicated in the development of severe forms such us pulmonary oedema and CM [166]. Immunohistochemical analysis of CM postmortem tissues, show loss of tight junctional proteins such as zonula occludens 1 (ZO-1), occludin and vinculin, in areas where infected erythrocytes were sequestered [178][179][180]. Moreover, blood brain barrier resistance is reduce by 70% upon contact with infected erythrocytes [181].

EPCR is expressed on endothelial cells and play a key role modulating blood coagulation, endothelial activation and barrier integrity. It binds and activates protein C, which once activated, prevents coagulation by inhibiting thrombin generation [182]. By reducing the level of thrombin, activated protein C strengthen the endothelial barrier integrity and prevents endothelial inflammation [182]. *P. falciparum* infected erythrocytes can bind to EPCR in brain, interfering with protein C binding and activation [63], thus exerting pro-coagulant and pro-inflammatory signaling by thrombin and leading to endothelial dysfunction [183].

Others

Few studies have suggested that endothelial apoptosis in brain can be induced by infected erythrocytes biding, however relation to severity has not be found [166]. On the other hand, not all signaling induced by infected erythrocytes are detrimental. It has been reported that anti-apoptotic and other genes involved in endothelial protection are induced by parasite binding. Thus, ensuring parasite survival and transmission [166]. Therefore, a balance between endothelial activation and protection are critical factors in dictating the severity of malaria outcome.

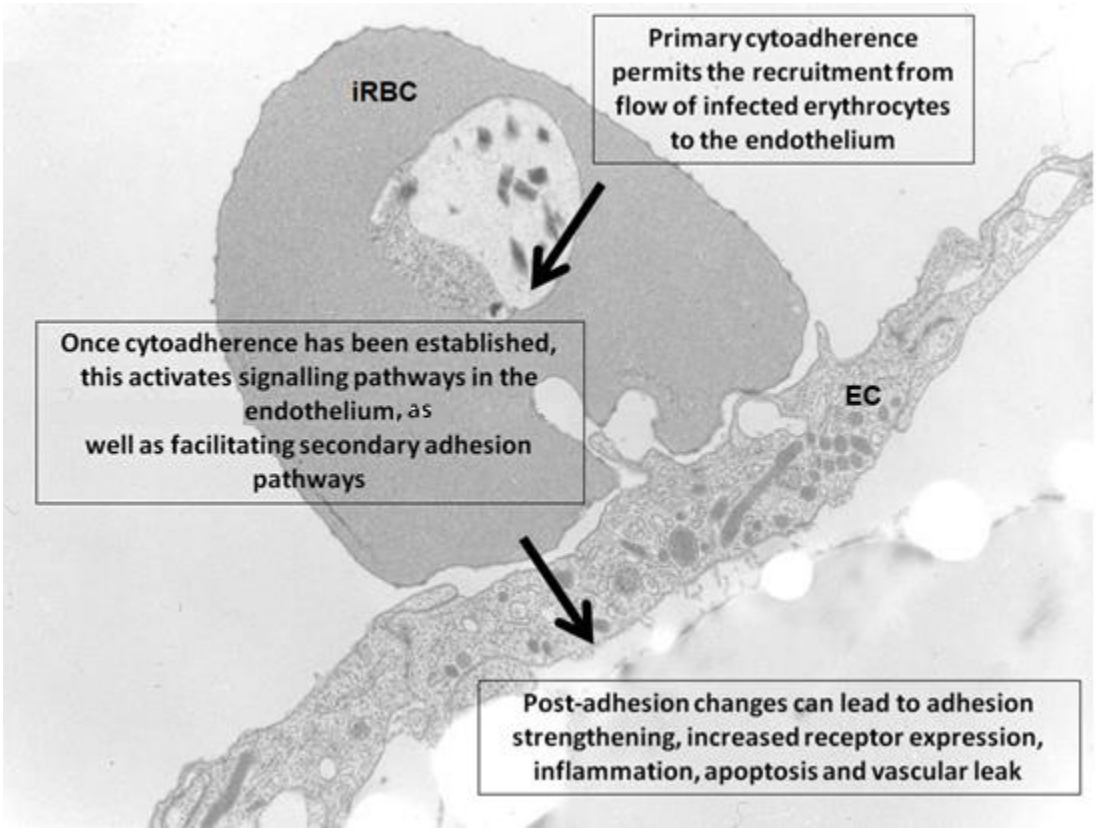

Figure 5 | Summary figure showing the endothelial cell responses to infected erythrocytes biding (adapted from Cruz *et al.,* (2012) [167]).

Cytoadherence might also localize parasite-derived compounds, which induce directly or indirectly endothelial cell activation and damage. For instance, GPI can induce the production of TNF-α from macrophages [25][26][27][28], which in turn upregulates the expression of endothelial adhesion molecules such as ICAM-1 and VCAM-1 [184][185]. Moreover, GPI and hemozoin release, can also disrupt the endothelial barrier integrity and increase vascular permeability [186].

Following infected erythrocytes rupture, other products such as hemoglobin and arginase are released into the plasma, which limit nitric oxide NO bioavailability [187]. Hemoglobin is a NO scavenger and arginase depletes L-arginine, the NO precursor [187][188]. NO is essential regulator of the microvascular blood flow, therefore, lower levels of NO produce loss of vasodilatory tone and might contribute to hypoperfusion [189]. Furthermore, the NO levels were found significantly reduced in severe malaria cases [190].

1.9. The impact of host genetic on red blood cells and protection against malaria

In endemic areas, *P. falciparum* has exerted a high selective pressure on the human population over thousands of years of co-evolution. As consequence, several polymorphisms within the human genome have emerged as positive selection by conferring distinctive resistance to severe malarial disease. Consequently, mutations in the globin gene are the most common monogenic disorders in humans, affecting around 7% of the world´s population [191].

The structure of the adult hemoglobin (HbAA) consist of a tetramer of two α and two β globin chains, each one attached to a heme prosthetic group which contains a ferrous iron (Fe^{+2}) that can bind oxygen. This property allows the hemoglobin to transport oxygen in erythrocytes [192]. Hemoglobin disorders can be classified as structural hemoglobinopathies, in which the hemoglobin molecule is altered, and quantitative hemoglobin disorders, in which the globin structure is normal but its synthesis, α or β-globin chain, is reduced (α- and β-thalassemias) [192]. The structural hemoglobinopathies, sickle hemoglobin (HbS), hemoglobin E (HbE) and hemoglobin C (HbC) reach very high frequencies in several populations probably as result of natural selection by malaria [193].

Hemoglobin S

Sickle hemoglobin results from a single amino acid substitution at position 6 of the β-globin chain (β 6Glu→Val) [194]. The exchange of hydrophilic glutamic acid residue by a hydrophobic valine creates and hydrophobic “sticky patch” on the outer surface of the β-globin chain. When Hb becomes deoxygenated, the sticky patch can interact and bind to another deoxygenated HbS [195]. This binding causes the deoxy-Hb aggregation and the cell to acquire a rigid sickle shape. Vascular obstruction, ischemia and tissue death can develop as consequence of the rheological changes of these erythrocytes [10]. Furthermore, instability of sickle erythrocytes shortens its lifespan (17 days instead of 120 days) additionally causing hemolytic anemia [196]. Homozygotes (HbSS, sickle cell) can suffer from hemolytic anemia, tissue damage and pain, and usually die before adulthood. The heterozygotes (HbAS, sickle cell trait), however, do not present clinical symptoms and have a normal lifespan [196].

The HbS allele is widely distributed throughout West Africa, Middle East and parts of India, were some populations can reach up to 40% allele frequencies [197]. HbAS confer up to 91% protection from severe malaria and death, and about 60% protection from clinical malaria [198][199]. Thus, HbS represents a classic case of balance polymorphism, in which the degree of protection experienced by the heterozygote balance the fitness cost of the homozygous form [200].

The mechanism of protection by this hemoglobin remains unclear, however, normal parasite invasion and growth is observed for HbAS erythrocytes *in vitro* [201] and comparable parasitemias can be found in children with HbAA and HbAS erythrocytes [202]. Interestingly, the ability of parasitized HbSS and HbAS erythrocytes to bind to microvascular endothelial cells under static and flow conditions is reduced [203]. Furthermore, infected HbSA and HbSS erythrocytes show abnormal distribution and reduced levels of PfEMP-1 molecules on the infected erythrocytes surface, along with abnormal knob morphology and distribution [203]. Adhesion of infected HbS erythrocytes to uninfected erythrocytes (rosetting) is also reduced [203][204].

Hemoglobin E

Hemoglobin E results from a single amino acid substitution at position 26 of the β-globin chain (β 26Glu→Lys). This causes reduced synthesis rate of the β-E chain [193]. The HbE allele is distributed throughout East India and Southeast Asia, with very high frequency among some populations in Thailand, up to 70% [197][205]. Worldwide, HbE represents the second most frequent hemoglobinopathy after HbS. It confers protection against severe malaria outcome [206][197][205] by reducing the parasite susceptibility to erythrocyte invasion and thus, preventing the development of high parasite burdens [207].

Hemoglobin C

Hemoglobin C allele distributions is restricted to West Africa [197], were some populations can reach up to 21% allele frequencies [208]. This hemoglobin variant results from a single amino acid substitution at position 6 of the β-globin chain (β 6Glu→Lys) [197]. This mutation might induce hemoglobin crystal formation and homozygotes might suffer from mild hemolytic anemia, while heterozygotes are

asymptomatic [209]. Hemoglobin C protects against severe malaria symptoms by ~80% [210] and reduces the risk of clinical malaria by 29% and 93% for HbAC and HbCC, respectively [211]. However, it does not protect against uncomplicated malaria and parasitemias, which indicates that HbC does not interfere with parasite replication or growth *in vivo* [210]. *In vitro* studies also show no major effect in invasion and growth on HbAC or HbCC erythrocytes [212][213][202]. Overall, these *in vivo* and *in vitro* studies suggest that HbC might not protect against severe malaria by impeding the development of high parasitemias.

Similar to infected HbS erythrocytes, the adhesion of infected HbAC and HbCC erythrocytes to microvascular endothelial cells is reduced, under static and flow conditions [203][214]. Moreover, infected HbC erythrocytes form less rosettes and are less prone to auto-agglutinate [214]. The reduced adhesive capabilities might arise from an abnormal and reduced PfEMP-1 surface display, together with, a lower knob density and abnormally large and widely separated knobs, present in infected HbCC and HbAC erythrocytes [214].

Aberrant knob formation and PfEMP-1 display on HbS and HbC infected erythrocytes

PfEMP-1 is directed to the erythrocyte surface via a traffic system established by the parasite within the host cytoplasm (see section 1.6.). For this, the parasite remodels the erythrocyte membrane skeleton and generates long actin filaments that connects Maurer's cleft to the knobs at the plasma membrane, where cargo vesicles, carrying PfEMP-1, are transported to the knobs [121]. When compared to HbAA, the Maurer´s clefts in infected erythrocytes containing hemoglobin S and C, show altered morphology together with shorter actin filaments, which do not interconnect with the knobs (Figure 6) [120].

HbS and HbC are unstable and tend to auto-oxidize. Consequently, elevated amounts of oxidized forms of hemoglobin, such as hemichromes and ferryl, accumulate within this cells [215][216]. Hemichromes can destabilize the membrane skeleton by decreasing the spectrin-protein 4.1-actin interaction [217] and ferryl hemoglobin can oxidize actin and interfere with actin filament dynamics [218]. Thus, high levels of oxidized forms of hemoglobin in HbS and HbC erythrocytes, might

interfere with parasite mediated actin reorganization [120]. As result of a distorted traffic system, infected HbS and HbC erythrocytes show reduced levels of PfEMP-1 at their surface. Moreover, distorted actin remodeling might explain the abnormal PfEMP-1 display and aberrant knob morphology observed for infected HbS and HbC erythrocytes [121].

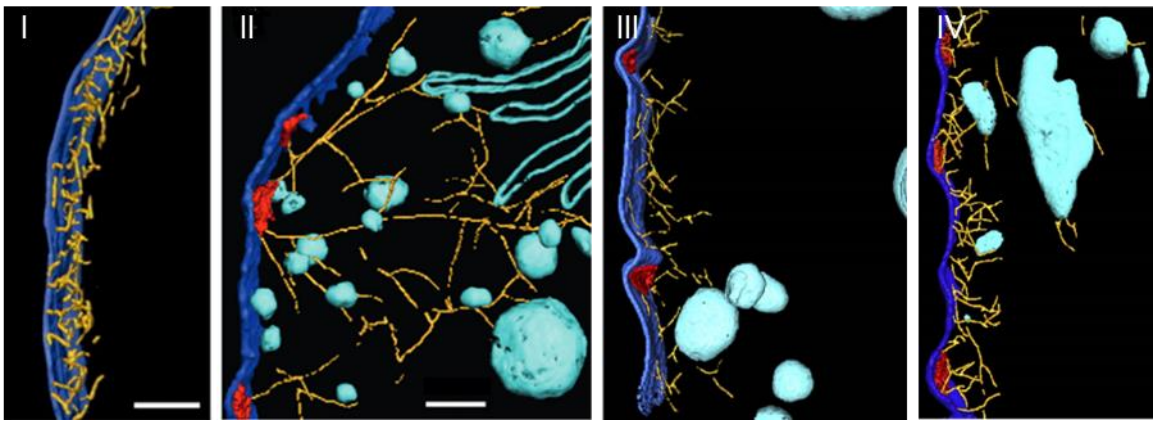

Figure 6 | Aberrant protein trafficking system observed in infected HbS and HbC erythrocytes (adapted from Cyrklaff *et al.,* (2011) (2016) [120][219]). Cyo-electron tomograms of uninfected HbAA erythrocyte (I) and infected HbAA (II), HbAS (III) and HbAC (IV) erythrocytes, showing the erythrocytes plasma membrane (dark blue), actin filaments (yellow), the knobs (red), the Maurer´s cleft and vesicles (light blue), scale bar 100 nm.

1.10. Aims of the study

In spite of reduced cytoadherence, substantial parasite densities have been observed in both malaria-infected HbAS and HbAC patients [210][199], with little or no effect on invasion and growth [203][214], indicating that parasites are able to invade and develop within HbS or HbC erythrocytes. These observations lead to the question: how does HbS and HbC protect against severe malaria without dramatically reducing the parasite density? We hypothesized that infected HbS and HbC erythrocytes can cytoadhere to the microvasculature strong enough to escape from splenic clearance mechanisms, but not enough to activate the endothelium and trigger life-threatening downstream inflammatory events.

A better understanding of the cytoadherence properties of parasitized HbS and HbC erythrocytes and their effect on endothelial cell activation may explain the mechanism by which these hemoglobinopathies confer protection against severe malaria. The aim of this project is therefore, to investigate in a quantitative manner, the dynamic and firm adhesion of infected hemoglobinopathic erythrocytes, as well as the response of microvascular endothelial cells to this binding interaction. Understanding the mechanism underpinning protection by HbS and HbC against severe malaria will help to identify novel strategies for future clinical interventions.

Specific aims:

- Isolate and characterize a parasite population capable of cytoadhering to microvascular endothelial cells.
- Study the cytoadhesive behavior of infected erythrocyte at differential intraerythrocytic developmental stages.
- Characterize in quantitative terms the firm and dynamic adhesion behavior of infected wild type and hemoglobinopathic erythrocytes under physiological flow conditions.
- Examine the effect of hemoglobin variants on infected erythrocytes binding strength to microvascular endothelial cells.
- Investigate the effect of infected hemoglobinopathic erythrocytes binding on endothelial cell activation.

2. Materials and Methods

2.1. Materials

2.1.1. Equipment

Equipment	Model	Company
Analytical balance	ABT 120-5DM	Kern & Sohn, Balingen, Germany
Atomic force microscope	NanoWizard 3	JPK Instruments, Berlin, Germany
Autoclave	ABT 120-5DM	Kern & Sohn, Balingen, Germany
	2540 EL	Tuttnauer, Breda, The Netherlands
Balance		Sartorius GmbH, Göttingen
Centrifuge	Biofuge fresco	Thermo Fisher Scientific, Dreieich, Germany
	Biofuge pico	Thermo Fisher Scientific, Dreieich, Germany
	Megafuge 1.0 R	Heraeus, Hanau, Germany
	Megafuge 2.0 R	Heraeus, Hanau, Germany
Confocal microscope	LSM510	Zeiss, Jena, Germany
Electrophoresis power supply	Power Pac 300	Bio-Rad, München, Germany
	Power Pac 200	Bio-Rad, München, Germany
Flow cytometer	FACSCalibur	Becton and Dickinson, Heidelberg, Germany
Syringe pump	55-2316	Harvard Apparatus, Holliston, MA
Freezer -20ºC	LGex 3410 MediLine	Liebherr, Biberach, Germany

Freezer -80ºC	HERAfreeze	Thermo Fisher Scientific, Dreieich, Germany
Fridge	LKexv 3910 MediLine	Liebherr, Biberach, Germany
Heating block	NeoBlock Mono I	NeoLab, Heidelberg, Germany
High precision pump	55-2316	Harvard Apparatus, MA, USA
	AL-4000	World precision instruments, Florida,USA
Ice machine		Ziegra, Isernhagen, Germany
Incubator	Heraeus Cytoperm2	Thermo Fisher Scientific, Dreieich, Germany
	HeraCell	Thermo Fisher Scientific, Dreieich, Germany
Inverted microscope	Zeiss Axio Observer Z1	Carl Zeiss, Oberkochen, Germany
	DM IL	Leica, Wetzlar, Germany
Light optical microscope	Axiolab	Zeiss, Jena, Germany
Liquid nitrogen tank	MVE Cryosystem 6000	Thermo Fisher Scientific, Dreieich, Germany
	LS 6000	Taylor-Wharton, Husum, Germany
	RS Series	Taylor-Wharton, Husum, Germany
Magnetic sorter	VarioMACS	Miltenyi Biotec, Bergisch Gladbach, Germany
Magnetic stirrer	RCT	IKA, Staufen, Germany
	COMBIMAG RCH	IKA, Staufen, Germany
Micro osmometer	Type 6	Löser Meßtechnik, Berlin, Germany

MiliQ water system	Purist ultrapure	Rephile, Germany
Particle counter	Z1	Beckman Coulter, Krefeld, Germany
pH meter	pH 7110	WTW, Weilheim, Germany
Pipets	P2, P10, P20, P1000	Gilson, Limburg an der Lahn, Germany
Pipetus	Forty\Standard	Hirschmann, Eberstadt, Germany
Adaptors for silicon tubing	Elbow connector	Ibidi, München, Germany
	Luer connector male	Ibidi, München, Germany
	Luer lock connector male	Ibidi, München, Germany
	Luer lock connector female	Ibidi, München, Germany
	Female luer lock coupler	Ibidi, München, Germany
Silicon tubing	1.6 mm	Ibidi, München, Germany
Scanning electron microscope	Leo Gemini 1530	Carl Zeiss Oberkochen, Germany
Shaker	KS 501 digital	IKA, Staufen, Germany
Sonicator	Sonoplus HD 2070	Bandelin, Berlin, Germany
Spectrophotometer	UVIKON 923	Kontron instruments, Munich, Germany
Sputter coatter	EM MED 020	Leica, Wetzlar, Germany
Sterile work bench	Herasafe	Thermo Fisher Scientific, Dreieich, Germany
	SterilGard Class II	The Baker company, Sanford, ME, USA

Thermocycler	Labcycler	Sensoquest, Göttingen, Germany
UV chamber	GS Gene linker	Bio-Rad, München, Germany
UV table	TFX-35M	Vilber Lourmat, Eberhardzell, Germany
Vacuum Workstation	PyroMark Q96	QIAGEN, Hilden, Germany
Vortex	Genie 2	Scientific Industries, Bohemia, NY, USA
Waterbath	MP	Julabo, Seelbach, Germany

2.1.2. Disposables

Disposable	**Company**
µ-slide VI$^{0.4}$ Treat	Ibidi, München, Germany
AFM cantilever with colloidal particule 2 µm Ø CP-9P-SCONT-SiO-A	NanoAndmore, Wetzlar, Germany
AFM tipless nitride cantilever MLCT-010	Brucker, CA, USA
Aluminium foil	Carl Roth, Karlsruhe, Germany
Cell culture plate (6 well, 12 well and 24 well)	Greiner bio-one, Frickenhausen, Germany
Cellulose swabs (Askina Brauncel)	B Braun, Melsungen, Germany
Centrifuge polypropylene (Cellstar) tubes (14 ml, 50 ml)	Greiner bio-one, Frickenhausen, Germany
Coverglass 15 mm Ø	Marienfeld , Lauda-Königshofen, Germany
Cryo.s, polypropylene, with screw cap	Greiner bio-one, Frickenhausen, Germany
Cuvettes Acryl 10x10x48 mm	SARSTEDT, Nümbrecht, Germany
Filter systems 500 ml	Corning, Kaiserslautern, Germany

Filters Millex GS (0,2µm)	Merck Millipore, Darmstadt, Germany
Glass bottom dishes 5 mm Ø	WillCo Wells, Amsterdam, The Netherlands
Gloves TouchNTuff	Ansell, München, Germany
MACS CS column	Miltenyi Biotec, Bergisch Gladbach, Germany
Micro tube (1 ml, 2 ml)	Sarstedt, Nümbrecht, Germany
Micro tube (1 ml, braun)	Carl Roth, Karlsruhe, Germany
Microscope glass slides 75 x 25 x 1mm	MarienFeld, Lauda-Königshofen, Germany
Parafilm	Bemis, Londonderry, UK
Petri dishes (60 mm Ø, 100 mm Ø, 145 mm Ø)	Greiner bio-one, Frickenhausen, Germany
Pipette tipps	Corning, Kaiserslautern, Germany
Plastic pipettes (1 ml; 2 ml; 5 ml; 10 ml; 25 ml; 50 ml)	Corning, Kaiserslautern, Germany
Polystyren round.bottom tubes (5 ml)	Corning, Kaiserslautern, Germany
Precision wipes (11x21cm)	Kimberly Clark, Mainz, Germany
SEM conductive tabs 18 mm Ø	Ted Pella, CA, USA
SEM pin stub 18 mm Ø	Ted Pella, CA, USA
SEM storage box and holder for pin stubs	Ted Pella, CA, USA
Sterile filter tips (200 µl, 1000 µl)	Denville scientific, Lambrecht/Pfalz, Germany
Syringe Luer-lok (1 ml, 10 ml, 20 ml and 60 ml)	Becton and Dickinson, Madrid, Spain
Thermowell tubes (0.2 ml tubes with dome cap)	Corning, Kaiserslautern, Germany
Transfer pipettes	Sarstedt, Nümbrecht, Germany

Transwell permeable supports, 12mmØ, 0.4 µm polycarbonate membrane, tissue treated	Corning Incorporated, ME, USA

2.1.3. Kits

Kits	Company
Ambion DNA-free kit	Invitrogen - Thermo Fisher Scientific, Vilnius, Lithuania
Blood and cell culture DNA mini kit	Qiagen, Düsseldorf, Germany
Endothelial cell detachment kit	Promocell, Heidelberg, Germany
Endothelial cell growth medium (MV 2) Kit	Promocell, Heidelberg, Germany
Human IL-6 ELISA Max Deluxe	Biolegend, London, UK
SuperScript III First Strand Synthesis	Invitrogen-Thermo Fisher Scientific, Vilnius, Lithuania
Taq DNA polymerase kit	Qiagen, Düsseldorf, Germany
Venor®GeM Classic mycoplasma detection kit for conventional PCR	MB Minerva Biolabes, Berlin, Germany

2.1.4. Chemicals

All chemicals used within this study were purchased from one of the following companies: Boehringer Ingelheim, Carl Roth, GE Healthcare, Amersham, Honeywell, ICN Biomedicals, MP Biomedicals, Merk, Millipore, Roche, Calbiochem, Novagen, Sigma-Aldrich, Fluka, Thermo Fisher Scientific, Gibco, Invitrogen, and Molecular Probes.

2.1.5. Biological materials

2.1.5.1. Antibodies

Antibody	Description	Clone	Clonality	Isotype	Company	Use
Alexa Fluor® 488 anti-rabbit IgG	Goat anti-rabbit	-	Polyclonal	IgG	Thermo-Fisher	IF
Anti-CD54 (ICAM-1)	Mouse anti-human	15.2	Monoclonal	IgG1	Serotec	Inhibition assay
Anti-CD36	Mouse anti-human	FA6-152	Monoclonal	IgG1	Abcam	Inhibition assay
PE anti-CD31 (PECAM-1)	Mouse anti-human	WM59	Monoclonal	IgG1	Biolegend, London, UK	Flow cytometry
PE anti-CD36	Mouse anti-human	5-271	Monoclonal	IgG2a	Biolegend, London, UK	Flow cytometry
PE anti-CD54 (ICAM-1)	Mouse anti-human	HCD54	Monoclonal	IgG1	Biolegend, London, UK	Flow cytometry
PE IgG1 isotype control	Mouse anti-human	MOPC-21	Monoclonal	IgG1	Biolegend, London, UK	Flow cytometry
PE IgG2a isotype control	Mouse anti-human	MOPC-173	Monoclonal	IgG2a	Biolegend, London, UK	Flow cytometry
Purified anti-NF-	Rabbit anti-human	Poly6225	Polyclonal	IgG	Biolegend, London,	IF

κB P65	UK

2.1.5.2. Dyes

Dye	Label	Ex/Em (nm)	Company	Use
Ethidium bromide		360/590	Roth	DNA visualization
SYBR® Green I	Nucleic acid, dsDNA	355/465	Sigma-Aldrich	Flow adhesion assay, parasite labeling
Hoechst 33342		361/497	ThermoFisher	Cell imaging, IF

2.1.5.3. Size markers

GeneRuler 1 Kb plus DNA ladder (Ambion - Thermo Fisher Scientific, Dreieich, Germany).

2.1.5.4. Cytokines

Recombinant tumor necrosis factor alpha (TNF-α) from *E. coli* (Promocell, Heidelberg, Germany).

2.1.5.5. Organismus and primary cells

Organisms and cells	Origin
Human dermal microvascular endothelial cells (HDMEC)	Single donor, Promocell, Heidelberg, Germany
Plasmodium falciparum FCR3 strain	Gambia [220]

2.1.5.6. Oligonucleotides

N°	Sequence	Company
63, for	gg act agt atg aaa ttc gca agt aaa aaa aat aat c	Eurofins

73, rev	gt tct ttt agc aaa aat tTt ttc aat tac aca tac	Eurofins

2.1.6. Buffers and solutions

***P. falciparum* culture**

Complete culture medium	RMPI 1640 medium supplemented with 2 mM L-glutamine, 25 mM HEPES, 100 µM hypoxanthine, 20 µg/ml gentamicin and 10% (v/v) human serum.
Freezing solution	6.2 M Glycerol, 140 mM Na-Lactat, 0.5 mM KCl, pH 7.2 adjusted with 0.5 M of $NaHCO_3$ at pH 9.
Thawing solution I	12% (w/v) sodium chloride.
Thawing solution II	1.8% (w/v) sodium chloride.
Thawing solution III	0.9% (w/v) sodium chloride, 0.2% (w/v) glucose.
Sorbitol lysis solution	280 mM D-sorbitol, 5 mM HEPES, pH 7.4. (300 mOsm). Hit sterilized.
MACS buffer	PBS, 2mM EDTA, 0.5% (w/v) BSA.
Gelatin solution	0.5% (w/v) gelatin (from porcine skin type A) was dissolved in RPMI 1640 supplemented with 2 mM L-glutamine and 25 mM HEPES.
RMPI incomplete	RMPI 1640, 2 mM L-glutamine and 25 mM HEPES.
Binding medium	RMPI 1640, 2 mM L-glutamine, 25 mM HEPES, 0.1% BSA (w/v) pH 7.2.

NaOH and HCl were used to adjust the pH, solutions were filter sterilized (0.2 µm) and stored at 4°C. Otherwise indicated.

Immunofluorescence methods (activation assays)

FACS buffer	PBS, 2% (v/v) FCS, 0.1% (w/v) sodium azide.
FACS fixing solution	2% (v/v) formaldehyde in PBS.
IF fixing solution	4% (v/v) paraformaldehyde in PBS.
IF permeabilizing solution	0.5% (v/v) Triton X-100 in PBS.
IF blocking solution	3% (w/v) BSA in PBS.

TNF-α	10000 U/ml in PBS; 0.1% (w/v) BSA. Filter sterilized (0.2 µm).

DNA/RNA	
TAE buffer 1X	40 mM Tris, 20 mM acetic acid and 1 mM EDTA (0.5 M pH 8.0).
MOPS buffer 20X	0.4 mM MOPS, 40 mM sodium acetate, 5 mM EDTA (0.5 M pH 8.0).
DNA loading buffer (6x)	60% glycerol, 60 mM EDTA / 2.5 mg/ml Bromophenol blue.
RNA running buffer (20x)	400 mM MOPS, 40 mM $C_2H_3NaO_2$, 5 mM of EDTA.

NaOH and HCl were used to adjust the pH.

For all solutions and buffers MilliQ water was used.

2.1.7. Computer software and databases

Program	**Company**
Mendeley	Elsevier, London, UK
LSM imaging software	Zeiss, Jena, Germany
Cellquest	Becton and Dickinson, Heidelberg, Germany
JPK	JPK Instruments, Berlin, Germany
FIJI (v1.50a)	National Institute of Health, Bethesda, MD
SigmaPlot 13.0	Systat, CA, USA

2.2. Methods

2.2.1. Ethical clearance

This study was approved by the ethics committee of Heidelberg University, Mannheim University Hospital and the Biomolecular Research Center (CERBA/Labiogene). Blood samples were collected by venipuncture after obtaining written informed consent from the volunteers.

2.2.2. Blood collection and genotyping

Approximately 12 ml of citrated whole blood was collected. After centrifugation at 800 x g for 10 min at RT, the plasma and buffy coat were discarded. The remaining erythrocytes were washed three times with three volumes of RPMI-1640 basal medium and stored until use at 4°C. Erythrocytes were used within two weeks after collection. Hemoglobin genotypes were determined by cellulose acetate electrophoresis as previously described [211], a routine test performed by the Kooperatives Speziallabor of the Heidelberg University Hospital.

2.2.3. Cell culture methods

2.2.3.1. Endothelial cell culture and handling

2.2.3.1.1. Endothelial cell culture

Human dermal microvascular endothelial cells were purchased from Promocell (Heidelberg, Germany). These are primary cells isolated from a juvenile donor foreskin. Cells were grown in low serum containing medium (endothelial cell growth medium MV 2) at 37°C with an atmosphere of 5% CO_2. Neither antibiotics nor antimycotics were added. Cells between passage 4 and 7 were used for all assays. Cells were tested regularly for mycoplasma contamination using the mycoplasma detection kit (Venor®GeM classic, Invitrogen).

For sub-culturing, the PromoCell detachment kit was used. Confluent cells (T25 flask) were washed with 2 ml Hepes BSS solution and incubated at RT with 2 ml trypsin-EDTA until cells were detached. Since endothelial cell medium MV 2 contains low serum, 2 ml trypsin neutralizing solution was used. After centrifugation at 220 x g for

3 min, cell pellet was resuspended in MV 2 growth medium and placed into a new T25 culture flask and back into the incubator under regular cell culture conditions.

2.2.3.1.2. Freezing and thawing of endothelial cells

Cryopreservation was performed as recommended by the manufacturer. Confluent cells were detached as described previously (section 2.2.3.1.1.). After centrifugation cell were resuspended in 1 ml of serum-free freezing medium (Cryo-SFM) and freeze gradually (-1°C/min) to -80°C. Finally, cells were transferred into liquid nitrogen for long term storage.

Thawing of cryopreserved cells was performed as recommended by the manufacturer. Firstly, 9 ml of endothelial cell growth medium (MV 2) was added to a T25 cell culture flask and then placed into the incubator (37°C, 5% CO_2) for 30 min. After equilibration, cells were thawed for 2 min in the water bath at 37°C and transferred directly in to the T25 culture flask with the pre-warmed medium. Culture flask was placed into the incubator to let the cells attach. Medium was replaced after 16-24 h. Cells were sub-cultured after reaching confluence (80-90%).

2.2.3.2. *Plasmodium falciparum in vitro* culture and handling

2.2.3.2.1. *P. falciparum in vitro* culture

P. falciparum FRC3 strain was cultured as described by Trager and Jensen [221]. Briefly, parasites were cultured in type A^+ erythrocytes suspended in complete culture medium containing A^+ serum. Cells were grown at a hematocrit of 3.5% at 37°C under controlled atmospheric conditions (3% $C0_2$, 5% O_2 and 92% N_2). Hemoglobin variants infected erythrocytes were grown in complete culture medium containing AB serum, as the sugar group of the blood donor was unknown.

2.2.3.2.2. Blood smear preparation and light microscopy

Thin blood smears of the parasite culture were fixed in absolute methanol and stained with 10% (v/v) Giemsa solution for 20 min. After washing and air drying, smears were observed by light microscopy under oil immersion (100X) objective. Parasitemia was calculated as percentage from at least 1000 cells counted.

2.2.3.2.3. Cryopreservation of *P. falciparum* from *in vitro* cultures

Parasite culture of approximately 3-5% parasitemia in ring-stage was used for cryopreservation, since their membranes are more robust and therefore less prone to lyse during the thawing procedure. After centrifuging the parasite culture 500 x g for 2 min at RT, 1/3 cell pellet volume of freezing solution was added drop-wise, and the tube was let stand for 5 min at RT. Slowly, 4/3 cell pellet volume of freezing solution was then added, and the cells were carefully mixed, aliquoted into cryogenic-vials and stored at -80°C overnight. Cells were transferred to liquid nitrogen for long term storage.

2.2.3.2.4. Thawing of *P. falciparum* cultures

Cells were thawed for ~30 s in the water bath at 37°C, transferred into a 15 ml conical tube were 300 µl of thawing solution was added dropwise and the mixture was stand for 5 min at RT. Slowly 9 ml of thawing solution II was added, as well very slowly and cells were centrifuged for 2 min at 500 x g, RT. Finally, 7 ml of thawing solution III was added to the remaining pellet and suspension was centrifuged once again. Pellet was resuspended in complete culture medium and restored to normal culture conditions after adjusting the hematocrit to 3,5% with fresh packed blood.

2.2.3.2.5. Synchronization of *P. falciparum* with isosmotic D-sorbitol

During the late-intraerythrocytic development, approximately 16 h post-invasion *P. falciparum* increases the permeability of the red blood cell plasma membrane to a wide range of small solutes including D-sorbitol which have been shown to enter the red blood cell via a different pathway not operating in uninfected erythrocytes called the new permeation pathways [222]. As a result, in isosmotic solution of D-sorbitol, the infected erythrocytes at a late stage of development will swell and hemolyze and uninfected erythrocytes or early parasite ring stages will be not affected as they do not present NPP.

To perform this synchronization, parasite cultures were collected by centrifugation for 2 min 500 x g at RT and washed once with PBS. Twenty volumes (one volume = RBC pellet volume) of isosmotic sorbitol lysis solution were added to the culture

pellet and incubated at 37°C for 5 min. After an additional centrifugation, pellet was washed and resuspend in complete culture medium and restored to regular parasite culture conditions. Parasites were synchronized again after 10-12 h, keeping a tightly synchronized parasite population within a ± 4-6 h time window. Cultures were kept synchronized.

2.2.3.2.6. Enrichment of knobby mature-stage *P. falciparum*-infected erythrocytes by gelatin flotation

This method is used to enrich mature forms of infected erythrocytes however, does not generate pure parasite preparations. It is based on the sedimentation behavior of the iRBCs on gelatin solution [223] and it enriches only late-stage infected erythrocytes expressing knobs on the erythrocyte plasma membrane (+K, knobby parasites), since +K late stages sediment slower than uRBCs or ring-stage iRBCs.

After centrifuging the parasite culture (3-5% parasitemia, 3.5 hematocrit) at 500 x g for 2 min at RT, cell culture pellet was suspended in 10 volumes (one volume = RBC pellet volume) of 37°C pre-warmed gelatin solution. Cell suspension was then incubated for 30-60 min at 37°C. Supernatant was carefully transferred to a new tube and centrifuged (500 x g, 2 min, RT). Cell pellet was washed twice with RPMI incomplete medium and restored to normal culture conditions adjusting hematocrit to 3.5 % and parasitemia 0.5-1 % or used immediately for panning.

2.2.3.2.7. Magnetic isolation of *P. falciparum*-infected erythrocyte late-stages

Ingestion of hemoglobin during the intraerythrocytic development, results in the accumulation of free heme, which is highly toxic to the parasite as it lacks heme oxygenases [224]. For instance, the parasite possesses a very efficient detoxification mechanism where heme is aggregated into an insoluble non-toxic crystals termed hemozoin (malarial pigment), which is accumulated in the parasite digestive vacuole [225]. During this process, the $Fe+^{2}$ ions (diamagnetic) contained in the oxyhemoglobin are transformed in the hemozoin into $Fe+^{3}$ ions (paramagnetic) [226]. Accumulation of hemozoin in the digestive vacuole is noticeable microscopically in the most metabolically active parasite stages such as trophozoites and schizonts and

this fact permits the purification of mature iRBC up to ≤ 98% parasitemia with high parasite viability [227].

To perform this method, the magnetic activated cell sorting (MACS) separation column was placed into the vario MACS magnetic support and equilibrated by adding pre-warmed MACS buffer for 20 min at RT. The suspended parasite culture (3-5% parasitemia, 3.5% hematocrit), was loaded into the magnetic column and led flowed through at low flow rate (1 drop/sec). The column was washed then with approximately 50 ml of pre-warmed MACS buffer. The effluent which contained the uninfected erythrocytes and ring-stage-infected erythrocytes was discarded. After washing, the column was then removed from the magnetic field and the late-stage erythrocytes were eluted by applying 10 ml MACS buffer into the column. After centrifugation (500 x g, 2 min, RT), purified iRBCs were washed twice with RPMI 1640 medium. After purification iRBCs were used either for binding assays, endothelial cell activation assays, SEM, AFM or for hemoglobin variants infection.

2.2.3.2.8. Hemoglobin variants infection

Tightly synchronized parasites (time window of ± 6 h) at the trophozoite stage were magnetically enriched. iRBCs were suspended in *P. falciparum* culture medium containing AB serum after washing and added to fresh HbAS or HbAC blood to a parasitemia of 1-2% and 3.5% hematocrit. Thin blood smears were made to monitor parasite invasion and development. Hemoglobin AA erythrocytes were infected in parallel and used as control.

2.2.3.2.9. Estimation of the parasite multiplication rate, development and multiple infectivity

The parasite multiplication rate was determined for hemoglobin variants AS and AC erythrocytes, both as the parasitized erythrocyte multiplication rate (PEMR) and as the viable parasite multiplication rate (VPMR) as previously described [228]. Tightly synchronized parasite culture (± 6 h time window) at the schizont stage were magnetically purified, washed twice with complete RPMI medium and adjusted with fresh blood to a 0.05-1% parasitemia at 3.5% hematocrit and cultured under regular *in vitro* culture conditions. The number of newly invaded red blood cells was determined by light microscopy after preparing thin blood smears stained with

Giemsa of pre-invasion and 24 h post-invasion samples. The PEMR was calculated by dividing the final parasitemia at the ring stage by the starting parasitemia at the schizont stage (erythrocyte containing ≥ 2 parasites were counted as single infected erythrocyte), while for the VPMR estimation, the percentage of total ring-stage parasites present in all infected erythrocytes were divided by the starting parasitemia before schizogony. At least 1000 RBCs from each slide were counted.

Parasite multiple infectivity (PMI), defined as an iRBC cell containing ⩾ 2 parasites, was estimated by counting the number of multiply invaded red blood cells in 300 infected red blood cells. The percentage of single, double, triple and quadruple infections was quantified for infected HbAA and hemoglobinopathic erythrocytes. Furthermore, the parasite development was estimated by dividing the percentage of rings by the percentage of late-throphozoites after 24 hr. All assays were repeated a minimum of three times, from at least three different blood donors.

2.2.3.2.10. Selection of *P. falciparum* FCR3 strain for cytoadhesion to human dermal microvascular endothelial cells

The panning procedure was done as previously described by Claessens and Rowe [229]. Only cells between passage 4 and 7 were used, as during these stages the expression of surface receptors is constant [230]. After 48 h cells reached confluence and cells were activated with TNF-α (100 U/ml) for 24 h to induce ICAM-1 expression. After that, panning was performed. For this, late stages at approximately 5% parasitemia were selected for knobs by gelatin flotation. +Knob iRBCs were then collected from the gelatin supernatant and washed twice with RMPI-1640 basal media. The final pellet was suspended in 4 ml binding medium and added to the confluent endothelial cells (60-mm dish) previously washed with HBSS. Cells were co-cultured for 1 h at 37%. During the incubation, the parasites were suspended twice carefully by gently rocking the dish and rotating it clockwise and anti-clockwise. Once finished the incubation, the dish was washed ≤ 5 times with RPMI incomplete media by aspirating the medium and gentle rocking, until uninfected cells or non-bound iRBCs were completely gone. Remaining adherent cells were placed back in the incubator overnight after adding 3 ml parasite culture medium and 40 µl of packed fresh blood. The following day, infected erythrocytes were harvested by washing them out of the plate vigorously with RPMI incomplete medium. After

centrifugation (800 x g, 2 min, RT) the cell pellet was suspended in complete culture medium and placed back to culture after adjusting hematocrit to 3.5 %. Panned parasites were termed here FCR3^{HDMEC}.

After every panning, the parasite binding capability to HDMEC was monitored by static adhesion assay (see section 2.2.4.1). Once a high binding population was obtained, adhesion and activation assays were performed. Infected erythrocytes were repeatedly selected for knobs by gelatin flotation and for binding to HDMEC (every 3-4 weeks).

2.2.4. Binding assays

2.2.4.1. Static adhesion assay (wash assay technique)

2,5x10^5 HDMEC were seeded in 24 well plates pre-coated for 20 min at RT with fibronectin (10 mg/ml in PBS). HDMEC reached confluence after 48 h. Highly synchronized FRC3^{HDMEC} iRBCs late-stages were purified by MACS. IRBC pellet was washed with RPMI incomplete medium and resuspended in binding medium. Purification yield was evaluated by Giemsa stained blood smear and the number of cells was determined using a particle counter. Confluent HDMEC were washed twice with HBSS and incubated with 500 µl of iRBCs suspension (5x10^6 iRBCs/ml) in binding buffer for 1 h at 37 °C. During the incubation, the parasites were suspended twice carefully by gently rocking the dish and rotating it clockwise and anti-clockwise. Cells were washed ≤ 5 times with RPMI incomplete medium by aspirating the medium and gentle rocking until non-bound iRBCs were completely gone. Remaining adherent cells were washed once with PBS and fixed with 2% (v/v) glutaraldehyde in PBS for 30 min at RT and stained with 10% (v/v) Giemsa for 30 min at RT. Adhered cells were observed under an inverted microscope at 10X magnification air objective. Images of at least 6 fields of view were taken and the number of adhered cells per area was calculated using an automated cell counter plugin from ImageJ (v2.7.3). Duplicates were done for each sample and uninfected erythrocytes were assessed in parallel as negative binding control.

2.2.4.2. Flow chamber adhesion assay

30 µl of $1.3x10^5$ cells/ml were seeded in Ibidi µ-slide $V^{0.4}$ pre-coated with fibronectin (10 µg/ml in PBS) and place back into the incubator to let the cells sit and adhere for 30 min. Cells were then fed with 120 µl (reservoir volume). Cells were fed twice a day and they reached confluence within 48h. If needed, cells were incubated with TNF-α (100 U/ml) for 24h in HDMEC medium without hydrocortisone before the experiment to induce ICAM-1 expression.

Tightly synchronized trophozoites were magnetically purified and parasitemia calculated by Giemsa stained thin blood smear. After washing them twice with RPMI incomplete medium, cells were resuspended in binding medium and incubated with 0.4 µl/ml SYBR Green for 30 min at 37°C (in dark), for parasite labeling and therefore, automated cell tracking. After ≤ 5 washes, the cells number was determined using the particle counter and iRBCs were then resuspended in binding medium at a concentration of $1x10^6$ iRBCs/ml. At this point, confluent HDMECs were washed with binding medium and parasite suspension at 37°C was flowed through the cell monolayer on the flow chamber at different flow rates to create shear stress ranging from 0.03 to 0.3 Pa. This range of shear stress is typically found in post-capillary venules [231]. 5 ml of parasite suspension was flowed through the chamber (a total of $5x10^6$ iRBCs) at each shear stress. Unbound cells were washed out by flowing binding medium alone for 5 min at the same wall shear stress. For each shear stress condition, number of adherent cells was quantified from at least 6 fields of view at the center of the channel, were flow is found to be homogenous.

To study iRBCs motion behavior on HDMEC, videos at each of the previous shear stresses were recorded (time interval 0.033) using an inverted microscope (Zeiss Axio Observer, 40X objective, EGFP HC Filter set Ex: 456-490 nm Em: 500-540 nm). Mean translational velocities and fluorescence intensity profiles were obtained after video analysis using the TrackMate plugin from ImageJ (v2.7.3). Only cells that showed an end to end motion were used for analysis.

The generation of a desired wall shear stress from a flow rate was obtained by following the formula:

$$T = \eta \cdot 176.1 \cdot \Phi$$

Were T indicates the wall shear stress (Pa); η corresponds to the viscosity of the medium which was 0.7 mPa s, Φ corresponds to the flow rate (ml/min) and 176.1 is a factor obtained from the dimensions of the channel (provided by the manufacturer).

Table 1. Correspondent flow rate used to generate the different shear stresses in the µ-slide VI$^{0.4}$ chamber.

T (Pa)	Φ (ml/min)
0.03	0.24
0.05	0.39
0.075	0.59
0.10	0.79
0.15	1.18
0.20	1.58
0.25	1.97
0.30	2.37

2.2.4.3. Tracking analysis of single infected erythrocytes

The TrackMate plugin from ImageJ (v2.7.3) was used in order to track iRBCs motion on HDMEC. The DoG detector was used to detect small size particles. The estimated blob diameter was set to 7 µm and the threshold to 4. The Simple LAP tracker with a linking distance of 25 µm was selected to reduce the branched tracks. Translational velocity and fluorescence intensity amplitude profiles were obtained. These profiles served for classification of the iRBC motion as rolling/flipping or non-interacting cells and for further quantification of the cytoadhesive behavior.

2.2.4.4. Quantification of infected erythrocytes cytoadhesive behavior

Since the focus was maintained on top of the endothelial cells, the maximum points in the fluorescence amplitude data corresponded to the parasite approaching the focal plane whereas the minimum points corresponded to the parasite when leaving the focal plane. Amplitude difference (Δa) was determined by estimating and averaging the maximum $\langle a_{max} \rangle$ and minimum $\langle a_{min} \rangle$ points on the fluorescence

amplitude profile, by using the peak detection algorithm in python, performed by Dr. Anil Dasanna, Institute of Theoretical Physics, Heidelberg University:

$$\Delta a = \langle a_{max} \rangle - \langle a_{min} \rangle$$

Knowing that the maximum points on the fluorescence amplitude profile represent the parasite in closest proximity to the substratum, a threshold (-0.05 a.u.) was applied to maximum amplitude values. All data points above the threshold were then summed and the contact time estimated (since each data point corresponds to 0.033 sec). Pearson correlation coefficient between fluorescence amplitude and translational velocity profile was used to determine the regularity of flipping as previously described [232]. Furthermore, the mean translational velocity were obtained for all trajectories. All calculations were done after normalizing all fluorescence amplitude profiles with the minimum intensity value, since the florescence intensity signal was not constant for all the samples.

2.2.4.5. Adhesion using blocking antibodies

Adhesion assay was performed as described in section 2.2.4.2., were HDMEC were pre-incubated with saturating concentrations of monoclonal antibodies (FA6-152 and 15.2) against CD36 or/and ICAM-1 PfEMP1 binding sites (4 µg/ml in HDMEC culture media, for 1 h under regular culture conditions) before the experiment. No monoclonal antibody control was evaluated in parallel.

2.2.4.6. Flow-based adhesion assay / detachment assay

Flow chambers (Ibidi µ-slide V $^{0.4}$) were coated with fibronectin (10 µg/ml in PBS) for 30 min at RT. After washing the channels with PBS, 30 µl of 1.3x10^5 cells/ml were seeded per channel and cells were place back into the incubator to let them sit and adhere for 30 min. Reservoir volume were filled (120 µl) with medium. Cells were fed twice a day with HDMEC cell complete medium and they reached confluence within 48 h. If needed, cells were incubated with TNF-α (100 U/ml) for 24h in HDMEC medium without hydrocortisone before the experiment to activate the endothelial cells.

Tightly synchronized infected erythrocytes at late stages were purified trough the magnetic column and iRBCs pellet was washed twice with incomplete RPMI-1640 medium. For automated cell counting, iRBCs were labeled with 0.4 µl/ml SYBR Green for 30 min at 37°C in dark. After ≤ 5 washes with incomplete RPMI-1640 medium, cells were counted and resuspended in binding medium at a concentration of $1x10^6$ iRBCs/ml. A total of 5 ml of parasite suspension at 37°C was flowed through the HDMEC monolayer on the flow chamber, at a wall shear stress of 0.05 Pa. Unbound cells were washed out by flowing binding medium alone for 5 min. At least 6 fields of view at the center of the channel were imaged and initially bound iRBCs were quantified. After this step, shear stress was increased stepwise up to 4 Pa. Each wall shear stress was applied for 5 min and initial shear stress of 0.05 Pa was applied while images were taken, that the flow conditions were always present. Infected hemoglobin variants and wild-type erythrocytes were run in parallel. Binding strength was estimated by calculating the critical shear stress at which the 50% of the initially bound iRBC population detached (τ_{50}).

2.2.5. Assessment of endothelial cell activation

2.2.5.1. Co-culture of HDMEC and *P. falciparum*-infected erythrocytes

Activation assay was done as described by Viebig *et al.* [165]. HDMEC were seeded in fibronectin pre-coated 12 well plates (10 mg/ml in PBS). After reaching confluence, endothelial cells were washed with HBSS and co-cultured with $5x10^6$ iRBCs at the trophozoite stage (enriched by MACS) resuspended in 1 ml of HDMEC culture medium without hydrocortisone (hydrocortisone prevents activation and therefore was depleted during this assay) for 16 h under regular culture conditions. After the incubation period, supernatant was collected, centrifuged for 1 min at 10000 x g and 4°C. The supernatant was frozen to -20°C until ELISA for IL-6 detection was performed (see section 2.2.6.1.). The remaining endothelial cells were used for flow cytometry in order to measure ICAM-1 endothelial cell surface levels after iRBCs exposure (see section 2.2.6.2.).

Alternatively, HDMEC were seeded in Ibidi µ-slide $V^{0.4}$ pre-coated with fibronectin (10 µg/ml in PBS). After reaching confluence, endothelial cells were incubated as described previously, with 150 µl of parasite suspension ($5x10^6$, $2x10^7$, $7x10^7$ or $1x10^8$, iRBCs/ml) for 2 h under static normal culture conditions. When assessed in

flow conditions, infected erythrocytes ($1x10^8$ iRBCs in 5 ml) were flown through the confluent HDEMC seeded on the channel at a wall shear stress of 0.03 Pa (30 min) and incubated for another 90 min. After this period, endothelial cells were washed 3X with cold PBS and proceed to NF-κB immunolocalization (see section 2.2.6.3. and 2.2.7.1.). For all activation assays, HDMEC in parallel were incubated with endothelial cell culture medium without hydrocortisone and uninfected erythrocytes as negative controls, and TNF-α (100 U/ml) as positive control for endothelial activation.

2.2.6. Immunofluorescent methods

2.2.6.1. Enzyme-linked immunosorbent assay for IL-6 quantification

Enzyme-linked immunosorbent assay (ELISA) is used to detect and quantify specific antigen or antibody using an enzyme chemically linked to the antibody directed to the antigen/antibody of interest. The capture or sandwich ELISA is a modification of the classical ELISA used to detect secreted products such as cytokines. Instead of coating the plastic plate with antigen to detect antibodies, it is coated with antigen-specific antibodies, which are then able to bind with high affinity to the specific antigen, thus concentrating it on the plate surface even if the antigen its present at very low concentrations in the suspension. A secondary antibody chemically linked to an enzyme, usually HRP, is directed against another epitope of the captured antigen, thus it can be detected by an enzyme color change reaction that can be read in multichannel spectrometer [233].

Capture ELISA was used to quantify IL-6 released from HDMEC after co-culture with infected erythrocytes (human IL-6 ELISA MAX™ Deluxe set) as recommended by manufacturer, after performing the activation assay (see section 2.2.5.). Duplicates from at least three independent experiments were evaluated.

2.2.6.2. ICAM-1 cell surface levels measured by flow cytometry

Flow cytometry allows to measure multiple physical parameters of a cell such as cell relative size, internal complexity and granularity and relative fluorescence intensity, while the cell flows in a fluid stream through a beam of light. These parameters are determined using an optical-to-electronic coupling system that records how the cell

scatters incident laser light and emits fluorescence. Side-scattered light is collected at approximately 90° to the laser beam and corresponds to the cell granularity or internal complexity and forward scatter light is collected at 0-10° to the laser beam and indicates the relative cells size. By using specific labeled antibodies to tag cell surface proteins, it is possible to identify individual cells and quantify the levels of protein expression on their surface. The scatter light and fluorescence signals are detected and amplified by the photomultiplier tube and the amount of signal detected is proportional to numbers of fluorochrome molecules on the cell [233].

To quantify the ICAM-1 levels on endothelial cells after exposure to FCR3^{HDMEC} infected erythrocytes, endothelial cells were first washed with pre-warmed PBS and detached with trypsin-EDTA. After detachment, trypsin was inactivated using trypsin-inhibitor (1:1 trypsin volume) and cells were centrifuged at 300 x g for 5 min at RT. Cell pellet was washed once with 400 µl FACS buffer and cells were counted. 2-10x10^5 cells were used per staining. For this, cell pellet was resuspended in 50 µl FACS buffer with PE-labeled antibody at a 1:50 dilution and incubated for 30 min on ice in dark. Cells were washed with 100 µL FACS buffer and fixed with 100 µL of 2% (v/v) formaldehyde in PBS. Fluorescence intensity (Ex: 488 nm, Em: 575 nm) and forward scatter light was recorded. Post-analysis was performed using CellQuest software. Quantification of CD36 was also performed in order to corroborate stable levels expression on HDMEC in the different cell passages and donors.

2.2.6.3. NF-κB immunolocalization

Immunofluorescence (IF) microscopy make the use of a specific antibody to localize a target molecule with accuracy in single cells or in tissue sections. Indirect fluorescence makes the use of a secondary antibody labeled covalently with a fluorescent dye. The stained cells can be the examined under the microscope were exposed to a specific light wavelength to excite the fluorochrome. Which once excited emits light at a characteristic wave length that is collected through a selective filter. Different than a fluorescence microscope, confocal microscopy allows as to produce a very thin optical section of a cell or tissue. In this way the fluorescence emission itself can be restricted to the optical section [234].

Immunolocalization of p65 NF-κB in HDMEC was evaluated by confocal microscopy after co-culturing them with FCR3^{HDMEC} infected erythrocytes as previously described [169]. Endothelial cells were washed three times with ice cold PBS and fixed with 4% (v/v) paraformaldehyde in PBS for 15 min at RT. Cells were then rinse three times with cold PBS and permeabilized with 0.5% (v/v) triton X-100 in PBS for 10 min at RT. After washing, cells were blocked with 3% BSA in PBS for 30 min at RT. Cells were incubated with 1:200 rabbit polyclonal IgG anti-human NF-κB p65 subunit diluted in blocking solution overnight at 4°C. After washing three times with PBS, Alexa-488 conjugated goat anti-rabbit IgG was added to a dilution of 1:400 in blocking solution and incubated for 1h at RT in the dark. After washing, nuclei were counterstained with Hoechst (5 µM) for 10 min at RT. Cells were imaged immediately or kept in 0.02% (w/v) sodium azide in PBS for longer storage. Images were acquired by confocal microscopy and post-analyzed as described by Vora *et al*., 2010 [235].

2.2.7. Microscopy techniques

2.2.7.1. Confocal imaging acquisition and analysis

Fluorescence imaging of P65-NF-κB translocation was performed using a Zeiss confocal microscope. The Hoechst (excitation: 351 nm, emission: 385-470 nm), Alexa-488 (excitation: 488 nm, emission: 505-550) and DIC images were acquired from at least 6 random fields of view (63X/ 1.2 NA W objective) for each sample. Images were recorded using a pin hole Ø of 1.71 airy units, a scan speed of 1.6 µs/pixel and a frame averaging of 2. The PMT gain and offset were adjusted to obtain sub-saturating fluorescence intensity with an optimal signal-to-noise ratio. The percentage positive p65-NF-κB immunolabeled nuclei from the total number of nuclei observed by Hoechst staining (nuclear labeling index; NLI) was estimated as previously described [235] and expressed as mean ± SEM from at least three biological replicates.

2.2.7.2. Scanning electron microscopy

The resolution power obtained from optical microscopes depend on the wavelength of light, which is limited then to 0.2 µm, when using green light illumination. Electron microscopes use instead of a light beam an electron beam, producing shorter wavelengths that allow resolving ~0.1 nm structures [117]. For this reason, scanning

electron microscopy (SEM) was performed to resolve and quantify the nano-scale knobs presented on the infected erythrocytes plasma membrane.

Magnetic purified infected erythrocytes were fixed with 2% (v/v) paraformaldehyde and 2% (v/v) glutaraldehyde in PBS for 1h at RT and loaded onto coverslips previously coated with 0.01% poly-L-lysine (v/v in water) for 15 min. Cells were washed three times with PBS and dehydrated by ethanol series of 30%, 50%, 70%, 90% and 3 x 100%, 10 min each; followed by immersion in 1:1 solution of hexamethyldisilazan:ethanol for 5 min and hexamethyldisilazan 100% overnight. Dehydrated samples were sputter-coated with 10 nm gold/palladium (EM MED 020 Leica, Germany) and viewed at 10000X magnification on a scanning electron microscope (Leo1530, Carl Zeiss, Germany). Quantification of knobs was done by manual counter using imageJ and the knob number was expressed per μm^2.

2.2.7.3. Atomic force microscopy (AFM)

Atomic force microscopy allows imaging with a high magnification and with very high resolution. It requires minimal and inexpensive sample preparation and can be used as well to image living cells. It can be used to resolve the topography of a specimen by scanning the sample in the x and y directions with the AFM cantilever, which will bend when encounter an uneven surface. The detected cantilever deflection is translated into a 3D topographic image [236]. In contrast to SEM, AFM provides quantitative information on the height [236]. On the other hand, AFM force spectroscopy permits the measurement of forces in the range of pico Newton. By approaching and retracting the AFM cantilever in the z-direction, a force-distance curve can be generated, which directly give information on the interacting forces between the cantilever and the substratum [236].

2.2.7.3.1. Sample preparation for knob imaging by scanning AFM

Highly synchronized *P. falciparum* cultures were magnetically purified and washed twice with PBS. 4 µl from pellet were resuspended in 10% (v/v) Giemsa in PBS for 10 min at 37°C. From this a thin blood smear was made and air dried. AFM imaging was performed by Katharina Quadt (Center for Infectious Diseases, Heidelberg University Hospital) as previously described [115].

2.2.7.3.2. AFM-Single cell force spectroscopy (AFM-SCFS)

The quantification of the infected erythrocytes binding strength to HDMEC at the single cell level was performed as previously described by Davis et al., (2012) [162]. The Nanowizard III atomic force microscope was equipped with a CelHesion module (JPK Instruments, Berlin, Germany) and mounted on an inverted microscope stage. The set was enclosed in a chamber in order to keep the temperature and atmosphere constant at 37°C and 5% CO_2. Measurements were performed using a relative contact mode with a relative set point of 0.15 nN, z-length of 50 µm, extend and retract speed of 1.5 µm/s, sample rate of 256 Hz and extend delayed that vary between 0 and 30 s.

A triangular tip-less nitride cantilever with spring constant of 0.05 N/m was UV cleaned for 15 min and exposed to 4 mg/ml of dopamine hydrochloride in 10 mM Tris pH 8.5 for 1 h at room temperature and protected from light. Cantilever was washed with milliQ water and dried for 1 h at room temperature. In parallel, *P. falciparum*-infected erythrocytes magnetically purified were washed and resuspended in HDMEC basal medium without supplements at 0.5% hematocrit. At the same time confluent endothelial cells grown in the center of a 15-mm petri dish pre-coated with fibronectin (10 µg/ml in PBS) were washed with HBSS, suspended in endothelial cell basal medium without supplements and mounted into the base of the inverted microscope. The atomic force microscope was set to force spectroscopy (contact mode) and previously calibrated onto an empty petri dish. Infected erythrocytes suspension was lead into the petri dish (5 µl) in an area without endothelial cell and cantilever was approach on top of a cell for 60 s in order to lead the red blood cell adhere to the functionalized cantilever before it was brought into contact with the endothelial monolayer. Force curves were analyzed using the JPK software to determine the maximum force of detachment and the number of rupture events.

2.2.8. Molecular biology methods

2.2.8.1. *P. falciparum* RNA isolation for *var* gene transcriptional profiling

Var gene transcription profiling of $FCR3^{HDMEC}$ was performed by q-PCR in order to determine the major transcript expressed on the population selected to bind on HDMEC. For this, tightly synchronized parasites at ring stage (10-16 h post-invasion)

at 5-10% parasitemia were used. The parasite culture was collected by centrifugation at 800 x g for 2 min at 4°C, supernatant was discarded, and cell pellet was lysed in 4°C cold saponin lysis solution (0.1% (w/v) saponin in PBS) to get rid of uninfected erythrocytes. After mixing carefully and centrifuging at 2600 x g for 8 min at 4°C, remaining pellet was washed once with cold PBS and lysed with TRIzol (10 pellet volumes). Lysed cells were then kept at -80°C until RNA extraction.

TRIzol lysates were thawed at 37°C, mixed thoroughly by vortex to dissolve clumps and divided into 1 ml aliquots. To the sample 0.2 TRIzol volumes of chloroform were added and after shaking vigorously for 15 s suspension was incubate at RT for 2 min and centrifuged 12000 x g for 30 min at 4C°. The aqueous phase containing the RNA was carefully removed and transferred to a new tube. 0.5 TRIzol volumes of 4°C cold isopropanol was added and solution was incubated for 10 min at RT to precipitate the RNA. Followed by a centrifugation at 12000 x g for 30 min at 4°C RNA pellet was washed with 1 TRIzol volume of ethanol 75%. Pellet was air dried at RT for approximately 10 min and resuspended in 20 µl of RNAase free water. RNA pellet was incubated for 10 min at 60°C to dissolve completely. RNA yield was determined by measuring the absorbance at 260 nm. Samples with an OD_{260}/OD_{280} ratio close to 2.0 were used for q-RT-PCR. RNA integrity was further assessed in agarose gel electrophoresis (0.7% agarose/ 20% formaldehyde in running buffer) for 1 h at 100 V. RNA was visualized with ethidium bromide.

To proceed with the cDNA synthesis, contaminant genomic DNA (gDNA) was eliminated from the sample RNA by DNAse treatment using the TURBO DNA-free™ kit (Ambion). cDNA was produce from RNA using the kit Superscript III First-Strand Synthesis SuperScript (invitrogen). To corroborate complete elimination of gDNA from the original sample, a PCR to detect PfCRT intron was performed as follow:

PCR Master Mix	**For one reaction (µL)**
10 Reaction Buffer Tag -$MgCl_2$	2,5
dNTPs 2mM	2,5
$MgCl_2$ (50 Mm)	1,25
Tag Polymerase (5U/µl) PFX	0,25

Primer 1	1
Primer 2	1
DNA Sample	1

Program for thermocycler:

1 Cycle	94°C for 4 min
30 Cycles	94°C for 45 sec 54°C for 45 sec 68°C for 45 sec
1 Cycle	68°C for 10 min
Cool down to 4°C ∞	

Samples were visualized in agarose gel electrophoresis (2% in TAE buffer) for 1 h 100 V. *P. falciparum* gDNA was used as positive control.

The real time qPCR was performed by Marilou Tétard and Benoit Gamain (Inserm, Paris, France). For this, a total of five micrograms of starting RNA were used to compare the full set of primers. The quantitative real-time PCR reactions were performed using the CFX96 thermocycler (BioRad) in 20 µl volume using Advanced Universal SYBR Green Supermix (BioRad) and specific primer pairs for each IT4 *var gene* [237] . Relative transcription was obtained after normalization with seryl-tRNA synthetase (housekeeping control gene) [PlasmoDB: PF07_0073] and converted to relative copy numbers.

2.2.8.2. *P. falciparum* gDNA isolation

P. falciparum culture at the trophozoite stage with a parasitemia of approximately 5% was collected by centrifugation at 800 g for 2 min at RT, washed with ice cold PBS and lysed in 0.1% (v/v) saponin in PBS. DNA was isolated using the tissue and blood DNA extraction kit as indicated by manufacturer. DNA integrity was evaluated by 0.8% agarose gel electrophoresis with 3 µl ethidium bromide.

2.2.9. Spectrophotometric assays

2.2.9.1. Quantification of hemoglobin content by spectroscopy (new permeation pathways activation)

Highly synchronized infected red blood cells were evaluated for hemolysis capability over the entire intraerythrocytic life cycle. In detail, every four hours a total of $1x10^7$ iRBC were washed in PBS and then suspended in 800 µl of isosmotic sorbitol lysis solution for 10 min at 37°C. After centrifugation at 500 x g for 2 min, 700 µl of the supernatant were collected and used to measure the absorbance at 540 nm in order to estimate the hemoglobin concentration. Hemolysis of uninfected erythrocytes was assessed in parallel as negative control. Duplicates of at least two independent samples were done.

3. Results

3.1. Selection and characterization of a *P. falciparum* FCR3 binding population to HDMEC

3.1.1. Selection of *Plasmodium falciparum* (FCR3) binding to HDMEC

The predominant receptors for *P. falciparum* microvascular sequestration in field isolates are CD36 and ICAM-1 [238][239]. Both, CD36 and ICAM-1, are constitutively expressed on human dermal microvascular endothelial cells (HDMEC), at a reported density of 86 ± 14 x 10^6 and 6 ± 3 x 10^6 molecules per mm^2, respectively [161]. Therefore, these cells were used within this study as model for substratum for *P. falciparum* cytoadherence. HDMEC are very flat primary cells isolated from human neonatal foreskin. HDMEC obtained from different donors, were evaluated for their levels of CD36 and ICAM-1 surface expression by flow cytometry (Figure 7A). The results showed variations in the CD36 and ICAM-1 density expressed at the cell surfaces and therefore in the cell population homogeneity regarding the receptor expression. For instance, cells isolated from donor one and three presented a subpopulation of cells lacking or expressing very low amounts of CD36 on their surfaces, while the other part of the population expressed high levels. These results showed the heterogeneity regarding CD36 surface expression in those endothelial cell isolations. Similar observation was made for ICAM-1 expression in the cells derived from donor three. On the other hand, the cell population obtained from donor two showed to be more homogeneous for both CD36 and ICAM-1 receptor expression and therefore was selected for all future assays.

During malaria infection, systemic release of pro-inflammatory cytokines such as tumor necrosis factor alpha (TNF-α), increases [25][26][27][28]. This in turn, upregulates the expression of various endothelial adhesion molecules, such as ICAM-1. As expected [233], stimulation of HDMEC with TNF-α (100 U/ml) for 24 h induced a pronounced increase in ICAM-1 endothelial cell surface expression but did not markedly change the levels of CD36 expression (Figure 7B). After selection and characterization of HDMEC, a long-term *P. falciparum* culture was selected by panning over these microvascular endothelial cells.

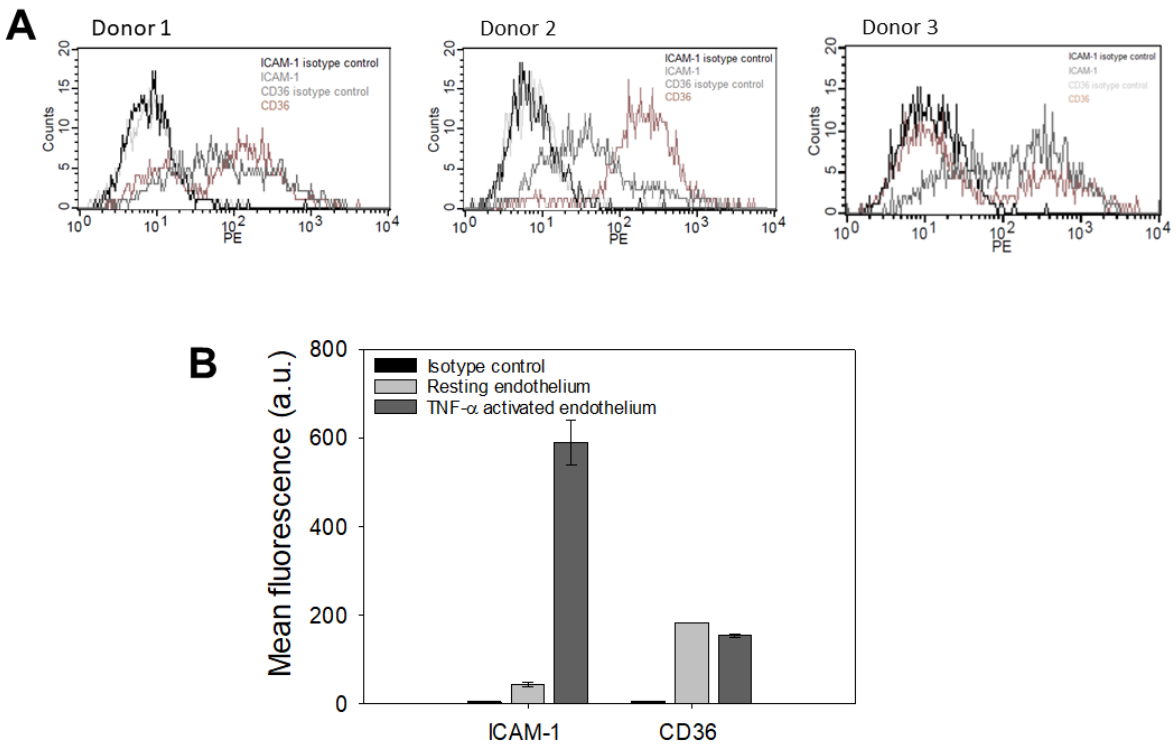

Figure 7 | Surface expression of ICAM-1 and CD36 on HDMEC. (A) Expression levels of CD36 and ICAM-1 on the surface of HDMEC of different cell donors, measured by flow cytometry (phycoerythrin fluorescence, PE). (B) Geometric mean fluorescence of CD36 and ICAM-1 for resting and TNF-α activated endothelial cells (donor two, *n = 2*).

Long-term *in-vitro* parasites populations usually show a very heterogeneous nature with respect to their binding properties [66]. Because of the absence of selective pressure, the parasite population can express many different *var* gene variants at any given time. Therefore, the *P. Falciparum* clone FCR3 (Gambia), was selected by panning for binding to HDMEC expressed ligands (Figure 8A). Initially, only few cells adhered to the endothelial monolayer, however, panning resulted in an approximately 160-fold enrichment for parasites binding to the HDMEC already after the fourth round of selection (Figure 8A/B). The selcted population was termed FCR3^{HDMEC}. These parasitized erythrocytes were capable of adhere to HDMEC under physiological flow conditions (0.05 Pa wall shear stress) as show in Figure 8C. The hemozoin crystals (malarial pigment) inside the parasite food vacuole can be appreciated in the phase contrast image as a black dot (Figure 8C, arrow), and its movement was used as indicator of parasite viability. Once selected, the binding

preference of *P. falciparum* FCR3^{HDMEC} to CD36 and ICAM-1 on HDMEC was characterized.

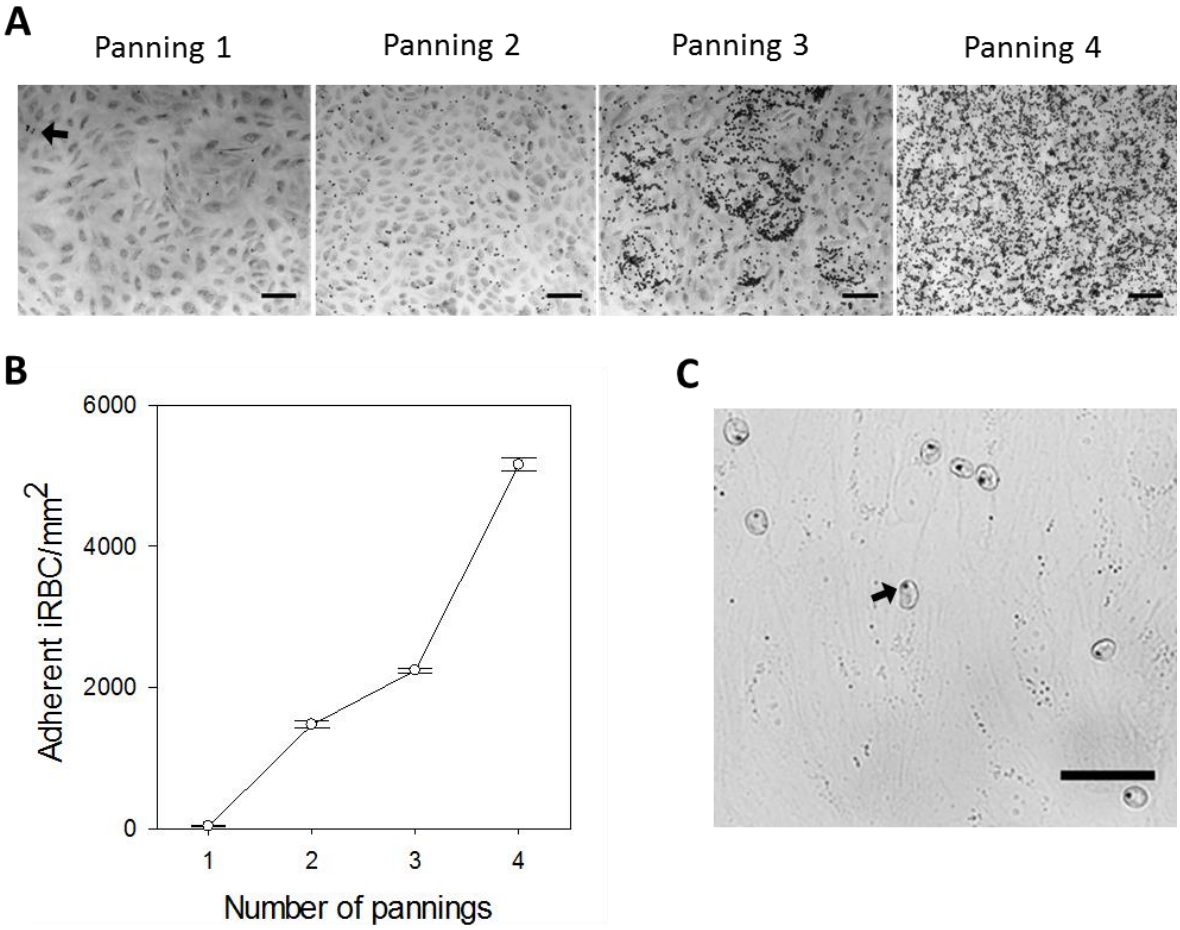

Figure 8 | Selection of *P. falciparum* FCR3 strain for binding to HDMEC. (A) Representative differential interference contrast (DIC) images (scale bar 100 µm, arrow points out the infected erythrocyte bound on the endothelial monolayer) and (B) the correspondent absolute number of *P. falciparum* parasitized erythrocytes cytoadhering under static conditions to confluent HDMEC after every round of selection. The mean ± SEM are shown, *n = 2*. (C) Representative phase contrast image (live cell imaging) of infected erythrocytes remaining adherent on HDMEC under flow conditions at a wall shear stress of 0.05 Pa, scale bar 20 µm. Arrow points to the hemozoin crystal present in the infected erythrocyte.

3.1.2. Characterization of FCR3^{HDMEC} receptor binding preference

In order to characterize the binding preference of FCR3^{HDMEC} infected erythrocytes, cytoadhesion on HDMEC was studied using saturating concentrations of FA6-152 and 15.2 antibodies. The monoclonal antibodies 15.2 and FA6-152 have been shown to completely block the binding of infected erythrocytes to ICAM-1 [238] and CD36

[240], respectively. Under flow conditions, the antibodies FA6-152 and 15.2 blocked the adhesion of FCR3^{HDMEC} infected erythrocytes to CD36 and ICAM-1 on HDMEC by approximately 93% and 17%, respectively (Figure 9). When applied in combination, the antibodies blocked the infected erythrocytes adhesion by ~99%.

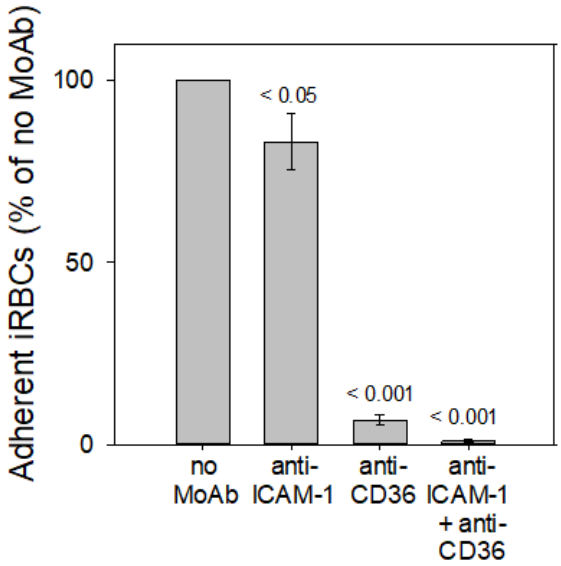

Figure 9 | Effect of blocking antibodies on FCR3^{HDMEC} binding to HDMEC. Percentage of parasitized erythrocytes remaining adherent on HDMEC at wall shear stress of 0.05 Pa, after blocking CD36 and/or ICAM-1 parasite binding sites on the endothelial cells with specific monoclonal antibodies (MoAb). Values are expressed relative to the no MoAb binding control group. The mean ± SEM are shown (*n = 3*). Significant differences are indicated; One-way ANOVA for multiple comparisons.

To further characterize the FCR3^{HDMEC} population, the *var* gene transcription profile was studied in colaboration with Marilou Tétard (PhD student) and Dr. Benoît Gamain from the French National Institute of Health and Medical Research in Paris. The results showed that the major *var* gene transcripts expressed in the parasite population were IT4var13, IT4var25 and IT4var66 (Figure 10). These *var* genes belong to the subgroup UpsB and UpsC, which encode for PfEMP-1 variants predicted to bind to CD36 and ICAM-1 [241]. IT4var13 and IT4var25 have been characterized to confer binging to ICAM-1 and CD36 [242][243][244]. The percentage of *var* gene transcripts remained relatively constant within the parasite population over periodical selections, particularly the IT4var25 and IT4var66. Once selected and

characterized for its binding preference, the *P. falciparum* FCR3^{HDMEC} growth and replication in wild-type and hemoglobinopathic erythrocytes was investigated.

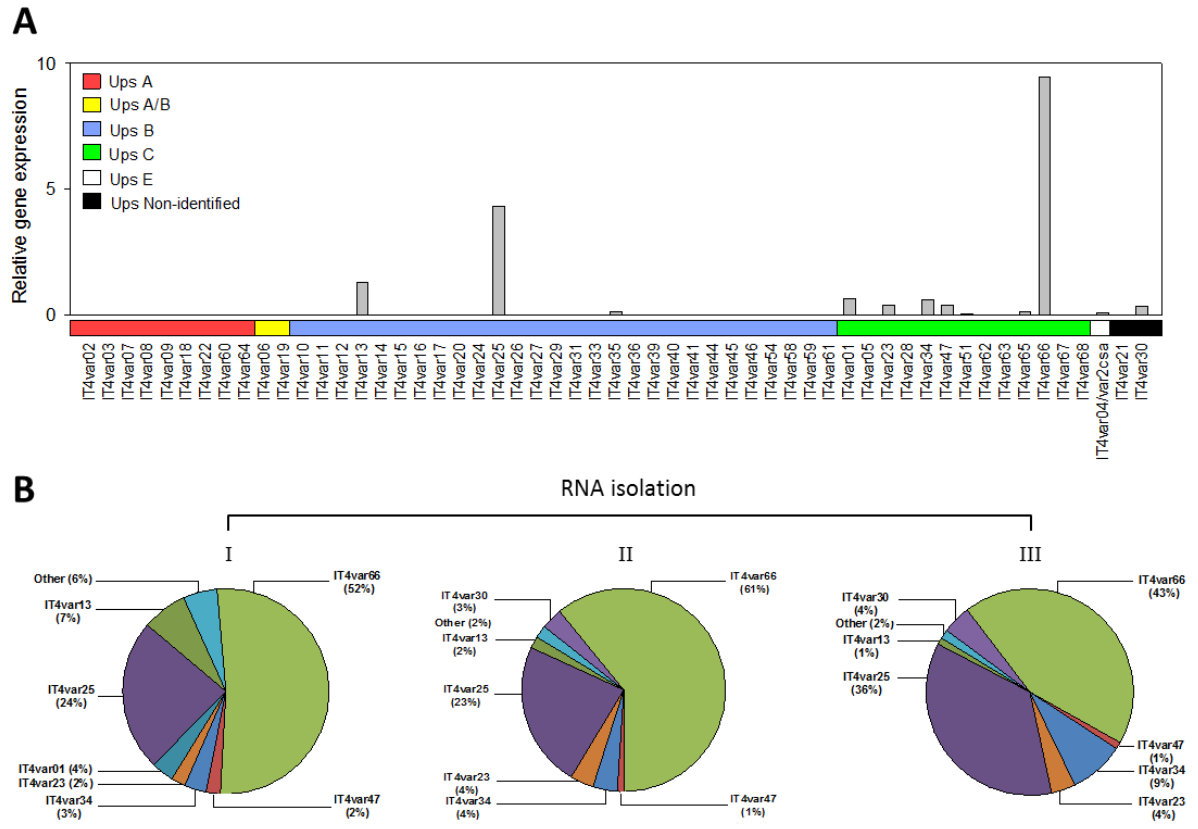

Figure 10 | Characterization of FCR3^{HDMEC} *var* gene transcription. (A) Transcription profile for the *var* genes was assessed after repeated selection of *P. falciparum* (FCR3 strain) infected erythrocytes on HDMEC. Results were normalized to the housekeeping control gene *seryl synthetase*. Genes were organized based on the upstream sequence (Ups) group into UpsA (red), UpsA/B (yellow), UpsB (blue), UpsC (green), UpsE (white), and others (black). (B) Pie chart showing the percentage of each *var* gene transcript expressed in the parasite population from three RNA samples isolated from independent panning selections.

3.1.3. Parasite multiplication rate, multiple infectivity and development

The number of newly infected red blood cells starting from one schizont determines the parasite multiplication rate (PMR). The intrinsic ability of parasites to multiply at high densities has been correlated with disease severity [228]. The PMR was determined both as the parasitized erythrocyte multiplication rate (PEMR) and as the viable parasite multiplication rate (VPMR). PEMR considers multiple invaded cells as

one infected erythrocyte, while VPMR considers all viable merozoites that were able to invade new red blood cells, thus considering multiple infectivity. *In vivo* and during *in vitro* cultures, especially under static conditions, *P. falciparum* shows multiple infectivity [245], i.e. more than one parasite resides within the same erythrocyte. Microscopic examination of Giemsa-stained thin blood smears revealed multiple infected erythrocytes carrying a maximum of four parasites (Figure 11A, upper panel), which were capable of developing normally to later stages (Figure 11A, lower panel).

The PEMR was estimated to be 6.6 ± 0.3, 6.4 ± 0.3 and 6.2 ± 0.4 for infected HbAA, HbAS and HbAC erythrocytes, respectively (Figure 11B). No significant difference between groups was found (between HbAA and HbAS $p = 0.731$, between HbAA and HbAC $p = 0.783$, One-way ANOVA). On the contrary, infected HbSS erythrocytes had significantly lower PEMR values (3.6 ± 0.8) when compare to wild-type control group ($p < 0.001$, One-way ANOVA). Compared to the PEMR, the VPMR values were higher for all the groups. They increased to 8.5 ± 0.7, 8 ± 0.6, 8.1 ± 0.8 and 4.7 ± 1 for HbAA, HbAS, HbAC and HbSS, respectively (Figure 11C). These results reflect the numerous multiple invaded erythrocytes found for the *P. falciparum* FCR3 strain growing under static culture conditions. No significant difference for VPMR between HbAA, HbAS and HbAC was found (between HbAA and HbAS $p = 0.856$, between HbAA and HbAC $p = 0.710$, One-way ANOVA), but infected HbSS erythrocytes showed significantly lower VPMR values, when compared to the HbAA group ($p < 0.01$, One-way ANOVA).

The biological reason for multiple invaded erythrocytes remains unclear, but it is has been correlated with severity, probably by increasing the amount of adhesins exported to the infected erythrocyte surface [245]. Furthermore, the amount of knobs positively correlates with the amount of intracellular parasites [245]. Therefore, when comparing infected wild-type and hemoglobinopathic erythrocytes in future adhesion assays, it is highly important to consider the levels of multiple invaded cells. The percentage of *P*. *falciparum* multiple invasions (parasite multiple infectivity, PMI) was found to be ~24% and did not vary significantly between groups (Figure 11D) (p = 0.860, One-way ANOVA). Double invaded cells were the dominant form, representing ~80% of the multiple invaded erythrocytes, followed by triple (~16%)

and quadruple invasions (~4%) (Figure 11E). No significant differences between infected wild-type and hemoglobinopathic erythrocytes were found (2 parasites p = 0.303; 3 parasites p = 0.457; 4 parasites p = 0.303, One-way ANOVA).

Determining the parasite development in infected HbAA and hemoglobinopathic erythrocytes was also of relevance in our study since the iRBC adhesion increases as the parasite matures [116][118]. Parasites growing in HbAA, HbAS and HbAC erythrocytes developed normally from rings to late stages (between HbAA and HbAS p = 0.457; between HbAA and HbAC p = 0.361, One-way ANOVA comparing the ring to trophozoite ratios), but not when growing in HbSS erythrocytes (Figure 11F). For these cells, the number of parasites capable of developing through the end of the erythrocytic cycle significantly declined by 27% ($p < 0.050$, One-way ANOVA). Some of the HbSS erythrocytes showed sickling under normal *in vitro* culture conditions (Figure 11G; arrow a,b). Few parasites, however, were still able to grow inside these morphologically disturbed cells (Figure 11G; arrow b). Nevertheless, approximately 13.6 ± 4% of the parasites growing in sickle erythrocytes arrested at late stages of maturation (Figure 11G; arrow c). These results were obtained microscopically by thin blood Giemsa smears from highly synchronized parasite cultures. For sickle cell hemoglobin, blood from only one donor was processed.

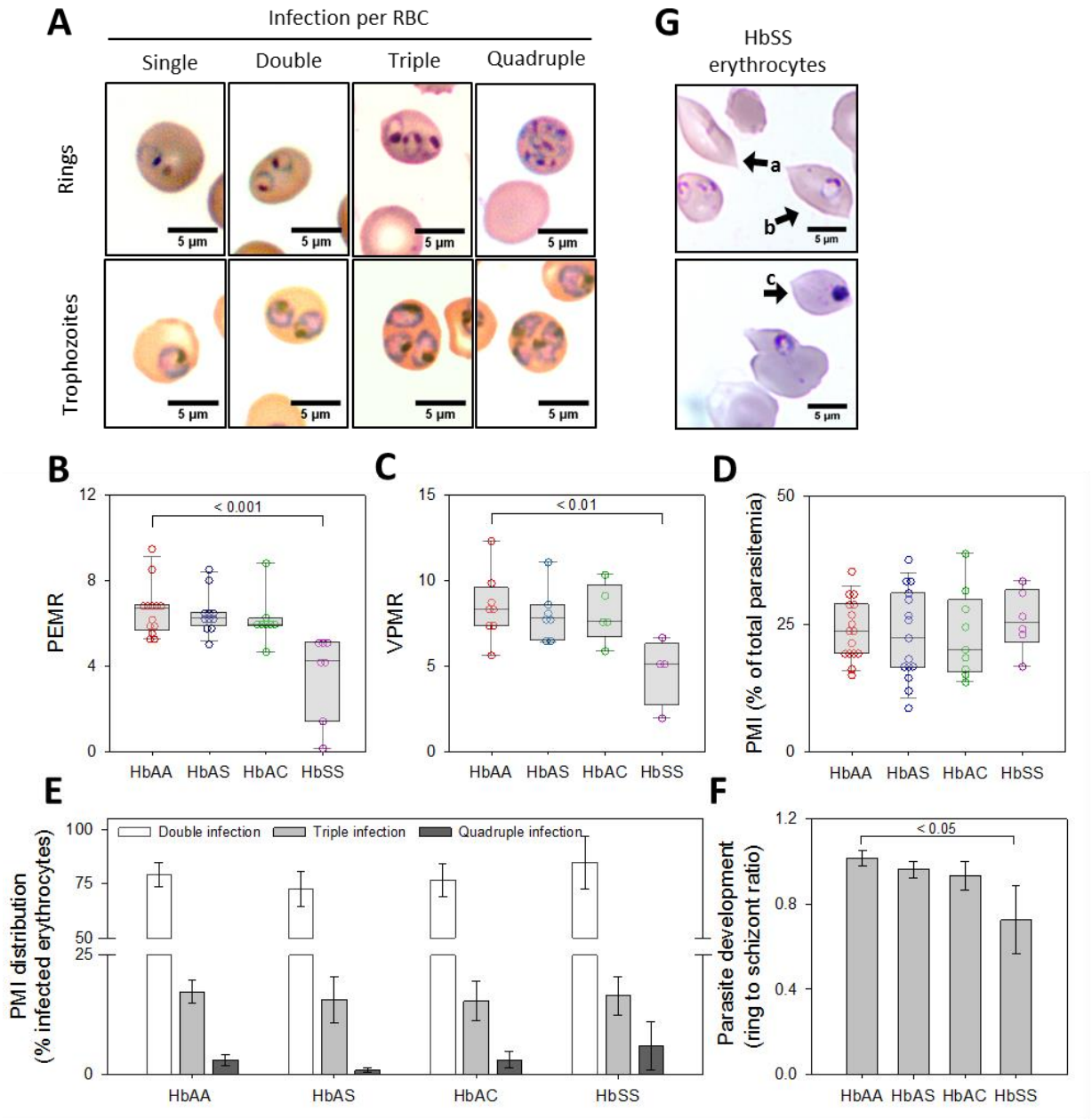

Figure 11 | Characterization of *Plasmodium falciparum* FCR3^{HDMEC} growing in hemoglobinopathic erythrocytes. (A) Representative light microscopy images of intraerythrocytic *P. falciparum* infection containing ≤ 1 parasite per cell during the ring and trophozoite stage. Box plot showing the (B) parasitized erythrocyte multiplication rate (PEMR), (C) viable parasite multiplication rate (VPMR) and (D) the percentage of parasite multiple infectivity (PMI). Bar chart showing (E) the parasite multiple infectivity distribution and (G) the parasite development for infected HbAA, HbAS, HbAC and HbSS erythrocytes. The means ± SEM are shown for at least three independent biological replicates. Significant differences are indicated; One-way ANOVA. (G) Representative light microscopy images of uninfected sickle erythrocytes (HbSS) (arrow; a), *P. falciparum*-infected (arrow; b) and arrested parasite growth in HbSS erythrocytes (arrow; c), scale bar 5 µm.

3.2. Characterization of infected hemoglobinopathic erythrocytes adherence to HDMEC

3.2.1. Adherence of FCR3^{HDMEC} *P. falciparum*-infected hemoglobinopathic erythrocytes under static conditions

The study of cell adhesion includes the process of cell attachment and cell detachment. It can be performed at a population or at single cell level. Adhesion studies at a cell population level can be further investigated via static or flow adhesion through the wash assay technique and flow chamber technique, respectively [246]. The attachment studies focus on the mechanism of adhesion to a specific substratum, while detachment studies give emphasis to the response of adherent cells to an applied force. The attachment capabilities of FCR3^{HDMEC} infected erythrocytes was studied at a population level under static and flow conditions. The ability of infected hemoglobinopathic erythrocytes to adhere to microvascular endothelial cells was initially assessed under static conditions. The results obtained showed a marked reduction in the number of infected HbAS and HbAC erythrocytes adhering to HDMEC as compared to HbAA-iRBCs at the same developmental stage (Figure 12A/B). Cytoadhesion of infected HbAS and HbAC erythrocytes to HDMEC was reduced by ~61% and ~82%, respectively. As expected, uninfected erythrocytes, evaluated in parallel, did not adhere to the endothelial monolayer (Figure 12A, upper panel).

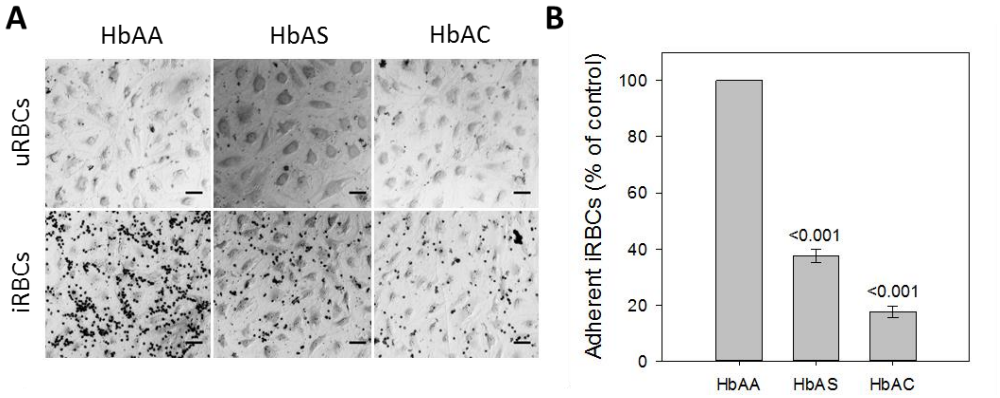

Figure 12 | Comparative adherence of infected HbAA, HbAC and HbAS erythrocytes to HDMEC under static conditions. (A) DIC images of fixed samples showing the degree of static adherence of uninfeced (upper panel) and infected (lower panel) HbAA, HbAS and HbAC erythrocytes, scale bar 50 µm. (B) Percentage of binding for infected HbAA, HbAS and HbAC erythrocytes to confluent HDMEC under static conditions. Data was normalized to the HbAA binding control group run in parallel. The means ± SEM are shown for at least three independent biological replicates and blood from at least two different donors. Significant differences are indicated, One-way ANOVA.

3.2.2. Adherence of FCR3^{HDMEC} *P. falciparum*-infected hemoglobinopathic erythrocytes under physiological flow conditions

The flow chamber permitted to evaluate the range of wall shear stresses at which the infected erythrocytes capture events occurred. *P. falciparum*-iRBCs cytoadhere *in vivo* under low flow conditions within a range of shears forces encountered in post-capillary venules and sinusoids. The effect of these shear forces on infected erythrocytes cytoadherence was studied in flow chamber experiments. iRBCs were flushed on confluent endothelial cells at different wall shear stresses ranging from 0.03 Pa to 0.3 Pa, which are physiological relevant values [231]. The results showed that iRBCs adhere to HDMEC in a shear dependent manner (Figure 14B). This means that the number of adherent cells decreased as the wall shear stress increased, 0.03 Pa being the most favorable shear stress for iRBCs adhesion to HDMEC. Consistent with our previous observations, fewer infected hemoglobinopathic erythrocytes adhered to the endothelial monolayer, compared to HbAA-iRBCs, at all shear stresses evaluated (Figure 13A/B). Considering binding at all shear stresses the binding was reduced by approximately 36.7 ± 14%, 62.2 ± 6% and 64.2 ± 1% for HbAS, HbAC and HbSS-iRBCs, respectively ($p < 0.001$, One-way ANOVA). As expected, uninfected erythrocytes evaluated in parallel did not adhere to the endothelium (Figure 13A, upper panel).

To estimate the binding strength of infected erythrocytes that adhered under flow conditions, detachment assays were performed. For this, infected erythrocytes were allowed to adhere to HDEMCs under flow conditions at a wall shear stress of 0.05 Pa. Remaining adherent cells were then exposed to gradually increased wall shear stress steps up to 4 Pa. The number of cells remaining adherent were quantified and displayed as function of the wall shear stress (Figure 14A). Overall, only a small fraction of the initially bound population detached after applying low wall shear stresses and the rest of the population remained adherent. After applying shear stresses above 0.7 Pa higher number of infected erythrocytes started to detach. A fraction of the iRBCs remained adherent even after applying a wall shear stress of 4 Pa. These results indicate that infected erythrocytes adhering under low flow conditions were able to resist higher shear forces before detaching. By fitting an exponential decay function to the number of infected erythrocytes remaining adherent as a function of the wall shear stress, the τ_{50} values were calculated. τ_{50} is

defined as the shear stress at which 50% of the initially bound cells detach and indicates the overall population binding strength [246]. When compared to a τ_{50} of 2.0 ± 0.4 for infected HbAA erythrocytes, similar τ_{50} values were observed for infected hemoglobinopathic erythrocytes, were infected HbAS, HbAC and HbSS τ_{50} values were estimated to be 1.7 ± 0.4, 1.5 ± 0.3 and 2.7 ± 1.6, respectively (*p = 0.532*, One-way ANOVA).

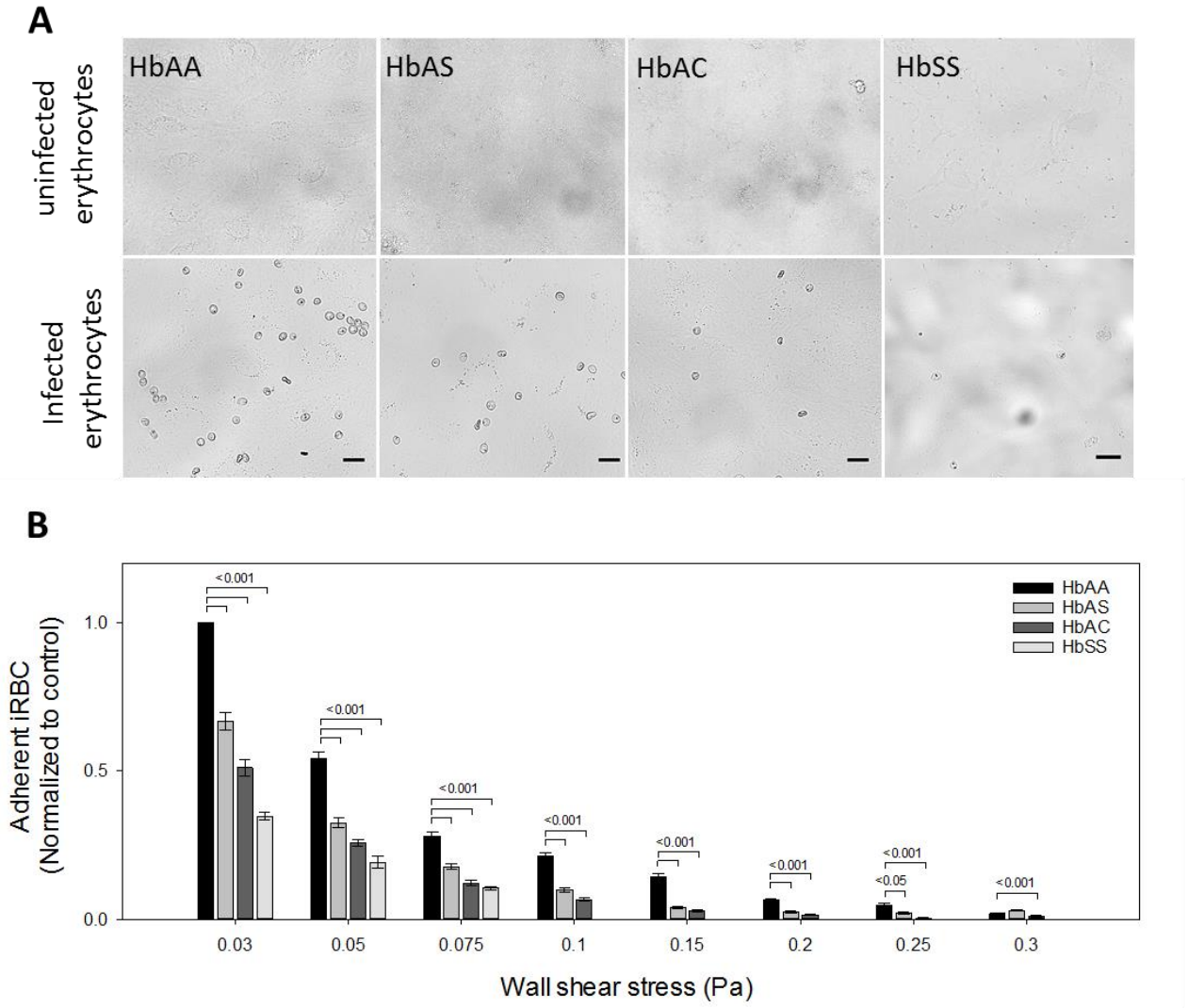

Figure 13 | Adherence of *P. falciparum*-infected erythrocytes under low physiological flow conditions. (A) Phase contrast images showing the degree of adherence for infected HbAA, HbAS and HbAC erythrocytes (lower panel) and control uninfected erythrocytes (upper panel), 0.05 Pa, scale bar 20 µm. (B) Percentage of adherent infected erythrocytes to confluent HDMEC under flow conditions ranging from 0.03 and 0.3 Pa. Data was normalized to the infected HbAA erythrocytes binding control group run in parallel. The means ± SEM are shown for at least three independent biological replicates and blood from at least two different donors. HbSS was evaluated only at 0.03 to 0.075 Pa and blood from only one donor. Statistical significance is indicated (One-way ANOVA).

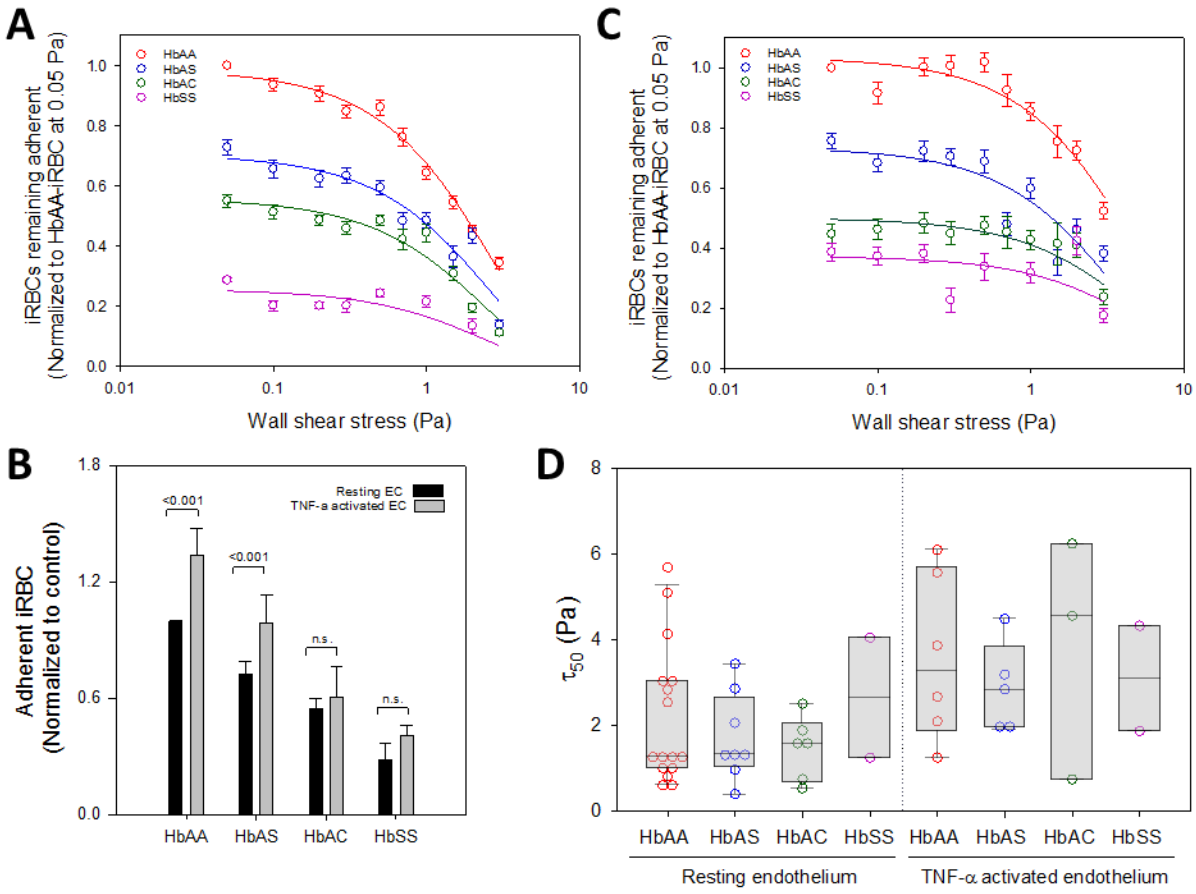

Figure 14 | Detachment assay for *P. falciparum*-infected erythrocytes bound under physiological flow conditions. (A) A total of $5x10^6$ infected erythrocytes were flushed over a confluent resting HDMEC at 0.05 Pa. The total number of adherent cells was quantified after washing unbound cells with the same shear stress. Wall shear stress was gradually increased up to 4 Pa. The number of cell remaining adherent after each shear stress applied was quantified and plotted as function of the wall shear stress. Mean ± SEM are shown for at least 3 independent replicates. (B) Adherent infected erythrocytes on resting and TNF-α activated HDMEC at 0.5 Pa. Mean ± SEM are shown for at least 3 biological replicates. Significant difference is shown (One-way ANOVA). (C) Remaining adherent iRBCs on TNF-α activated HDMEC. (D) Box plot showing the t_{50} obtained for infected hemoglobinopathic erythrocytes bound on resting and TNF-α activated HDMEC. The median, 25% and 75% quartile ranges and error bars are shown. No significant difference between groups was found (One-way ANOVA). For HbSS data from only two experimental replicates and one blood donor is shown.

During infection with *P. falciparum* the plasma levels of TNF-α increase [27][185]. Consequently, the surface expression of endothelial cells receptors, such as ICAM-1, also increases. This event may have a positive effect on parasitized erythrocyte sequestration [184]. To assess the effect of endothelial activation by TNF-α on

infected erythrocytes sequestration, flow chamber assays were performed using TNF-α activated HDMEC as a substratum. HDMEC activation with TNF-α provoked an increased binding of infected erythrocytes. For instance, at 0.05 Pa, the number of iRBC binding to HDMEC increase by ~34%, ~26%, ~6% and ~12% for infected HbAA, HbAS, HbAC and HbSS erythrocytes, respectively (Figure 14B). Interestingly, stimulation of endothelial cells with TNF-α not only provoked an increased number of infected erythrocytes binding, but also caused a slight increase in the τ_{50} values for all groups (Figure 14C). The τ_{50} values for infected HbAA, HbAS, HbAC and HbSS were 3.5 ± 1.9, 2.8 ± 1.0, 3.8 ± 2.8 and 3.1 ± 1.7, respectively. Nevertheless, no significant differences were found when comparing the τ_{50} values obtained for TNF-α activated endothelium and the τ_{50} values obtained for resting endothelium (*p = 0.166,* One-way ANOVA) (Figure 14D). Also, no significant differences were found between the τ_{50} values obtained for infected HbAA, HbAS, HbAC and HbSS erythrocytes binding to TNF-α activated endothelium (*p = 0.875,* One-way ANOVA).

Overall, the number of adherent cells was the major difference found between groups in both, resting and TNF-α activated endothelium. Nevertheless, the infected hemoglobinopathic erythrocytes capable of adhering under flow conditions adhered with comparable binding strengths to infected HbAA erythrocytes. This suggests the presence of a subpopulation of infected erythrocytes with similar binding capabilities as the HbAA group, identified as “strong binders”. The percentage of infected cells which did not adhere under flow conditions represents the subpopulation of weak binding infected erythrocytes. These weak binders showed a deficient firm adherence, probably as result of improper dynamic interaction on the endothelium.

3.2.3. Quantification of FCR3^{HDMEC} *P. falciparum*-infected erythrocytes cytoadhesive behavior on resting HDMEC

The adhesion behavior of *P. falciparum*-infected erythrocytes under flow conditions resembles the cytoadherence of leukocytes, where the cells tether, roll and firmly adhere to the endothelium [124]. To study in quantitate terms the iRBCs dynamic adhesive behavior, the presence of the intracellular parasite, labeled with a nuclear staining dye, was used. SYBR green was selected among other dyes for its low anti-plasmodial activity [247]. This feature makes SYBR green an optimal dye for tracking parasites with minimal or no interference with their viability [247]. Staining with SYBR

green showed low signal to noise ratio (Figure 15A) and had no effect on cytoadherence to HDEMC at 0.05 and 0.1 Pa (Figure 15B), as observed when labeled infected erythrocytes were compared to non-labeled ones (0.05 Pa, $p = 0.372$ and 0.1 Pa $p = 0.897$, Student´s t-test). Fluorescent labeling allowed for the tracking of infected erythrocytes in an automated manner and extracting relevant information from the erythrocytes motion, derived from the fluorescence signal.

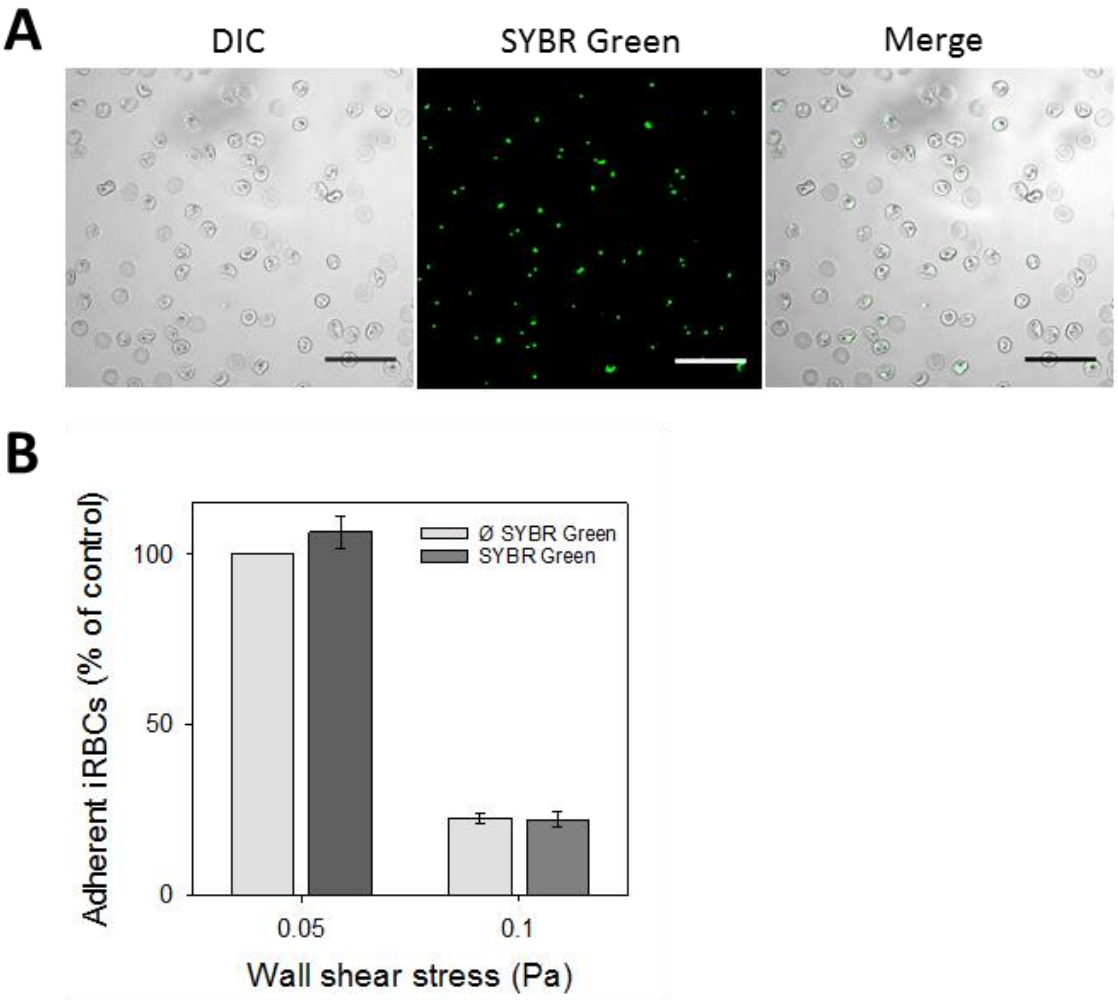

Figure 15 | Effect of SYBR Green staining on cytoadherence of FCR3^{HDMEC} to microvascular endothelial cells. (A) Representative phase contrast image of parasite nuclear staining after 1 h incubation with SYBR Green; scale bar 50 µm. (B) Absolute number of iRBCs adhering under flow conditions on confluent HDMEC after nuclear labeling with SYBR Green. Unlabeled iRBC were used as control for binding. Mean ± SEM are shown (*n = 3*). No significant difference was found between groups (Student´s t-test).

Fluorescent labeled infected erythrocytes were then assessed at different shear stresses using flow chambers (Figure 16A). By knowing the flow chambers dimensions and the medium viscosity, which was measured to be 0.7 mPa·s, the flow rate was calculated for each wall shear stress (Table 1, see section 2.2.4.2.). A precise syringe pump permitted the generation of specific flow rates to achieve a desired wall shear stress. A total of $5x10^6$ infected erythrocytes superseded in 5 ml of medium were allowed to flow over the endothelial monolayer seeded in the flow chamber. This concentration of cells permitted to record binding interaction with minimal interferences from other cells, simplifying the tracking process.

Inside the erythrocyte, the parasite is located at the periphery [20]. While the cell rotates by interacting with the endothelium and shear forces acting on its back, the fluorescence signal recorded results in a fluorescence amplitude (Figure 16B). As the focus is positioned on top of the endothelial monolayer, the maximum values recorded in the fluorescence amplitude correspond to the parasite in close proximity to the endothelium. Conversely, when the parasite finds itself away from the monolayer, the fluorescence intensity decreases to the lowest values recorded. By tracking the parasite nucleus, the iRBC translational velocity could also be obtained. Both, the fluorescence intensity and translational velocity profiles were used to describe and quantify the *P. falciparum*-infected erythrocytes motion behavior. In detail, from the fluorescence intensity and translational velocity profiles, four parameters were obtained: the mean translational velocity, the amplitude difference, the contact time towards the endothelium and the Pearson correlation coefficient between the fluorescence amplitude and the velocity profile.

Initially, the interaction between trophozoite-iRBCs and HDMEC was evaluated at low physiological flow conditions, using shear forces that ranged from 0.03 to 0.2 Pa. Four different interactions between trophozoite-iRBCs and endothelial cells were observed: firm adhesion, dynamic adhesion, dynamic adhesion followed by firm adhesion and non-adhering cells (Figure 17). A non-adhering cell showed low intensity values, since it was not in close proximity to the membrane, and high mean velocities (Figure 17A). An adherent cell was observed as the fluorescence intensity remained constant over the time, as well its mean velocity, which remained close to zero (Figure 17B). A dynamically adherent cell showed regular oscillation in the

florescence intensity profile as consequence of the out-off center intracellular parasite location. This feature caused the parasite position towards the focal plane on the endothelium to change while the infected erythrocyte moved along the endothelial monolayer. At the same time, a low, but oscillatory velocity profile, which was anti-correlative to the fluorescence amplitude, was observed (Figure 17C). The periodic oscillation in the velocity profile observed for dynamic adhesion resembled a flipping motion rather than a rolling motion. Some infected erythrocytes that dynamically adhered to the endothelium were capable of adhering firmly and remained adherent over the recording time, as seen in figure 17D.

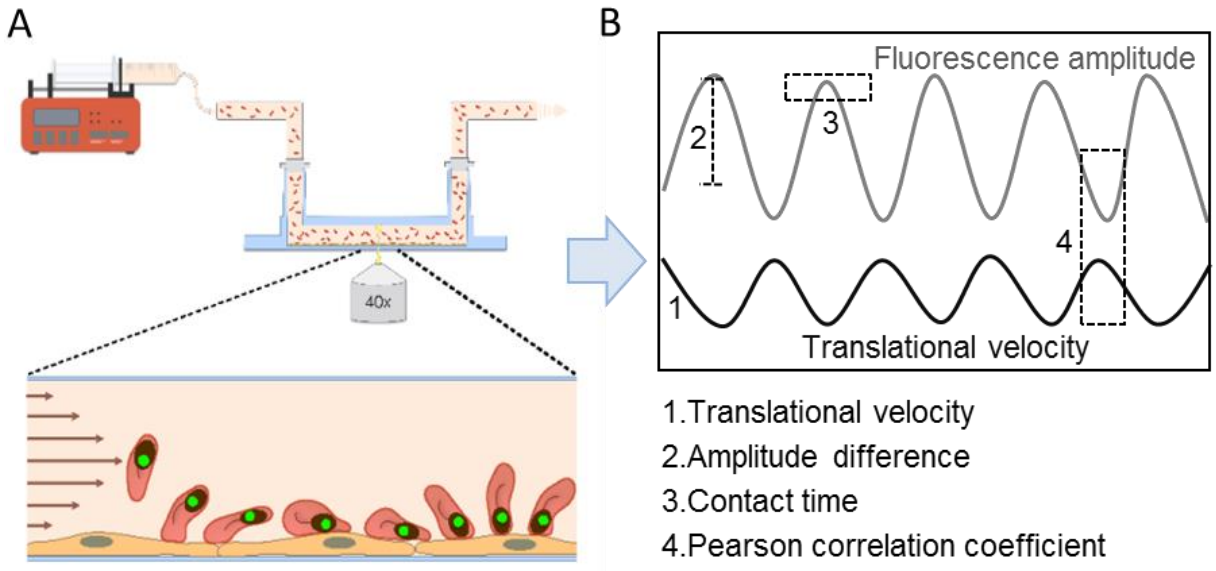

Figure 16 | Schematic of flow chamber experimental setup. (A) Using a precise syringe pump the infected erythrocytes were loaded at a desire wall shear stress into the flow chamber containing confluent endothelial cells. After positioning the focal plane above the endothelium, fluorescence from the labeled parasite nucleus was imaged and fast videos were recorded (300 frames / 9.9 sec). (B) During post-video analysis, the parasite nucleus of a single cell was tracked, and the correspondent fluorescence intensity amplitude and translational velocity were extracted. Using this information mean translational velocity, amplitude difference, contact time and Pearson correlation coefficient were calculated and used as measure for characterization of the infected erythrocyte cytoadhesive behavior. Courtesy of Dr. Britta Nyboer.

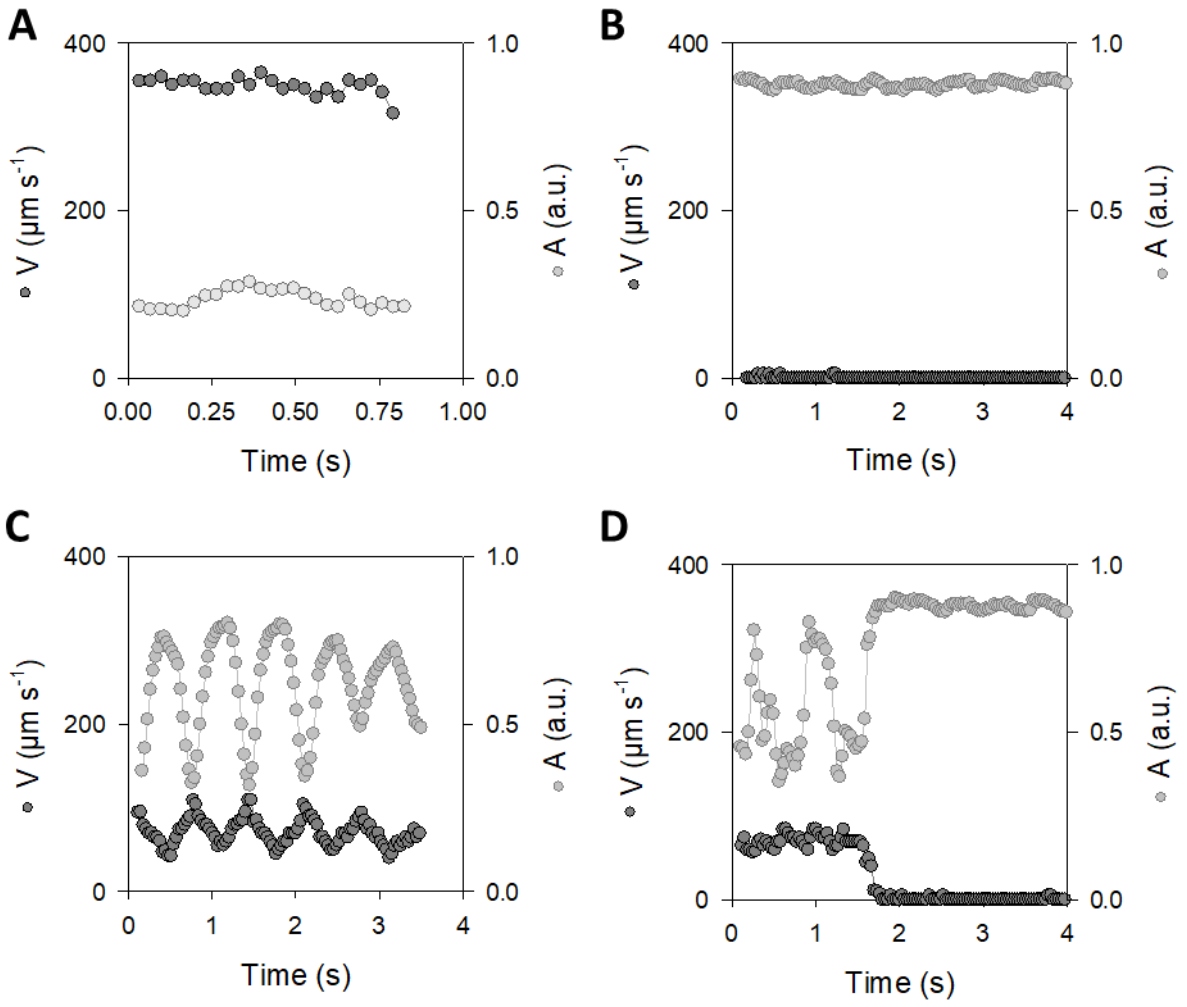

Figure 17 | Differential motion behavior of *P. falciparum*-infected erythrocytes under physiological flow conditions. Representative fluorescence amplitude and velocity profiles extracted from a (A) non-interacting, (B) firmly adhered, (C) dynamic adherent and (D) dynamic followed by firmly adhered infected erythrocytes flowing on confluent HDMEC at a wall shear stress of 0.03 Pa. a.u., arbitrary units.

3.2.4. Differential motion behavior for *P. falciparum*-infected erythrocytes at trophozoite and schizont stage on resting HDMEC

The erythrocyte shape [20], adhesiveness [248] and rigidity [249] highly influence the iRBC cytoadhesion behavior. Since these three parameters vary from early to late stages of the intraerythrocytic cycle, infected erythrocytes at the trophozoite and schizont stage were compared. After infected erythrocytes at the trophozoite stage (26 ± 6 hpi) adhered to HDMEC (Figure 18A, snapshot I) the hydrodynamic forces exerted on the iRBC back provoke the iRBC to peel off the endothelium (snapshot II). This reduction in the initial iRBC-HDMEC contact (snapshot III) provoked the flipping

of the cell over its other side (snapshot VI-V). In Figure 18C, representative fluorescence and velocity trajectories are showed for a trophozoite-iRBC. As described previously, the trophozoite trajectory revealed large fluorescence amplitude differences as well as periodical oscillations of the velocity profile, suggesting a flipping rather than a rolling motion. Furthermore, the velocity profile negatively correlated with the fluorescence amplitude (Figure 18C, indicated by the red circles).

On the other hand, the known increase in sphericity and rigidity at the schizont stage (36 ± 6 hpi) provoked infected erythrocytes to roll rather than flip. The cell movement along the endothelium was smooth and did not show large cell displacements (Figure 18B). Representative fluorescence and velocity trajectories are shown for an infected erythrocyte at the schizont stage (Figure 18D). For this trajectory, smaller amplitude differences and almost no oscillation in the velocity profile were observed. Furthermore, fluorescence and velocity amplitudes did not correlate. It was also noticed that the parasite was larger in the schizont stage than in the trophozoite stage, and that the parasite location changed from off-center to the middle of the erythrocyte.

The correlation between fluorescence amplitude and velocity profiles was estimated by the Pearson correlation coefficient. Values close to -1 indicated negative correlation or anti-correlation while the values close to zero indicated no correlation. For the representative trophozoite trajectory (Figure 18C) the Pearson correlation coefficient was -0.690, indicating a strong anti-correlation and therefore a flipping behavior. On the contrary, for the schizont trajectory (Figure 18D) the Pearson correlation coefficient was calculated to be -0.0151, indicating no correlation between fluorescence amplitude and velocity profiles, and therefore suggesting a rolling behavior. In this way, Pearson correlation coefficient was then used as a key parameter for characterization and quantification of *P. falciparum*-infected erythrocytes cytoadhesive behavior.

In Figure 19, flipping and rolling motion are shown as a series of phase contrast images over time. For the infected erythrocytes at the trophozoite stage, the erythrocyte discoid shape is visible as well as the intracellular parasite which

occupies approximately half of the erythrocyte space. The hemozoin crystals inside the food vacuole are visible as well (black dot). From these series of snap shots, the flipping, as described previously, can be appreciated. By following the hemozoin, the complete rotational cycles can also be observed. In these trajectories, the trophozoite completed three rotational cycles with variable durations. Furthermore, for trophozoites, it was noticeable that cells were sliding (large displacement without the cell rotating), this event is highlighted by the black square. On the other hand, a schizont infected cell showed a very homogeneous movement completing the rotational cycles with the same time duration. The almost spherical shape of the schizont infected erythrocyte could be noticed, which remained almost unchanged over the whole imaging recording.

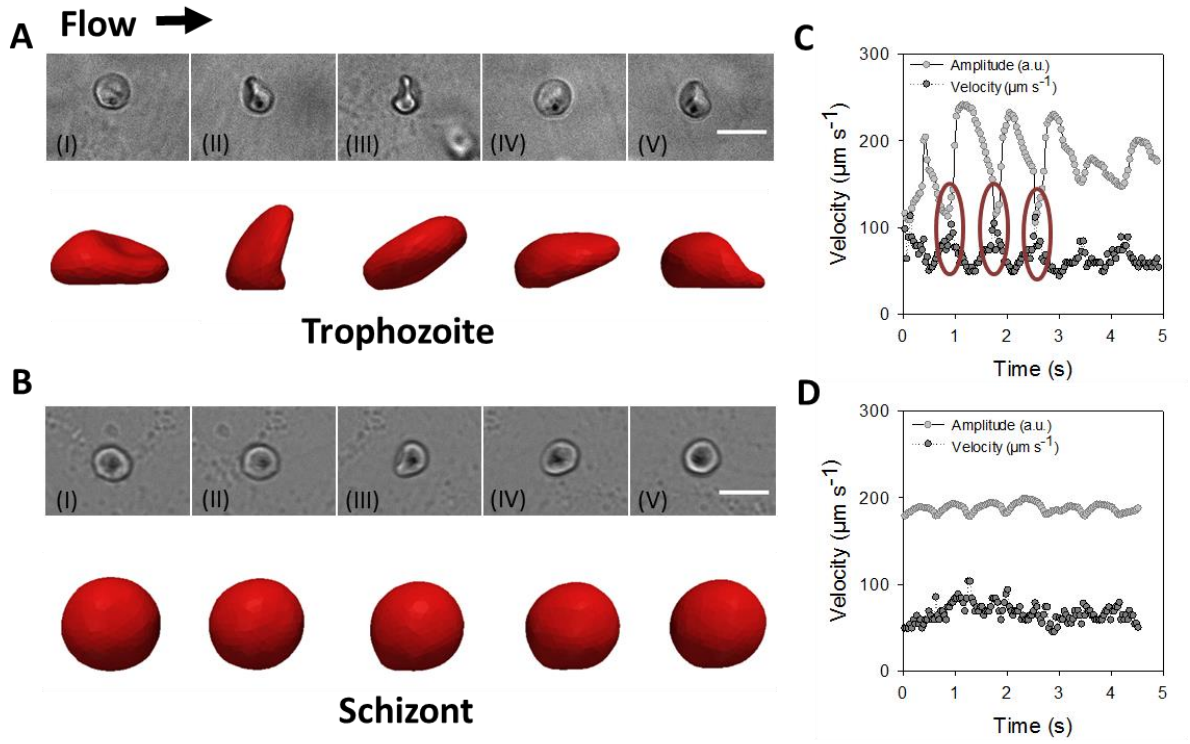

Figure 18 | Effect of the parasite developmental stage on the dynamic adhesion behavior. Snapshots obtained from experimental data (top view, phase contrast image) and computer simulations (side view, courtesy of Dr. Anil Dassana) illustrating an infected erythrocyte (A) flipping (trophozoite-stage) and (B) rolling (schizont-stage) over confluent HDMEC. Arrow indicates the direction of the flow; wall shear stress applied 0.05 Pa; scale bar 10 µm. The parasite can be identified in the phase contrast images by the hemozoin crystal, which is localized inside the parasites digestive vacuole. (C,D) Representative fluorescence and velocity amplitude profiles for infected erythrocytes at different developmental stage: (C) trophozoite stage (26 ± 6 hpi) and (D) schizont stage (36 ± 6 hpi). Red circles indicate the anti-correlation between fluorescence and velocity amplitudes. Wall shear stress applied 0.03 Pa. a.u., arbitrary units

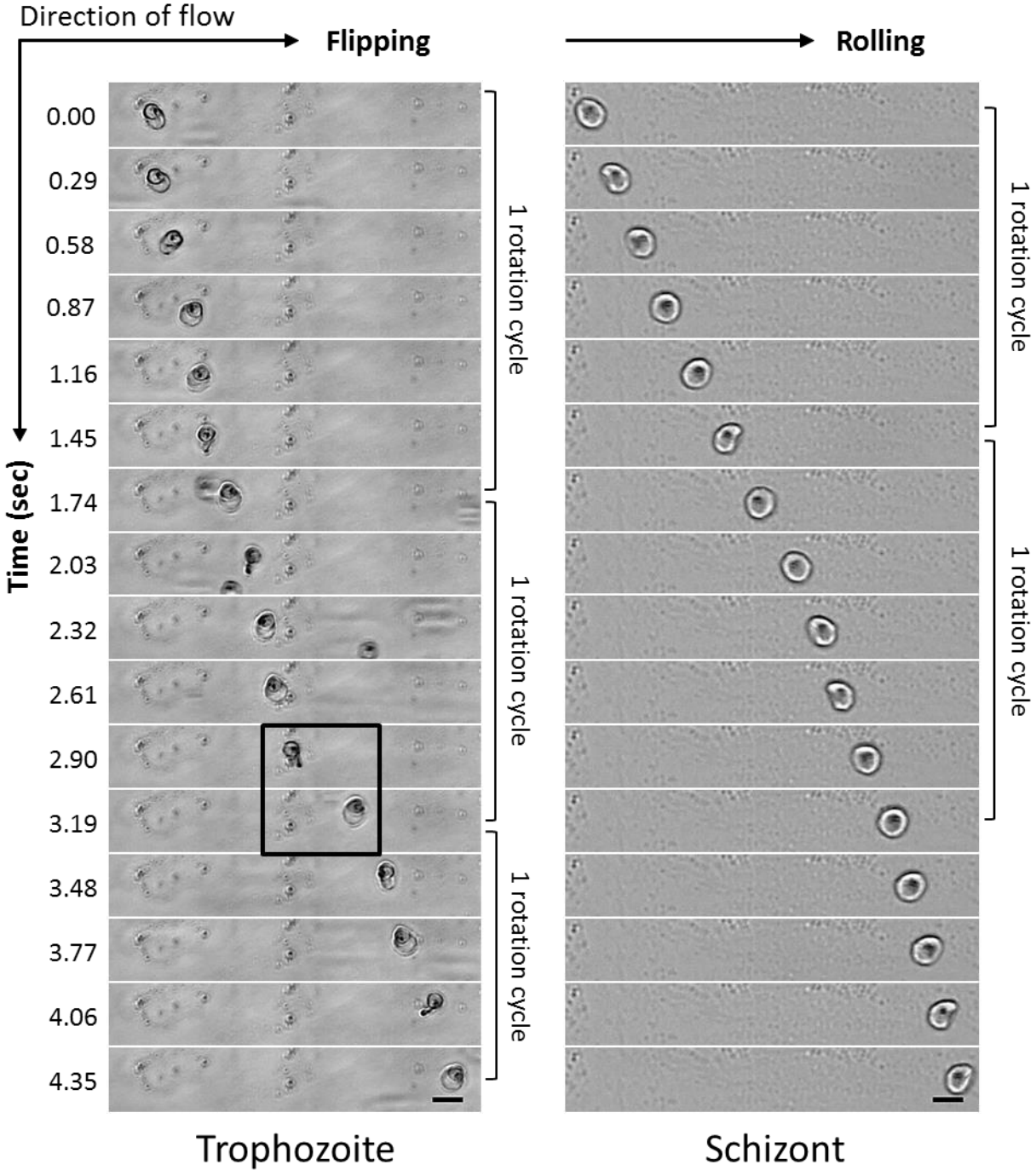

Figure 19 | Dynamic adhesion behavior observed for *P. falciparum*-infected erythrocytes at different developmental stages. Snapshots obtained from phase contrast videos recorded under low physiological flow conditions for trophozoite (26 ± 6 hpi) and schizont (36 ± 6 hpi). X-direction arrow indicates the direction of the flow; y-direction arrow indicates the time; black square indicates a sliding process; complete rotational cycles are shown by brackets; scale bar 10 µm.

3.2.5. Differential adhesion behavior for infected hemoglobinopathic erythrocytes on HDMEC

After characterization of trophozoite and schizont-iRBCs dynamic adhesion, HbAA and HbAS-iRBCs were compared. In the flow chamber assays, the percentage of non-adhering cells recorded was very high (Figure 20A/B). For instance, at 0.03 Pa approximately ~55% of all tracked cells did not adhere to the endothelium. The percentage of non-adhering cells rapidly increased by higher shear forces, reaching almost 100% at 0.2 Pa for both infected HbAA and HbAS erythrocytes. On the other hand, the number of dynamic adhesion events (includes flipping and rolling events) decreased as the wall shear stress increased. No more dynamic adhesion events were recorded above 0.1 Pa (figure 20A/B). From the dynamic adhesion events recorded for HbAA-iRBCs at the different shear stresses, approximately a third of them, cytoadhered in the field of view (31 ± 3%). Non-cytoadherence could reflect some heterogeneity on the binding capabilities of the FCR3 population, endothelial monolayer heterogeneity, or that the adherence happened out of the field of view.

The percentage of dynamic adhesion events for infected HbAS erythrocytes was comparable to the infected HbAA erythrocytes control group at all evaluated shear stresses (Figure 20C) (at 0.03 Pa $p = 0.326$, at 0.05 Pa $p = 0.528$, at 0.075 Pa $p = 0.403$, at 0.10 Pa $p = 0.825$, at 0.15 Pa $p = 1.0$ and at 0.20 Pa $p = 1.0$, t-test). Importantly, out of the total number of dynamically adhering cells, the percentage of cells that remained firmly adherent was significantly lower for HbAS-iRBCs as compared to HbAA-iRBCs ($p < 0.001$, exponential decay fit, F-test). Only ~19 ± 3% of the recorded HbAS-iRBCs firmly adhered in the field of view at different shear stresses (Figure 20D). It could be noticed that after 0.1 Pa, no dynamic adhesion events were recorded, but few infected erythrocytes adhered abruptly in the field of view after tethering.

For further quantification, only infected erythrocytes trajectories recorded at 0.03 and 0.05 Pa were processed, since the number of dynamic adhesion events was statistically sufficient only at those shear stresses.

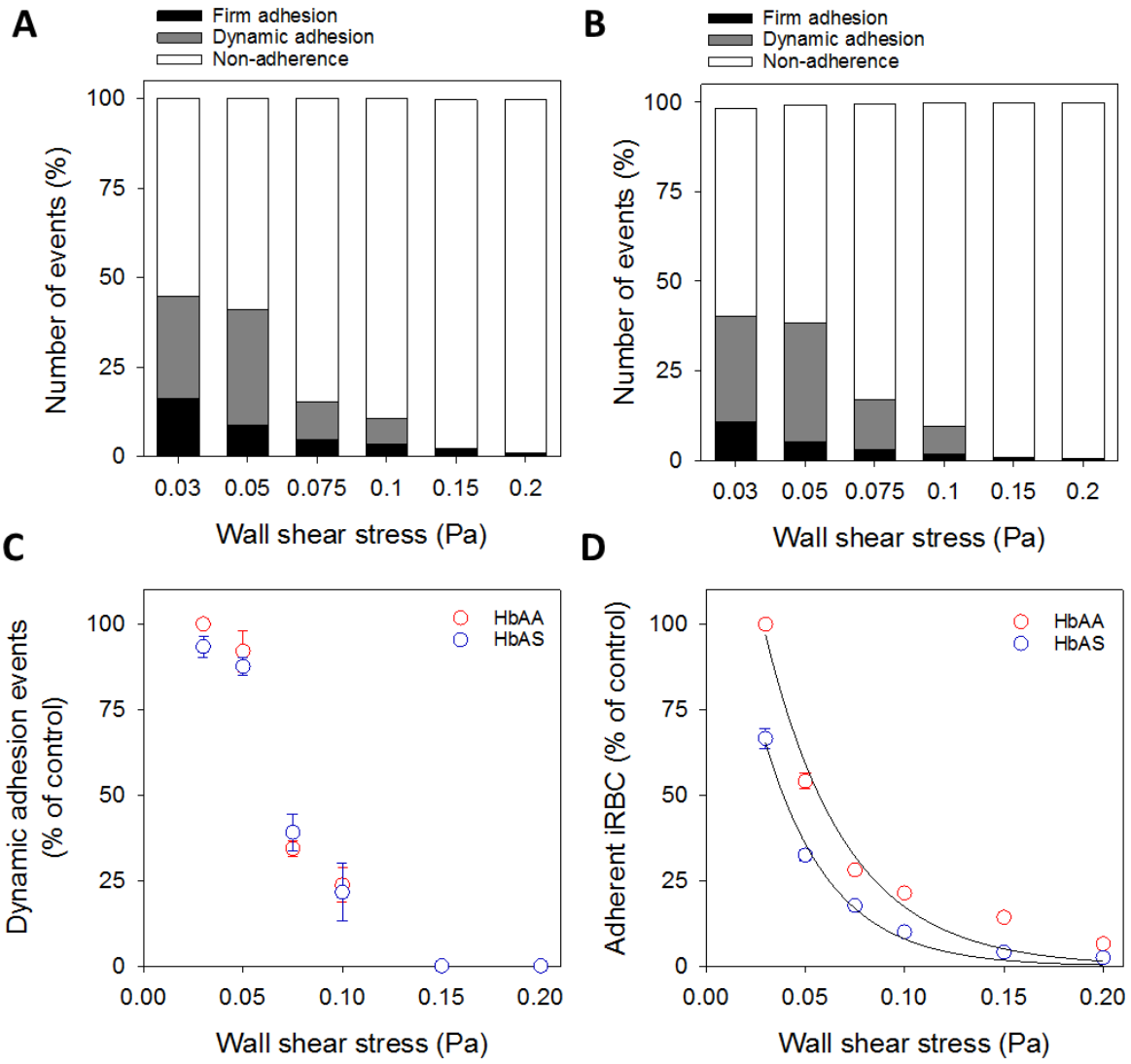

Figure 20 | Quantification of *P. falciparum*-infected erythrocytes dynamic and firm adhesion to HDMEC under low physiological flow conditions. Stacked bar charts representing relative proportions of various categories of motion behaviors observed for infected (A) HbAA and (B) HbAS erythrocytes flowing on confluent HDMEC at physiological shear stresses ranging from 0.03 to 0.2 Pa. (C) Percentage of dynamic adhesion events (*n.s.,* Student´s t-test) and (D) flow firm adherence ($p < 0.001$, F-test) of parasitized erythrocytes containing either HbAA (open circles) or HbAS (closed circles) to HDMEC. Values are expressed relative to the HbAA-iRBCs control group binding at a wall shear stress of 0.03 Pa. The mean ± SEM. are shown for at least four independent replicates.

Representative trajectories of infected HbAA and HbAS erythrocytes revealed also differences on the dynamic adhesion behavior for both groups, at trophozoite and schizont stage (Figure 21). For HbAS-infected erythrocytes at the trophozoite stage, the fluorescence amplitude and velocity profile showed the same evident anti-correlation as for HbAA-iRBCs trophozoites, but with larger fluorescence amplitude

difference. Additionally, the velocity shortly reached high values (showed by the arrows) which could indicate some degree of detachment of the iRBC from the substratum. At the schizont stage, infected HbAS erythrocytes also showed reduced amplitude differences and reduced velocities, however, it was not comparable with the schizont cells observed for the HbAA-iRBC group, which showed regular rolling.

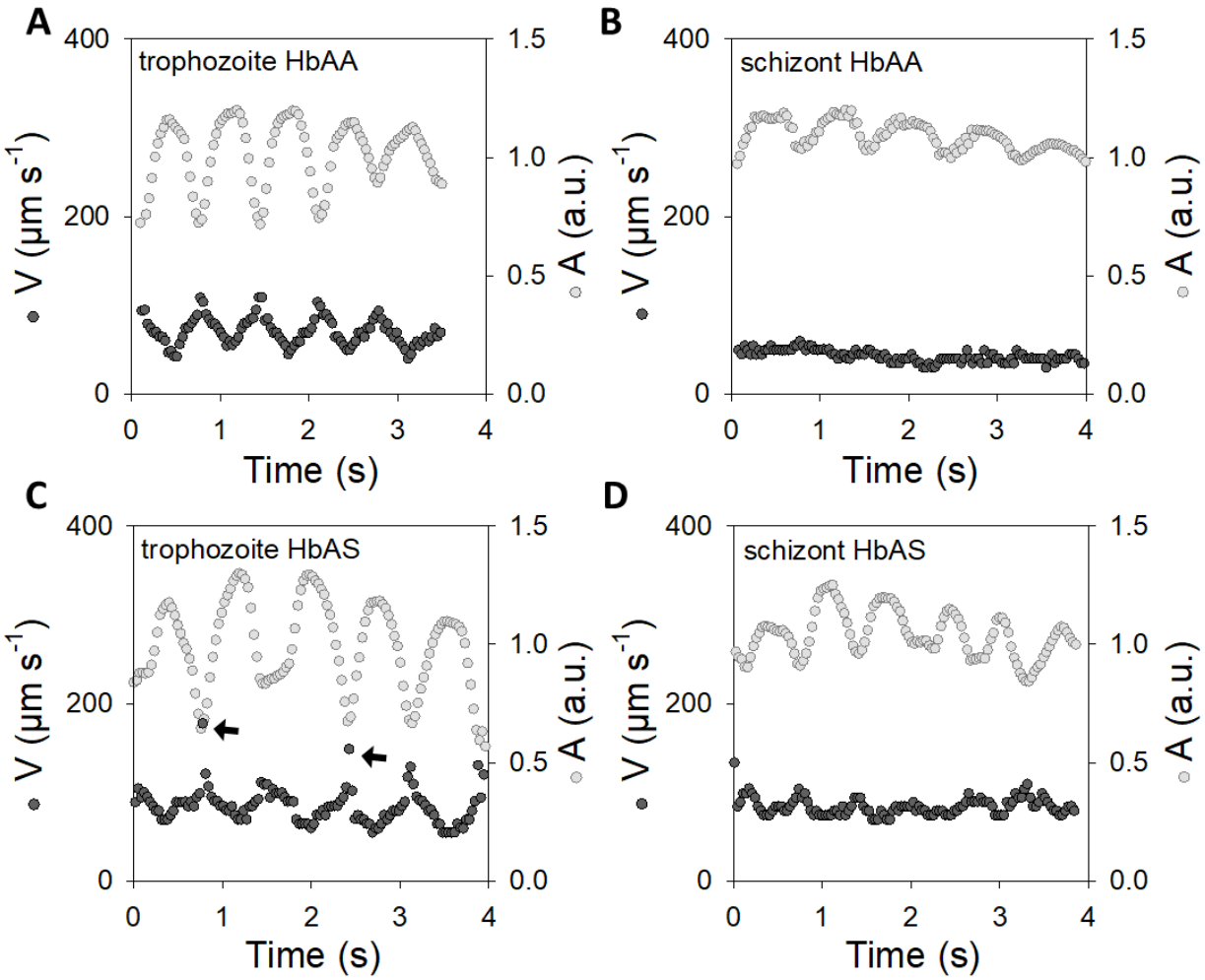

Figure 21 | Differential cytoadhesive behavior of *P. falciparum*-infected erythrocytes under low physiological flow conditions. Representative fluorescence and velocity amplitude profiles observed for infected HbAA and HbAS erythrocytes at different developmental stages flowing on confluent HDMEC at a wall shear stress of 0.03 Pa. (A) HbAA-IRBC (trophozoite), (B) HbAA-IRBC (schizont), (C) HbAS-IRBC (trophozoite) and (D) HbAS-IRBC (schizont). Arrows indicate jumps in the velocity values. a.u., arbitrary units.

From at least 27 trajectories and four independent biological replicates, infected HbAA and HbAS erythrocytes at the trophozoite stage (26 ± 6 hpi) and at the

schizont stage (36 ± 6 hpi) were compared for their motion behavior (Figure 22 and 23). Quantification of the iRBC cytoadhesive behavior was done for trajectories obtained at 0.03 and 0.05 Pa. At these wall shear stresses most of the rolling and flipping trajectories were observed and recorded. At 0.03 Pa (Figure 22), the resulted comparison showed that infected HbAS erythrocytes flipped and rolled at significantly higher velocities when compared to HbAA-iRBCs (trophozoites, $p < 0.001$ and schizonts $p < 0.001$, One-way ANOVA). When HbAA-iRBCs matured from trophozoites to schizonts, the velocity decreased significantly ($p < 0.001$, One-way ANOVA). This was not the case for HbAS-iRBCs, where the velocity between trophozoites and schizonts was shown to be comparable ($p = 0.145$, One-way ANOVA) (Figure 22A).

The amplitude difference decreased significantly from trophozoites to schizonts, for both HbAA- and HbAS-iRBCs (HbAA-iRBCs $p < 0.05$ and HbAS-iRBCs $p < 0.01$, One-way ANOVA) (Figure 22B). However, compared to HbAA-iRBCs, the amplitude differences observed for the HbAS-iRBCs trajectories were significantly larger at both developmental stages (trophozoite $p < 0.05$ and schizont $p < 0.001$, One-way ANOVA). The larger amplitude differences observed for infected HbAS cells suggested that the parasite nucleus, represented by the fluorescent signal, reached larger distances away from the substratum when compared to HbAA control group. This observation could indicate a transient detaching of the iRBC from the substratum during the flipping or rolling cycle.

Knowing that the maximum points on the fluorescence amplitude profile represent the parasite in closest proximity to the substratum, a threshold (-0.05 a.u.) was applied to maximum amplitude values. Since each data point corresponds to 0.033 sec, all data points above the applied threshold were summed up and the contact time was estimated (Figure 22C). The contact time increased significantly from trophozoite to the schizont stage for both infected HbAA and HbAS erythrocytes (HbAA $p < 0.05$; HbAS $p < 0.01$, One-way ANOVA). However, when compared to HbAA-iRBCs the contact time was significantly lower for HbAS-RBCs at both developmental stages (trophozoite $p < 0.01$ and schizont $p < 0.05$, One-way ANOVA).

Another parameter used for quantifying the cytoadhesive behavior was the Pearson correlation coefficient. This parameter is shown as function of the cumulative frequency (Figure 22D). The Pearson correlation coefficient values differed significantly for the groups at both developmental stages, as indicated by the F-test (between HbAA and HbAS at trophozoite stage $p < 0.001$; between HbAA and HbAS at schizonts stage $p < 0.001$). HbAS-infected erythrocytes trajectories were more anti-correlative with a median of -0.59 ± 0.03 compared to -0.44 ± 0.03 for HbAA-iRBCs. This indicated a more prominent flipping for HbAS-iRBCs at the trophozoite stage, as well as an inability of HbAS-schizont infected cells to reproduce the smooth rolling observed for infected HbAA erythrocytes at the same developmental stage.

At the higher wall shear stress of 0.05 Pa (Figure 23), similar behavior was observed for infected HbAS and HbAA cells. The mean translational velocities as well as the amplitude differences significantly increased for infected HbAS erythrocytes when compared to HbAA-iRBCs (velocity: trophozoites $p < 0.05$, schizonts $p < 0.001$; amplitude difference: trophozoites $p < 0.05$, schizonts $p < 0.05$, One-way ANOVA). The contact time was conversely significantly reduced for HbAS-iRBCs (significant for schizonts, $p < 0.001$). Moreover, a more pronounced anti-correlation was observed for HbAS-iRBCs, as indicated by the F-test (trophozoites $p < 0.001$, schizonts $p < 0.001$).

Overall higher velocities as well as slightly larger amplitude differences were reported for all groups when compared to 0.03 Pa. Higher shear forces may have induced the cells to shortly detach from the endothelial monolayer, therefore not only increasing the translational velocity but also the amplitude difference. This was reflected as well in the contact time which showed lower values compared to 0.03 Pa. All parameters together indicated clear differences between infected HbAA and HbAS erythrocytes motion behavior on resting endothelium at low shear stress conditions.

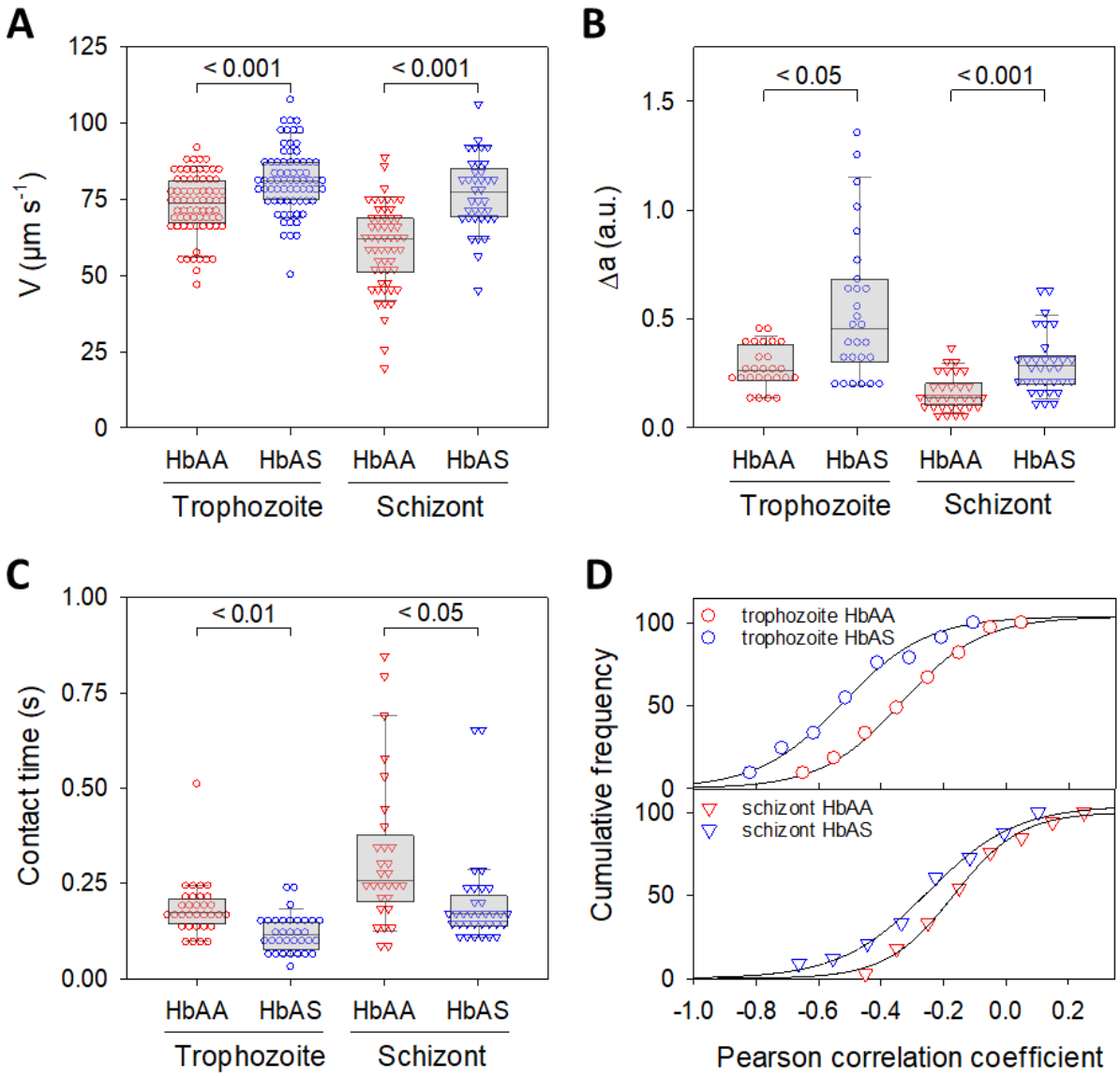

Figure 22 | Quantification of *P. falciparum*-infected erythrocytes cytoadhesive behavior at 0.03 Pa. Box plot showing (A) the mean translational velocity, (B) fluorescence amplitude difference and (C) contact time for infected HbAA and HbAS erythrocytes at different developmental stages (trophozoite and schizont) with an applied shear stress of 0.03 Pa. The median, 25% and 75% quartile ranges and error bars are shown from at least four independent experiments and 27 trajectories. Statistical significance is shown (One-way ANOVA). (D) Pearson correlation coefficient between fluorescence amplitude and velocity profile is expressed as function of the cumulative frequency for trophozoites ($p > 0.001$; F-test) and schizonts ($p > 0.001$; F-test); $n = 4$ (27 trajectories).

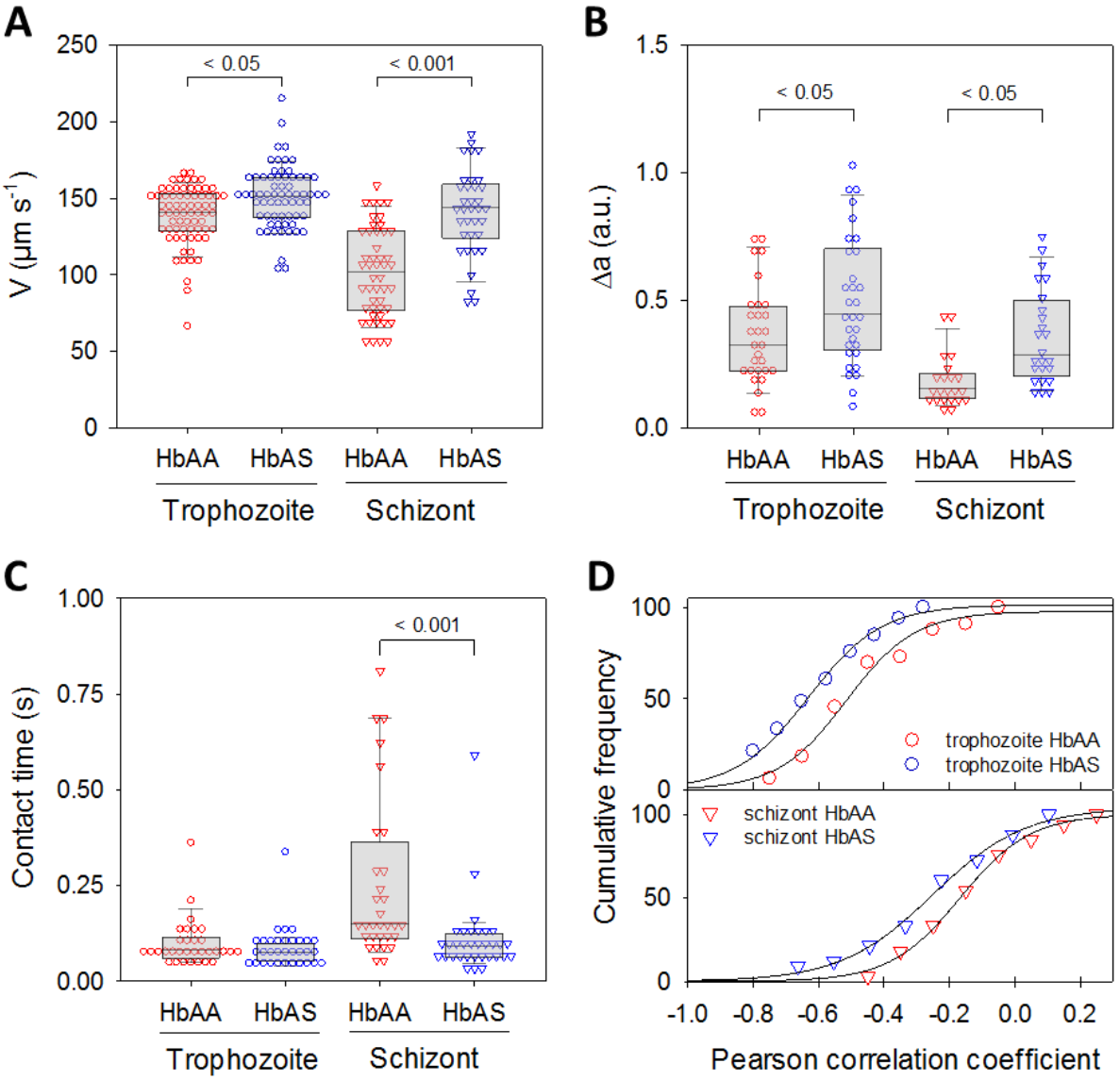

Figure 23 | Quantification of *P. falciparum*-infected erythrocytes cytoadhesive behavior at 0.05 Pa. Box plot showing (A) the mean translational velocity, (B) fluorescence amplitude difference and (C) contact time for infected HbAA and HbAS erythrocytes at different developmental stages (trophozoite and schizont) with an applied shear stress of 0.05 Pa. The median, 25% and 75% quartile ranges and error bars are shown from at least four independent experiments and 27 trajectories. Statistical significance is shown (One-way ANOVA). (D) Pearson correlation coefficient between fluorescence amplitude and velocity profile is expressed as function of the cumulative frequency for trophozoites ($p > 0.001$; F-test) and schizonts ($p > 0.001$; F-test); $n = 4$ (27 trajectories).

The effect of increased endothelial ligands on infected erythrocytes cytoadherence behavior was evaluated for infected erythrocytes at the trophozoite stage on HDMEC stimulated with TNF-α for 24 h (Figure 24). As expected, when compared to HbAA-iRBCs the mean translational velocity was significantly higher for HbAS-iRBCs ($p < 0.01$, t-test). Similarly, larger fluorescence amplitudes were observed for HbAS-iRBCs ($p < 0.05$, t-test). For HbAS-iRBCs, a lower mean contact time value was obtained, however, not statistically significant ($p = 0.084$, t-test). The Pearson correlation coefficient was shown again to be significantly lower for HbAS-iRBCs (more anti-correlative).

The red and blue lines in the graphs of Figure 24, correspond to the mean values of translational velocity, amplitude difference, contact time and Pearson correlation coefficient obtained for infected HbAA and HbAS erythrocytes flipping on resting endothelium, respectively. When compared to resting endothelium, infected HbAA and HbAS erythrocytes move at lower velocities on TNF-α activated endothelial cells, however statistical significance was only found for HbAA-iRBCs ($p < 0.01$, HbAS $p < 0.204$, One-way ANOVA) (Figure 24A). The contact time increased significantly for both HbAA- and HbAS-iRBCs ($p < 0.001$, One-way ANOVA) (Figure 24C). Moreover, the mean amplitude difference and the mean Person correlation coefficient obtained for HbAA- and HbAS-iRBCs flipping on TNF-α activated endothelium, remained comparable to the values obtained when resting endothelium was used as substratum (HbAA $p = 0.582$, HbAS $p = 0.397$ and HbAA $p = 0.808$, HbAS $p = 0.809$, respectively; One-way ANOVA).

Altogether these results indicate that the trend between HbAA- and HbAS-iRBCs was consistent within the different substratum. Therefore, the differences in behavior observed for both groups might arise mainly from the erythrocytic adhesive and/or mechanical properties. The increase of endothelial cells ligand density, especially ICAM-1, which is known to largely increase upon TNF-α stimulation, provoked significant variations in the cytoadhesive behavior, especially in translational velocity and contact time. The other parameters, i.e. the amplitude difference and the Pearson correlation coefficient were not dramatically changed, suggesting that these two parameters might be more dependent on other erythrocyte properties such as cell shape and rigidity, rather than in the number of ligand-receptor interactions.

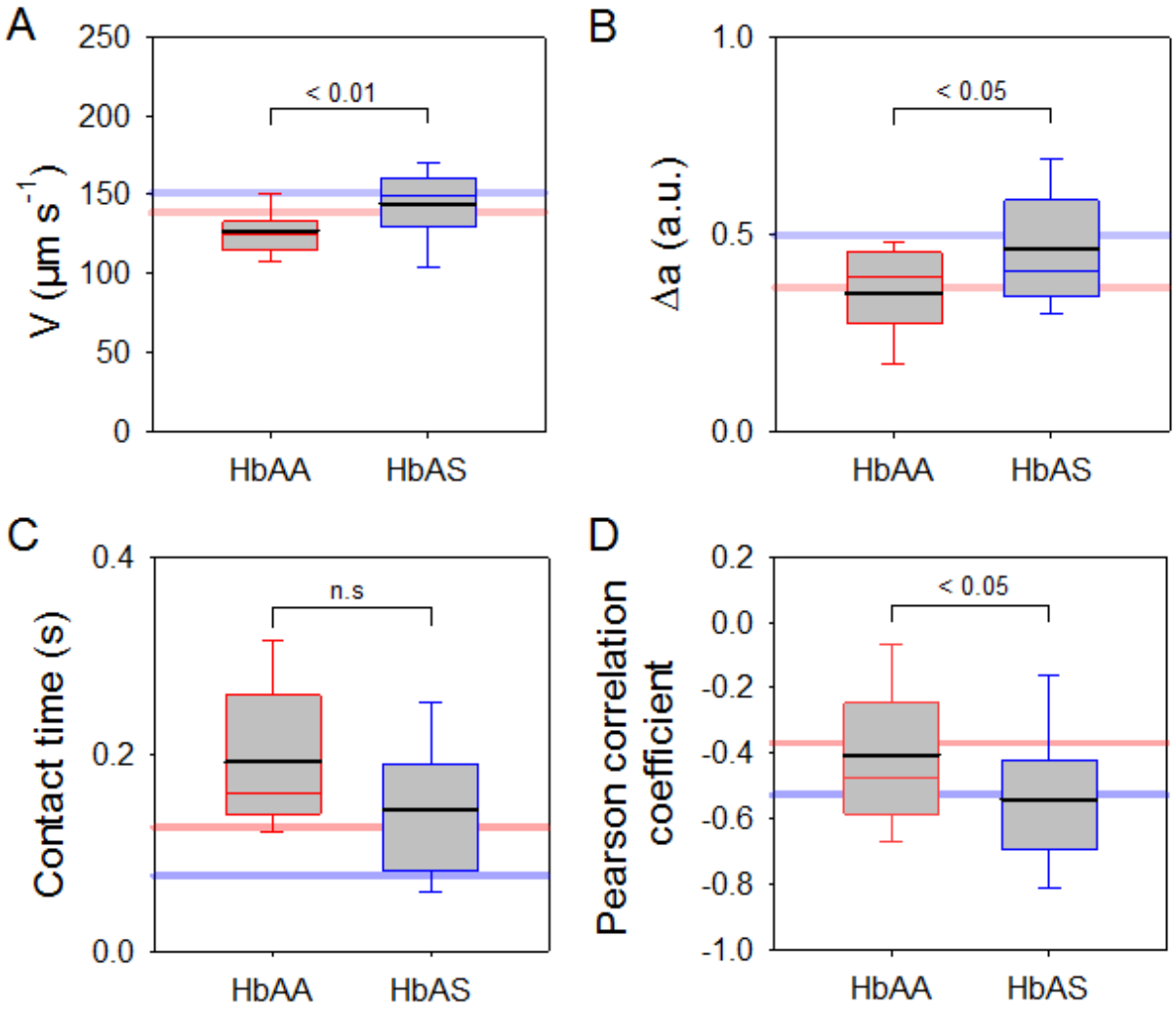

Figure 24 | Quantification of *P. falciparum*-infected erythrocytes cytoadhesive behavior on TNF-α activated endothelium at 0.05 Pa. (A) Mean translational velocity, (B) fluorescence amplitude difference, (C) contact time and (D) Pearson correlation coefficient between fluorescence amplitude and velocity profile for infected HbAA (Red) and HbAS (blue) erythrocytes at the trophozoite stage with an applied shear stress of 0.05 Pa. The median, 25% and 75% quartile ranges and error bars are shown, as well the mean values (thick black line) from three independent experiments and 21 trajectories. Mean values found for infected HbAA and HbAS erythrocytes flipping on resting endothelium are represented by the red and blue lines, respectively. Statistical significance is indicated (Student´s t-test).

Hemoglobin C erythrocytes showed a reduced static and flow adherence to HDMEC, and the characterization and quantification of the cytoadhesive behavior were originally part of the aims of the present study. However due to a limited sample access, the behavior quantification was not possible. Preliminary results showed

clear differences between trophozoite and schizont-stage infected HbAC erythrocytes (Figure 25). The typical flipping motion was observed for HbAC-iRBCs at the trophozoite stage (Figure 25A), characterized by large fluorescence amplitude and regular velocity oscillations, and by a strong anti-correlation (-0.669). Maturation to schizont-stage provoked reduced amplitude differences and fewer oscillations and variations in the velocity profile. However, similar to HbAS-iRBCs, schizonts HbAC-iRBCs showed a stronger anti-correlation (-0.266) when compared to schizonts of HbAA-iRBCs (Figure 25B). Therefore, preventing the smooth rolling observed previously for HbAA-iRBCs. Further repetitions and proper quantification could further reveal important differences in the cytoadhesive behavior of *P. falciparum* growing in this hemoglobin variant.

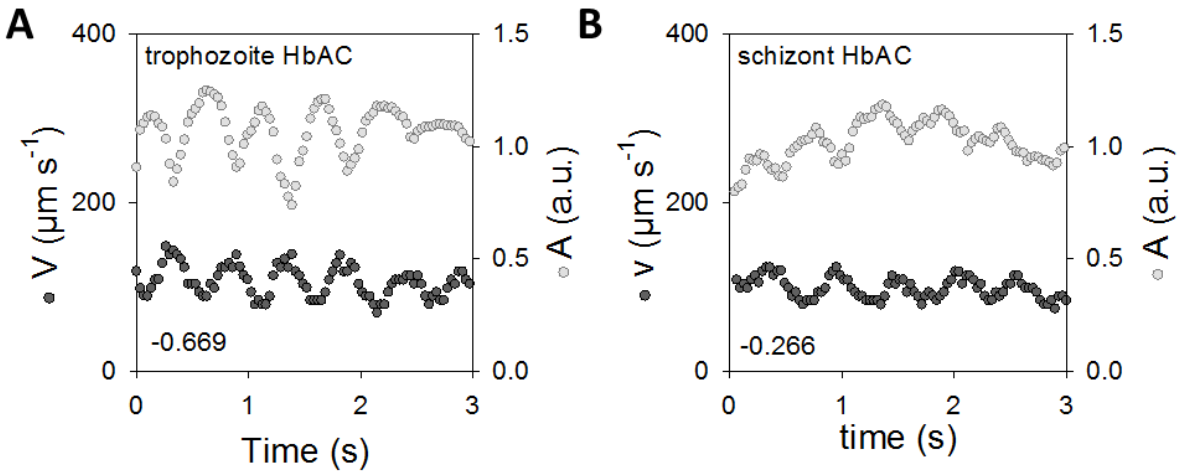

Figure 25 | Differential cytoadhesive behavior of *P. falciparum*-infected HbAC erythrocytes under low physiological flow conditions. Representative fluorescence and velocity amplitude profiles observed for infected HbAC erythrocytes at different developmental stages, (A) trophozoite and (B) schizont, flowing on confluent HDMEC at a shear stress of 0.05 Pa. Pearson correlation coefficient is shown for the selected trajectories.

3.2.6. Delayed activation of new permeation pathways in infected hemoglobinopathic erythrocytes

During the late-intraerythrocytic development *P. falciparum* increases the permeability of the red blood cell plasma membrane to a wide range of small solutes which have been shown to enter the red blood cell via a different pathway not operating in uninfected erythrocytes. This pathway is referred as new permeation pathways (NPP) and is permeable to anions as well as cationic and electroneutral

solutes including sugars like D-sorbitol [250]. As soon as the NPP are activated, the electrochemical Na^+ and K^+ gradients are gradually dissipated, subsequently, the cell starts to swell due to an influx of Na^+ and accompanied water [251], increasing the infected erythrocyte volume by 60% [20]. This feature contributes to the spherical shape observed at the schizont stage-infected erythrocytes [20]. Rolling adhesion seems to be highly dependent on the cell sphericity, therefore differences in the rolling behavior observed for schizont-infected hemoglobinopathic erythrocytes suggested altered erythrocyte morphology at this stage. Since the NPP activation contributes to the spherical shape at the end of the erythrocyte cycle, the NPP activation was evaluated for infected HbAA, HbAS and HbAC erythrocytes.

For this, highly synchronized $FCR3^{HDMEC}$ cultures on HbAA, HbAS and HbAC erythrocytes were studied over the whole intraerythrocytic developmental cycle (~48 hours post invasion (hpi)) for their induction of NPP using iso-osmotic D-sorbitol solution (Figure 26 A). D-sorbitol is permeable to the NPP and lead to cell lysis by driving water with it into the cell. The released hemoglobin from lysed cells was quantified by spectroscopy at a wavelength of A540 nm. Thus, the amount on hemoglobin corresponded to the levels of NPP activation. NPP activation coincides with the transition from ring to trophozoite stage at ~20 hpi. For parasitized HbAA erythrocytes the measured hemoglobin from lysed cells starts rising after 20 hpi. These cells reached the half maximum NPP activation at 26 ± 2 hpi, consistent with previous reports [252]. According to the F-test NPP activation was found to be significantly different for infected HbAS ($p > 0.001$) and HbAC ($p > 0.001$) erythrocytes when compared to HbAA control group. No difference between parasitized HbAS and HbAC erythrocytes was found ($p > 0.77$). NPP induction was delayed by ~4 h in both infected HbAS and HbAC erythrocytes. In both cases, the 50% maximum NPP activation was reached at 30 ± 2 h. Additionally, the NPP in hemoglobinopathic erythrocytes did not reach the maximum activation observed for infected wild type cells. The delay in NPP activation in these infected hemoglobinopathic erythrocytes might prevent the infected erythrocyte to become as spherical as HbAA-iRBCs at the end of the intraerythrocytic cycle.

In parallel to the NPP assessment, parasite development was monitored microscopically every 4 hours by Giemsa-stained thin blood smears and no

difference in the intraerythrocytic parasite development was found between groups over the 48 h time course (Figure 26B).

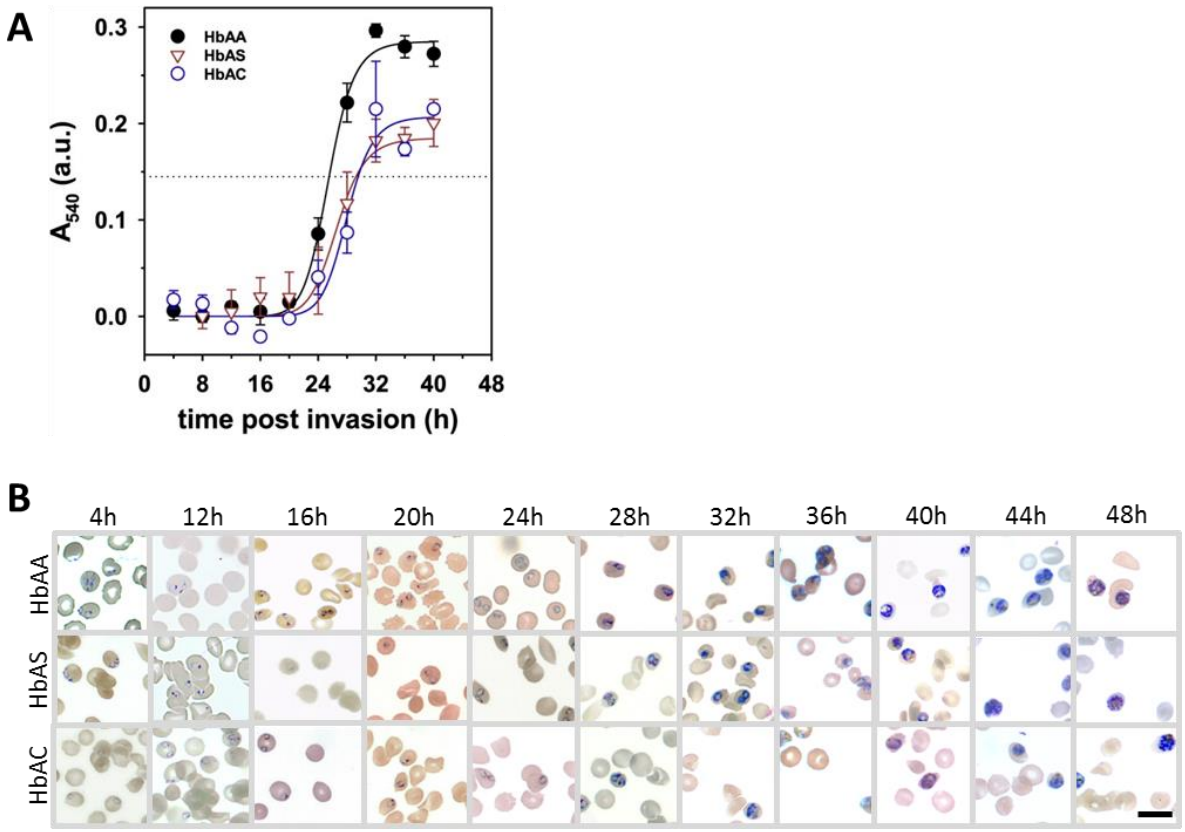

Figure 26 | New permeation pathways activation for parasitized HbAA, HbAC and HbAS erythrocytes. (A) Induction of NPP was assessed by spectroscopy by measuring the hemoglobin content at 540nm after exposing the infected erythrocytes to iso-osmotic D-sorbitol solution every 4 h during the whole intraerythrocytic cycle. The means ± SEM are shown for three independent biological replicates and blood from at least two different donors. The 50% NPP induction in infected HbAA erythrocytes is indicated by the dotted line. Statistic comparison between groups was performed using the F-test after fitting the data points to a three-parameter Hill function. a.u., arbitrary units. (B) Bright field images of the Giemsa-stained blood smears showing the parasitic stage and morphology for infected HbAA, HbAS and HbAC erythrocytes at every time point (4 h) during the time course. Scale bar 10 µm.

3.2.7. Knob characterization of hemoglobinopathic *P. falciparum*-infected erythrocytes

When compared to HbAA-iRBCs, larger amplitude differences were observed for infected HbAS erythrocytes, together with higher translational velocities and reduced contact times. These features could emerge as consequence of reduced knob densities in infected hemoglobinopathic erythrocytes. Knobs density and morphology

were investigated by scanning electron microscopy (SEM) and atomic force microscopy (AFM). AFM experiments were performed by Katharina Quadt (PhD student, Center for Infectious Diseases, Heidelberg University Hospital).

Scanning electron microscopy images permitted the quantification of knobs and the estimation of knob diameter from well preserved samples at the trophozoite stage. In Figure 27A, a representative SEM image is shown for an uninfected erythrocyte, lacking the electron dense protrusions, and infected HbAA, HbAS and HbAC erythrocytes displaying knobs on their surfaces. Fewer and slightly larger knobs were observed for the infected hemoglobinopathic erythrocytes. Compared to HbAA-iRBCs (Figure 27B), infected hemoglobinopathic erythrocytes showed significant lower knob densities on the surface of hemoglobinopathic erythrocytes (between HbAA and HbAS $p < 0.01$; between HbAA and HbAC $p < 0.001$, One-way ANOVA), but no difference was found between hemoglobin variants (between HbAS and HbAC $p = 0.702$). Knob diameter (Figure 27C) was found to be significantly larger for infected HbAS and HbAC erythrocytes when compared to wild-type control group (between HbAA and HbAS $p < 0.001$; between HbAA and HbAC $p < 0.001$) but not when compared to each other (between HbAS and HbAC, $p = 0.423$).

For the measurement of knob height, SEM is not the most appropriate technique. Therefore, knob density, diameter and height were measured by atomic force microscopy. These measurements were only performed for infected HbAA and HbAS erythrocytes at the trophozoite (26 ± 6 hpi) and schizont stage (36 ± 6 hpi) (Table 2). The results reveal discrepancies in the knob density, showing lower mean values when measured by AFM than when measured by SEM. For instance, the mean knob density for HbAA-iRBC quantified by SEM and AFM were 12.6 ± 1 knobs/μm^2 and 5.7 ± 0.4 knobs/μm^2, respectively. While for HbAS-iRBC the mean knob density obtained by SEM and AFM was estimated to be 5.8 ± 1 knobs/μm^2 and 3.3 ± 0.5 knobs/μm^2, respectively. Nevertheless, the difference in knob reduction between infected HbAA and HbAS erythrocytes at the trophozoite stage remained constant between AFM and SEM (about a factor of 2). The mean knob diameter values were comparable when measured by SEM and AFM.

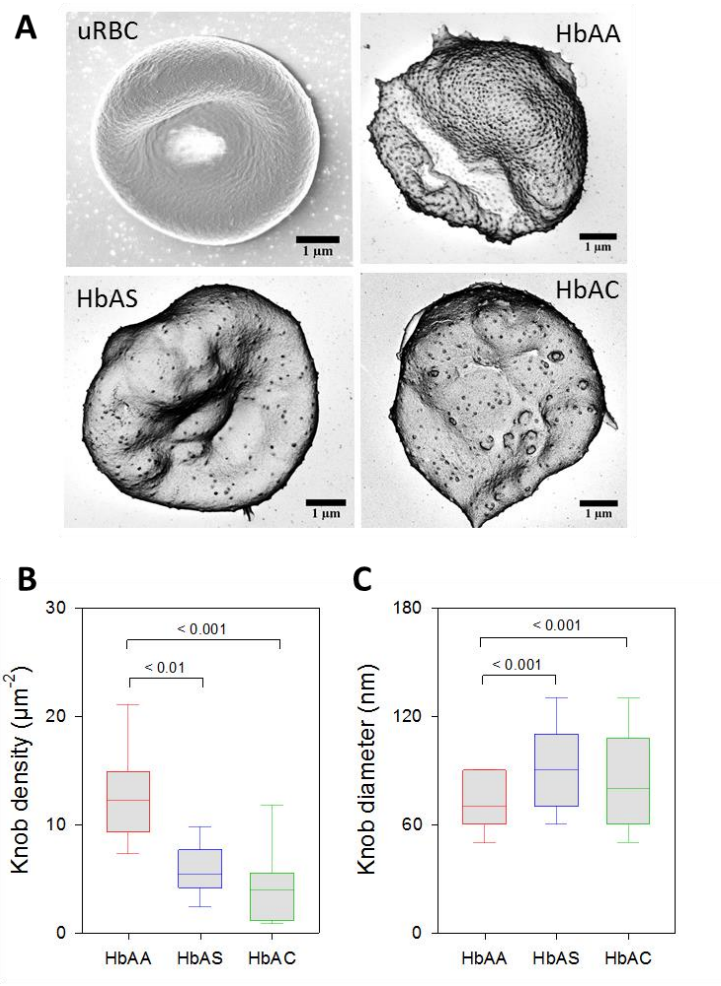

Figure 27 | Knob characterization for hemoglobinopathic infected erythrocytes. (A) Representative scanning electron microscopy images of uninfected erythrocytes and Pf-infected HbAA, HbAS and HbAC erythrocytes at the trophozoite stage. Box plots showing the (B) knob density and (C) the knob diameter for infected HbAA, HbAS and HbAC erythrocytes (trophozoite-stage). The median, 25% and 75% quartile ranges and error bars are shown from at least 14 cells. Statistical differences are indicated; one-way ANOVA.

The AFM data showed that the mean knob height significantly increased for HbAS-iRBCs when compared to HbAA-iRBCs ($p < 0.001$, t-test). Furthermore, the number of knobs increased from trophozoite to schizonts stage for both HbAA- and HbAS-iRCBs, but it remained significantly lower for HbAS group when compared to HbAA-iRBCs ($p < 0.05$, t-test). Knob diameter as well as knob height remained relatively constant from trophozoite to schizont and were significantly larger for HbAS-infected erythrocytes ($p < 0.001$, t-test) (Table 2).

The discrepancies in the knob density measured by SEM and AFM could be partly explained by the sample preparation. Infected erythrocytes are osmotically fragile cells and could have shrunk during the SEM preparation [117]. The erythrocyte diameter measured by SEM was about 5.5 µm while the erythrocytes diameter measured by AFM was about 6.5 µm. This could clarify the increased knob densities observed for infected erythrocytes when measured by SEM. Similar discrepancies in the knob densities measured by AFM and SEM in parallel have been previously observed [116].

Table 2. Knob characterization of infected HbAA and HbAS erythrocytes at the trophozoite and schizont stage by AFM. Statistical significance was obtained by Student's t-test.

	Trophozoites			**Schizonts**		
	HbAA	HbAS	*P value*	HbAA	HbAS	*P value*
Knob density (μm^{-2})	5.7±0.4	3.3±0.5	<0.001	7.6±0.8	5.8±0.6	<0.05
Knob diameter (nm)	83±2.4	103±2.5	<0.001	89±2	101±3	<0.01
Knob height (nm)	6.5±0.3	9.2±0.4	<0.001	9.4±0.6	11.3±0.6	<0.05

In order to interpret all the data in a more meaningful way, principal component analysis (PCA) was performed (Figure 28). For the analysis, the Pearson correlation coefficient, translational velocity, amplitude difference, contact time and knob density were included as variables. Since cell rigidity is thought to play an important role in the iRBCs dynamic adhesion, membrane bending rigidity values previously measured for iRBC-HbAA and iRBCs-HbAS [253] were also included in the PCA analysis. The mean values reported for infected HbAA and HbAS erythrocytes bending modulus were 3.4±1.4 (10^{-19} J) and 5.9±1.2 (10^{-19} J), respectively, indicating the increase in membrane bending rigidity for HbAS-iRBCs [253].

In the PCA, the two major components in which the data differed more were obtained. The PC1 showed the highest variation (84%, 86%) and the PC2 the second highest variation (8%, 10%). The score graph showed clear separation between infected HbAA and HbAS erythrocytes at both, trophozoite and schizont-

stage. In the PCA, it is also visible that the infected HbAA erythrocyte population was dominated by high knob density, larger contact times, no correlative Pearson correlation coefficient, lower amplitude differences and lower bending modulus. While infected HbAS erythrocytes were dominated by high translational velocities, higher bending modulus, larger amplitude differences, lower knob densities, reduced contact times and anti-correlative Pearson correlation coefficient.

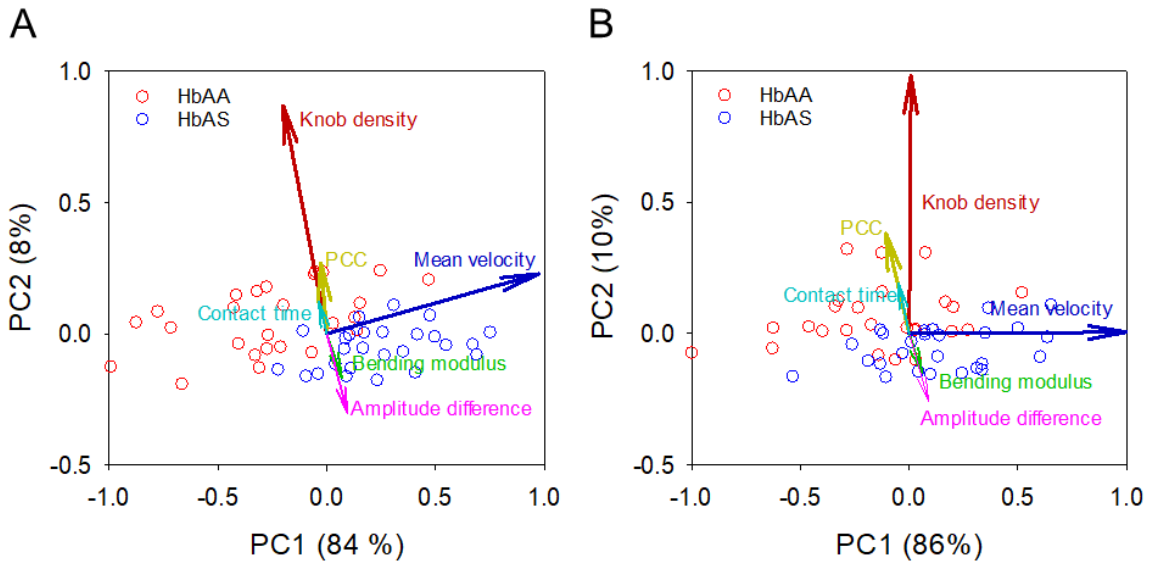

Figure 28 | Principal component analysis. Features analyzed include knob density, Pearson correlation coefficient (PCC), mean translational velocity, bending modulus, contact time and amplitude difference. Data is showed in a score graph for infected HbAA and HbAS erythrocytes at the (A) trophozoite-stage and (B) schizont-stage. *n* = *4* (27 cells). Loadings are shown for every variable: knob density (red arrow), Pearson correlation coefficient (yellow arrow), mean translational velocity (blue arrow), bending moduli (green arrow), contact time (light blue arrow) and amplitude difference (pink arrow).

Experimentally measured values of membrane bending modulus [253] and knob density from AFM were used by our collaborator Dr. Anil Dasanna (Prof. Ulrich Schwarz's group, Institute of Theoretical Physics, Heidelberg University) in mesoscopic computer simulations. The computer simulations studied the adhesion of iRBC under shear flow to a substratum that mimics HDMEC, by modeling deformable cell and explicit hydrodynamics which requires relevant parameters of the system such as bending modulus and knob density. From simulations a 2-factor decreased knob density and 2-factor increased bending modulus, resulted in increased velocity, increased amplitude difference, reduced contact time

and stronger anti-correlation [254]. This data indicated that lower knob density and increased bending modulus were responsible for altered cytoadhesive behavior that is observed for infected HbAS erythrocytes.

Other important information, such as the adhesion footprints, was then extracted from the simulations. The footprints patterns resultant from the dynamic adhesion of infected HbAA and HbAS erythrocytes at the trophozoite and schizont stage were visualized (Figure 29). Every dot corresponds to one ligand-receptor formation. At the trophozoite stage, infected erythrocytes showed larger contact areas compared to the infected cell at schizont stage. This results as consequence of the spherical shape and overall cell stiffness. On the other hand, the infected HbAS erythrocyte showed, in this representative trajectory, an inconsistent adhesion pattern, with areas depleted of contact (Figure 29C). At the schizont stage, infected HbAS erythrocytes showed a more regular footprint, nevertheless, less contact points were obtained when compared to the infected HbAA erythrocyte trajectory (Figure 29D). The reduced contact area and time, together with a reduced iRBCs ability to firmly adhere might have a strong impact on the direct endothelial cell activation by HbAS-iRBCs.

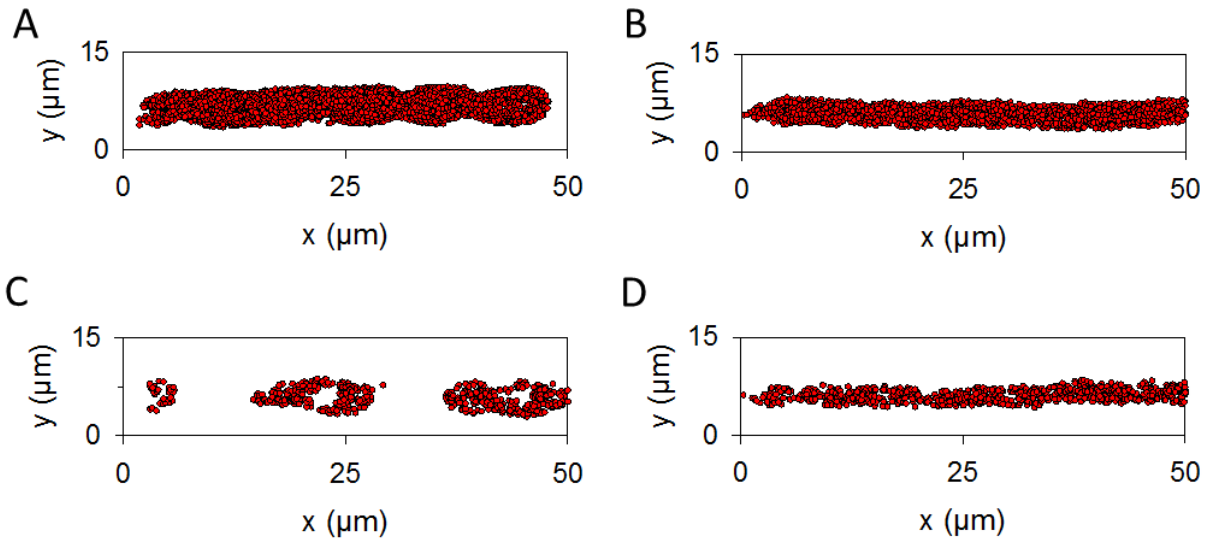

Figure 29 | Adhesion foot prints patterns for infected erythrocytes. Representative foot prints originated from infected HbAA (A,B) and HbAS (C,D) erythrocytes dynamically adhering on HDMEC-like substratum, at the trophozoite stage (A,C) and schizont stage (B,C). Data was obtained from mesoscopic simulations using the knob density obtained experimentally and the bending modulus [253]. Simulations were performed by Dr. Anil Dasanna, Institute of Theoretical Physics, Heidelberg University.

3.3. Endothelial cell activation by *P. falciparum* infected erythrocytes

3.3.1. NF-κB nuclear translocation induced by infected erythrocytes binding

It has previously been shown that direct interaction of *P. falciparum* infected erythrocytes caused activation of several signaling cascades in the microvascular endothelial cells [96][165][169]. NF-κB is a fast-acting transcription factor located in its inactive form inside the cell cytosol and upon infected erythrocytes binding, NF-κB is quickly translocated into the endothelial cells nucleus where it binds to consensus sequences of the DNA to initiate transcription of genes involved in immune response [170]. NF-κB is a dimer composed by several subunits, including p65 and p50. It is known that *P. falciparum* infected erythrocytes binding induce the fast nuclear translocation of p65 subunit in human brain microvascular endothelial cells [171][169].

To assess activation of HDMEC by infected erythrocytes, immunofluorescence of p65-NF-κB subunit followed by confocal microscopy imaging was performed. For this, confluent HDMEC were co-cultured with different parasitized erythrocytes loads for various incubation times (Figure 30). The level of activation was quantitatively represented as the nuclear labeling index (NLI) or the percentage of cells with p65-NF-κB positive labeled nuclei. NF-κB nuclear translocation in HDMEC upon infected erythrocytes binding was found to be concentration dependent, as the number of activated cells rose by increasing the infected erythrocytes load. However, an increase on the time of incubation had no major effect on activation. Interestingly, areas fully covered by infected erythrocytes showed fully activated endothelial cells (Figure 30B, arrows), further suggesting the importance of the number of adherent cell on endothelial cell activation. Uninfected erythrocytes (1.5×10^7 uRBC/well) and medium served as negative control and showed none or basal activation. TNF-α served as positive control and induced ~100% of the cells to be activated. It is appreciable that 2 h of incubation gave the lowest variation in the data. Therefore, this condition was used in future comparisons.

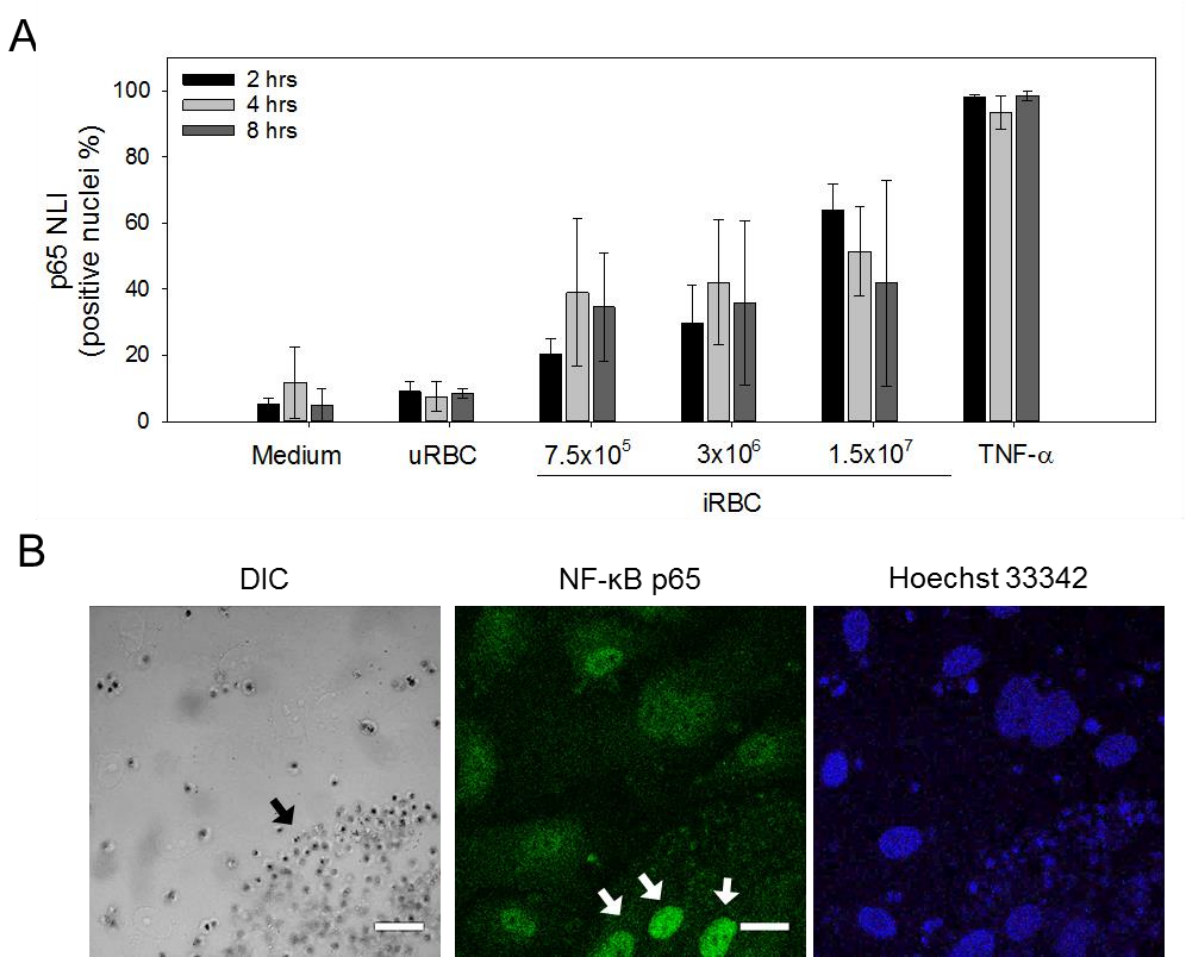

Figure 30 | *P. falciparum*-infected erythrocytes induce nuclear translocation of NF-κB in a dose dependent manner. (A) Percentage of positive p65-NF-κB nuclear labeled cells (nulear labeling index, NLI) is shown after co-culturing confluent HDMEC with different parasitized erythrocytes loads for different incubation times under static conditions. HDMEC co-cultured with uninfected erythrocytes and medium alone served as negative control while TNF-α served as positive control (*n = 2*). (B) Representative confocal microscopy image of p65-NF-κB obtained for HDEMC after co-culturing endothelial cells with infected HbAA erythrocytes adhering under static condition for 2 h ($1x10^7$ iRBCs). In the DIC the parasitized erythrocytes can be appreciated. In the Hoechst staining the nuclei are shown.

3.3.2. Endothelial ICAM-1 surface expression and IL-6 secretion upon infected erythrocytes binding

Once in the nucleus, NF-κB can bind to consensus sequences and initiate the transcription of several target genes including ICAM-1, VCAM-1 and IL-6 [255]. Therefore, NF-κB nuclear translocation is thought to induce a state of hyperadhesiveness, further worsening the degree of vascular obstruction, endothelial dysfunction and inflammation. Previous studies showed increased ICAM-1 endothelial surface expression and IL-6 secretion upon infected erythrocytes binding

on human umbilical vein endothelial cells (HUVEC) [165]. To assess if this response occurs in HDMEC, flow cytometry was performed after co-culturing HDMEC with parasitized erythrocytes to quantify the levels of ICAM-1 cell surface expression. In parallel, IL-6 secreted levels were quantified using a specific capture ELISA. Our results clearly showed an increase of ICAM-1 surface expression on HDMEC ($p < 0.05$, One-way ANOVA) and increased IL-6 levels ($p < 0.05$, One-way ANOVA) upon infected erythrocytes binding (Figure 31). To evaluate whether the observed activation was due to a binding of iRBCs to endothelial cell or due to parasite derived soluble factors, trans-well assays were performed. For this, HDMEC were cultured in the bottom of the chamber, while iRBCs were loaded into the top, separated by a porous membrane. Results clearly showed no activation in the trans-well assay, indicating that increased endothelial surface expression of ICAM-1 and IL-6 secretion was caused by direct contact between infected erythrocytes and the endothelium. TNF-α was used as positive control, and clearly caused an increase in both ICAM-1 surface expression and IL-6 secretion. Opposite to that, co-culture of endothelial cells with uninfected erythrocytes or medium caused no changes on ICAM-1 surface expression or IL-6 secretion to the medium.

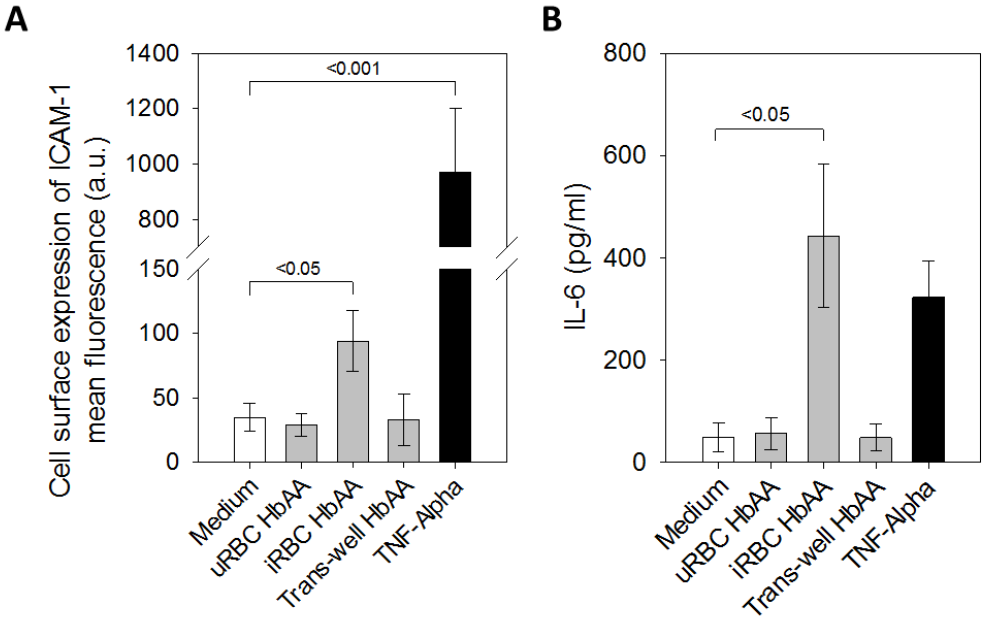

Figure 31 | *P. falciparum*-infected erythrocytes directly activate HDMEC. The levels of ICAM-1 endothelial surface expression (A) and IL-6 secretion (B) were quantified by flow cytometry and ELISA, respectively, after co-culturing confluent endothelial cells with infected erythrocytes for 20 hr. Medium and TNF-α were used as negative and positive control, respectively. Trans-wells were used to prevent direct contact between endothelial cells and infected erythrocytes but allowed the exchange of soluble factors. Mean ± SEM are shown for three independent experiments. Significance is shown (One-way ANOVA), a.u., arbitrary units.

Due to technical issues such as high requirement of cell material and extensive incubation times, ICAM-1 surface detection and IL-6 secretion quantification could not be performed under flow conditions. Therefore, only NF-κB nuclear translocation was used as marker for endothelial cells activation under flow conditions. Infected wild-type and HbAS erythrocytes were then compared on their ability to activate HDMEC under static and flow conditions.

3.3.3. Reduced endothelial cell activation by infected HbAS erythrocytes

Confluent HDMEC were co-cultured with different parasitized erythrocytes loads for 2 h (Figure 32). In the confocal images (Figure 32A), it can be appreciated that without any stimulus, the p65-NF-κB signal inside the endothelial cells was distributed homogenously inside the cell. The number of nuclei can be visualized by the Hoechst nuclear staining (Figure 32B, lower panel). Stimulation with the pro-inflammatory cytokine, TNF-α, caused the translocation of p65-NF-κB to the nuclei of almost 100% of the cells (positive control). p65-NF-κB nuclear translocation was also observed when HDMEC were co-cultured with infected HbAA erythrocytes. The parasite nuclei staining shows the high number of infected erythrocytes adhering to the endothelial monolayer. In the case of infected HbAS erythrocytes, high number of adherent parasitized erythrocytes were observed. However, the percentage of endothelial cells showing activation was lower when compared to the achieved by infected HbAA erythrocytes.

Quantitatively, the level of activation was represented as the nuclear labeling index or the percentage of cells with p65-NF-κB positive labeled nuclei. Parasitized erythrocytes bound under static conditions to HDMEC (Figure 32B) showed a clear increase in the percentage of activated cells as the infected erythrocyte load increased. Addition of $15x10^6$ iRBC caused the full coverture of the endothelium. The same trend was observed for infected HbAS erythrocytes, however, the level of endothelial cell activation was significantly decreased as evaluated by the F-test ($p < 0.01$), when compared to HbAA-iRBC applying the same parasitized erythrocyte load. Again, no activation was observed for the medium or uninfected red blood cells control. Stimulation with TNF-α caused activation of almost 100% of the endothelial cells.

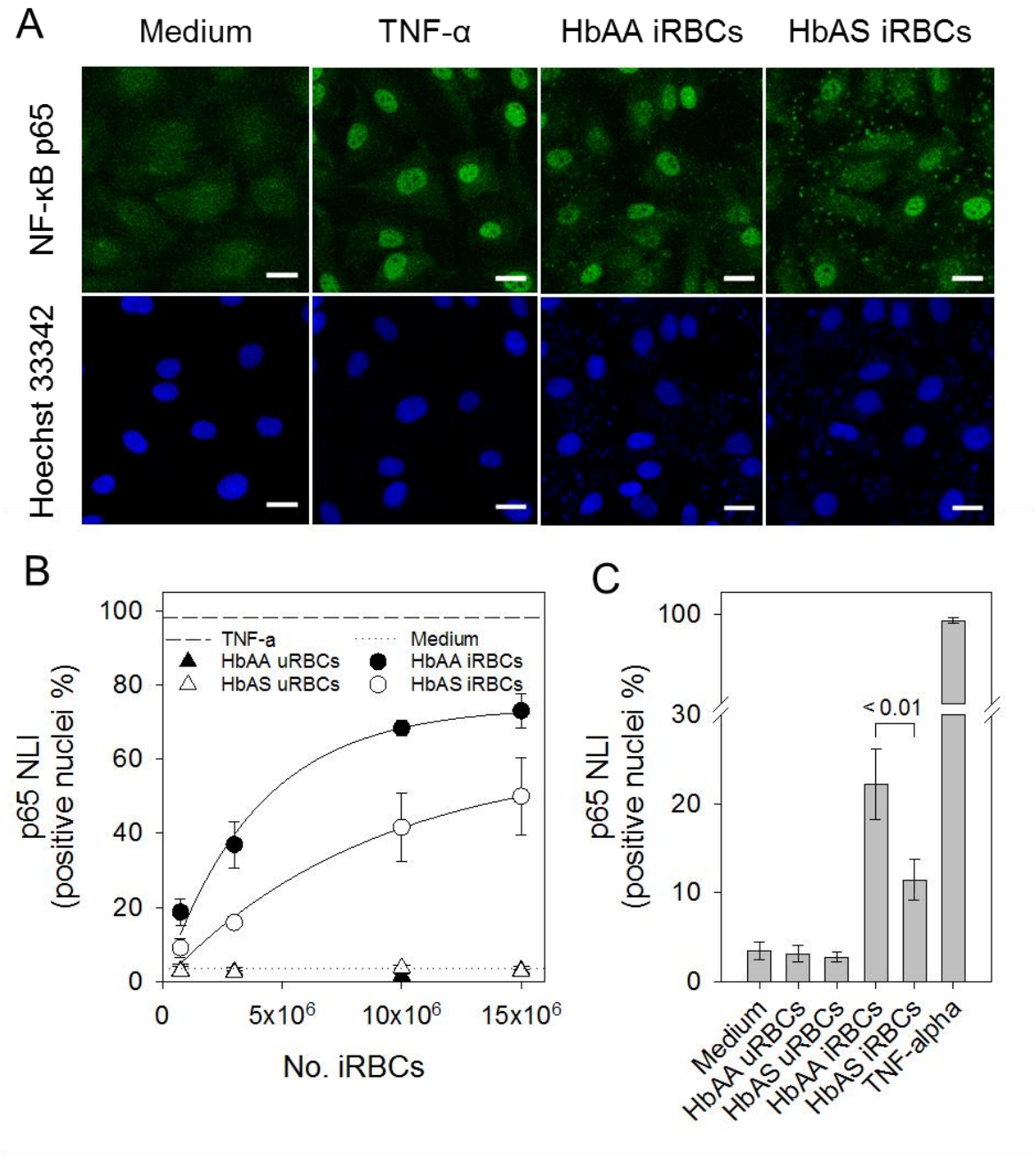

Figure 32 | Reduced endothelial cell activation by infected HbAS erythrocytes. (A) Representative confocal microscopy images of p65-NF-κB subunit obtained for HDEMC after co-culturing endothelial cells with infected HbAA or HbAS erythrocytes under static condition ($1x10^7$ iRBCs). Medium and TNF-α served as negative and positive controls, respectively. Total number of nuclei is shown by Hoescht 33342 stain. Scale bar 20 µm. (B) Percentage of positive p65-NF-κB nuclear labeled cells (nulear labeling index, NLI) is shown after co-culturing confluent HDMEC with different parasitized erythrocytes loads under static conditions ($p < 0.01$, F-test). HDMEC co-cultured with uninfected erythrocytes served as additional negative control. (C) Percentage of positive p65-NF-κB nuclear labeled cells after co-culturing confluent HDMEC with infected erythrocytes ($1x10^8$) that remained adhered after flushing the parasite suspension at a wall shear stress of 0.03 Pa. Medium, uninfected erythrocytes and TNF-α served as negative and positive control, respectively. Mean ± SEM are shown for at least five biological replicates from at least two blood donors. Statistical significance is shown (one-way ANOVA).

Contrary to static conditions, where almost all parasitized erythrocytes were able to interact with the endothelium and bind, fewer cells bound to the endothelium under flow conditions. However, the activation of endothelial cells by HbAA-iRBCs was clearly marked under flow conditions (Figure 32C) (between medium and HbAA iRBCs $p < 0.001$, between HbAA uRBCs and HbAA iRBCs $p < 0.001$, One-way ANOVA), activating approximately 22 ± 4% of the endothelial cells. When compared to HbAA-iRBCs, the percentage of activated endothelial cells by HbAS-iRBCs, after adhering under flow conditions, was reduced by ~50%, activating only 11 ± 2% of the endothelial cells.

3.4. Quantification *of P. falciparum*-infected erythrocytes binding strength at single cell level by atomic force microscopy-single cell force spectroscopy

Atomic force microscopy single cell force spectroscopy (AFM-SCFS) can been used to quantify the binding strength of infected erythrocytes at a single cell level, applying controlled forces. Within this study, the AFM-SCFS technology was simply established for future use and comparison. Infected erythrocytes were successfully functionalized to a tip-less AFM cantilever using the dopamine hydrochloride polymer (Figure 33A). Functionalized iRBCs were brought into direct contact with the endothelial cell with a constant force of 150 pN, which mimics the force that infected erythrocytes experience in post-capillary venules when being pushed from the centerline of the flowing cells towards the endothelium [164].

Infected erythrocytes were brought into contact with the endothelial cell for different periods of time: 0s, 5s and 30s. The retract/extend curves were obtained (retract curve, Figure 33B) and analyzed. The maximum force of detachment as well the number of rupture events were calculated from the obtained force curves. These two parameters described the binding strength between the two cells. In accordance with previous studies [164], longer contact durations provoked larger binding strengths as seen by an increase in the maximum force and rupture events. The binding strength of *P. falciparum*-iRBCs increased from 144 ± 18 pN at 0 s contact time to 489 ± 39 pN at 30 s contact time (Figure 33C). The number of rupture events also increased as well from 3.5 ± 0.6 at 0 s to 9.8 ± 1.3 at 30 s (Figure 33D). These results indicate

that initial contact permitted the formation of single or multiple bonds between iRBC-HDMEC, and this binding strength increased with the duration of the contact in agreement with previous results [162]. When the infected erythrocytes were brought into contact with BSA coated surface, negligible forces of detachment were observed, with almost no rupture events, suggesting no strong binding interaction between infected erythrocytes and BSA, as expected.

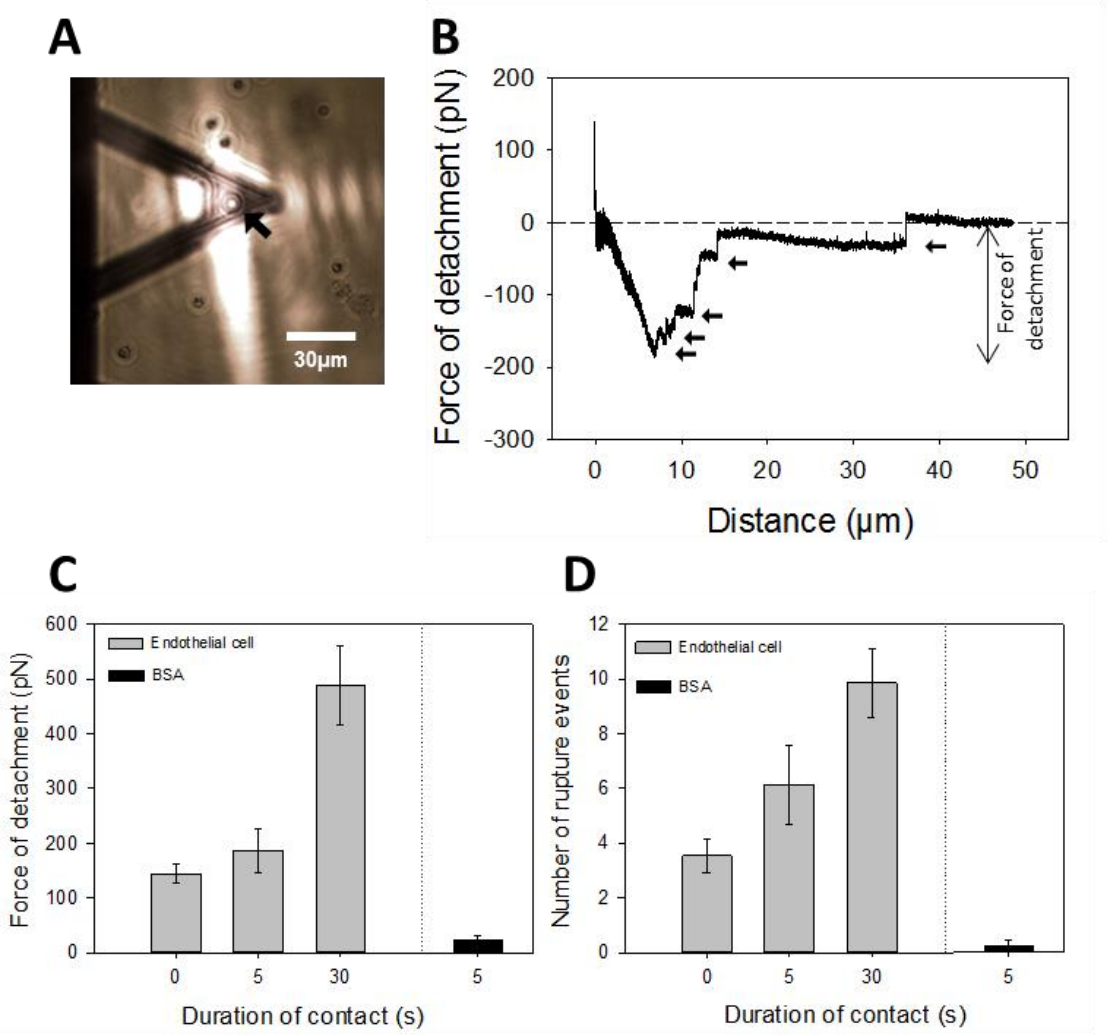

Figure 33 | Force measurements between *P. falciparum*-infected erythrocytes and HDEMCs at a single cell level. Phase contrast image of an infected erythrocyte mounted on the AFM tip less cantilever functionalized with dopamine hydrochloride, indicated by the arrow; scale bar 30 µm. (B) Representative force/retract curve obtained from the iRBC and HDMEC interaction at 0s contact time at a contact force of 150 pN. Maximum force of detachment is shown; rupture events are indicated by arrows. Bar charts showing the (C) maximum force of detachment and (D) number of rupture events for infected erythrocytes interacting for different times with HDMEC and with BSA for 5 sec as negative control. Mean ± SEM are shown from at least 7 curves per treatment (*n = 2*).

The increase on iRBC binding strength to HDMEC by increased duration of contact have been reported [162]. The initial binding of infected erythrocytes causes on microvascular endothelial cells the rapid actin recruitment and CD36 clustering in the adherent sites, strengthening the binding between cells. The increase in adhesive strength over time would allow the iRBC to resist, after the initial attachment, the shear stress present in the microcirculation [162]. Thus, by using this methodology, the iRBC-EC binding strength as well as the endothelial cell activation (adhesion strengthening) could be quantified at a single cell level, including all different cells present in a population, without excluding the weak binders, like it happens for the flow adhesion assays. However, the disadvantage of AFM-SCFS is that is expensive and high time consuming/low throughput technique [246].

4. Discussion

Several studies support the hypothesis that sickle trait hemoglobin and hemoglobin C are naturally selected due to the protection they confer against severe malaria and malaria-related deaths, reaching high frequencies in several populations [256][257][258]. However, the mechanism by which these erythrocyte variants confer protection remains unclear. Recent studies have associated these hemoglobin variants with reduced cytoadhesion to microvascular endothelial cells under static and flow conditions [203][52][214]. However, these studies only considered firm adhesion and have ignored the fact that infected erythrocytes interact dynamically with the endothelium. Our results indeed reveal major differences in the adhesion dynamics between infected wild-type and hemoglobinopathic erythrocytes. Additionally, we observed that the cytoadhesion behavior varied depending on the stage of the intraerythrocytic parasite, with trophozoites flipping and schizonts rolling. We further noticed that despite an overall reduced firm adherence and irregular dynamic adherence, a fraction of infected hemoglobinopathic erythrocytes bound to the endothelium with comparable strengths as infected HbAA erythrocytes. Nevertheless, infected HbAS erythrocytes activated the microvascular endothelial cells in a reduced manner under static and flow conditions.

4.1. Reduced cytoadherence of FCR3^{HDMEC} infected hemoglobinopathic erythrocytes to HDMEC under flow conditions

In order to survive, *P. falciparum* modifies its host erythrocyte extensively during the parasite intraerythrocytic development. This results in dramatic modifications of the infected erythrocyte´s morphological and rheological properties, which consequently leads to an increased membrane rigidity, reduced cell deformability and increased adhesiveness of infected erythrocytes to microvascular endothelial cell ligands [232][259]. Due to the overall decrease in cell deformability as well as changes in cell morphology, infected erythrocytes *in vivo* can no longer aggregate into the erythrocytes centerline as the blood enters low shear areas, such as the post-capillary venules. This promotes the margination of the infected erythrocyte towards the vessel wall after being pushed away of the center line by aggregated erythrocytes

[150]. This is the initial step for *P. falciparum*-infected erythrocytes adhesion to the endothelial cells lining the vessels. As soon as the infected erythrocytes are captured from flow, they interact dynamically with the endothelium, reducing their motion velocity and finally adhering firmly to the substratum [124]. Previous studies have demonstrated that alteration in the adhesive and mechanical properties of *P. falciparum*-infected erythrocytes plays a critical role in their ability to cytoadhere [12].

In the physiological range of shear stresses as well as under static conditions, the firm adhesion of FCR3^{HDMEC} infected hemoglobinopathic erythrocytes was highly affected. These results are supported by previous studies showing ~50% reduction for infected HbAS and HbAC to microvascular and about 80% for HbSS-iRBCs in binding to microvascular endothelial cells, when compared to HbAA-iRBCs *in vitro* [203]. *In vivo* the sequestration of infected HbAS erythrocytes is also reduced [260]. The reduction in microvascular sequestration might decrease parasite densities during an episode of malaria due to increased splenic clearance [260]. Infected HbSS erythrocytes showed the strongest reduction in the number of infected erythrocytes binding to microvascular endothelial cells, probably due to very low PfEMP-1 erythrocyte surface levels as well as larger and fewer knobs quantified in these cells [203]. Moreover, the multiplication rate and development of *P. falciparum* in HbSS was also altered. Reduced parasite invasion and growth in sickle erythrocytes have been reported under low oxygen conditions, which leads to erythrocyte sickling and parasite developmental arrest [245]. It seems that HbSS erythrocytes might further protect against severe malaria by preventing the development of high parasitemias due to a strong reduction of infected erythrocytes sequestration and interference with parasite intraerythrocytic growth. This idea is supported by reduced parasite densities reported in individuals homozygous for sickle hemoglobin compared to the HbAA control group [261][262]. Nevertheless, the protection conferred by HbSS is uncertain and difficult to evaluate in African populations due to the high mortality risk of HbSS and its derived complications such as sickle cell anemia [203].

By reducing microvascular sequestration, infected HbS and HbC erythrocytes can be trapped in the spleen where they will be recognized by the immune system and destroyed [263]. Infected hemoglobinopathic erythrocytes may have an increased

antigen presentation which leads to the fast development of acquired immune responses, including antibodies against PfEMP-1 [264]. In fact, individuals with HbAS and HbAC showed enhanced antibody responses against infected erythrocyte variant surface antigens including PfEMP-1 [265]. Additionally, a cohort study in Kenya showed that the protective effect of HbAS increased with age, implying a role of acquired immunity in the protection against severe malaria by hemoglobinopathies [266]. Antibodies against PfEMP-1 might further destabilize the cytoadhesive interactions, further reducing vascular obstruction.

Our results further revealed that, under flow conditions infected wild-type and hemoglobinopathic erythrocytes adhered in a shear dependent manner to HDMEC. This suggested that the main receptor(s) to which the infected erythrocytes were binding on HDMEC were slip-type bonds. Slip bonds are non-covalent bonds that become weaker and break after reaching a critical shear force. In agreement with this observation, AFM measurements describe the CD36-iRBCs binding as a slip-type bond interaction [267][268][269]. Furthermore, CD36 was found to be the dominant adhesion receptor for $FCR3^{HDMEC}$ binding under flow conditions. This can explain the shear dependent behavior observed for iRBCs to HDMEC. On the other hand, ICAM-1, the second dominant receptor for $FCR3^{HDMEC}$, is known to form catch bonds interactions with infected erythrocytes [267]. This means that the lifetime of the adhesive bonds is force enhanced, leading to shear enhanced binding [270]. By forming catch bond interaction, ICAM-1 can mediate adherence at higher shear stresses, while slip-bond CD36 mediate binding at lower shear stresses [267][271]. This could help explain the observation of few infected erythrocytes binding at higher shears stresses (above 0.15 Pa).

4.2. Differential cytoadhesion behavior for infected HbAS erythrocytes on HDMEC at trophozoite and schizont-stages

Before firmly adhering, infected erythrocytes roll on the endothelium [124]. This initial interaction permits the cell in motion to slow down until it stops completely and remains adherent over the rest of the intraerythrocytic cycle. For the first time, we showed experimentally, differences in the cytoadhesion behavior between trophozoite- and schizont-stage infected erythrocytes. While trophozoites showed a

flipping behavior, schizonts rolled on the substratum. Flipping has been previously predicted by simulations to occur for non-spherical and less deformable erythrocytes, such as trophozoite-iRBCs [272]. For smooth rolling on the other hand, adhesive dynamic simulations predicted that, besides rigidity and sphericity, a homogeneous coverage of the infected erythrocyte surface with knobs is required and that the rolling becomes more stable as the knob density increased [232]. In agreement with this prediction, the knob density on the infected erythrocytes surface increased from trophozoite to schizont stage, allowing the cell to smoothly roll on the substratum.

Both, HbAA and HbAS-iRBCs, were capable of flipping and rolling on HDMECs. However, HbAS-iRBCs showed pronounced differences in the adhesion behavior at both the trophozoite and schizont stages. The number of iRBCs that remained firmly adhered was largely reduced for HbAS erythrocytes, indicating that differences in the HbAS-erythrocyte properties such as adhesion, cell rigidity and cells shape might interfere with the proper dynamic and subsequently firm adhesion. Increased translational velocities and reduced contact times observed for HbAS-iRBCs may derive primarily from reduced knob densities. Reduced knob densities and larger and wider knobs were indeed observed for infected hemoglobinopathic erythrocytes, similarly to previous reports [203][214][219]. Reduced number and abnormal knob presentation has been associated with the instability of HbS and HbC and a tendency of these hemoglobin variants to spontaneously auto-oxidize, leading to a redox imbalance in the infected hemoglobinopathic erythrocytes. This in turn interferes with knob formation and PfEMP-1 display on the infected erythrocyte surface [120][219][121]. The values obtained in this study for HbAA- and HbAS-iRBCs knob densities varied from other published values [273][219]. Numerical discrepancies in the number of knobs can be due to the different PfEMP-1 variant expressed [116] and importantly due to the type of parasite *in vitro* cultivation method used within the studies [274].

Decreased erythrocyte deformability play as well an important role in the dynamic cell adhesion [275] and differences in this property could affect the adhesion behavior of infected erythrocytes. Uninfected HbAS erythrocytes are stiffer than uninfected HbAA erythrocytes by a factor of ~2 [276]. Moreover, erythrocyte membrane bending rigidity increases in infected HbAS and HbAC erythrocytes by a factor of ~2 compared to

infected wild-type erythrocytes [253]. It has been speculated that the increased rigidity in HbAS erythrocytes might derive from changes in the affinity between the actin and spectrin filaments that comprise the erythrocyte membrane skeleton [276]. Sickle erythrocytes have an up to 5 fold increased Ca^{2+} permeability [277]. The increased intracellular Ca^{2+} can interact and modulate band 3-ankyrin-spectrin and spectrin-protein 4.1-actin complexes interactions, leading to greater cytoskeleton rigidity by [278][279]. Additionally, an increase of intracellular Ca^{2+} concentrations leads to the activation of the Ca^{2+} dependent K^{+} channel (Gardos channel). Gardos channels activation leads to a loss of K^{+}, Cl^{-} ions and water [280], which results in red blood cell dehydration and cell shrinkage [281], further impairing cell deformability by increasing cytoplasmic viscosity and probably by promoting deoxy-hemoglobin to aggregate [282][283][284]. Aggregated hemoglobin fibers can bind to spectrin via band 3 [285]. Therefore, the interaction between hemoglobin fibers attached to the membrane and hemoglobin fibers in the cytoplasm could contribute to the increased rigidity observed for HbS erythrocytes [276]. Additionally, increased membrane rigidity in HbAS erythrocytes may come from elevated lipid peroxidation as a consequence of oxidative stress in these cells [286], which is known to have a negative effect on membrane erythrocyte deformability [287].

Our results further suggested that cell shape influenced the dynamic adhesion behavior. The infected erythrocyte shape was described to be comparable for HbAA- and HbAS-iRBCs at the beginning of the intraerythrocytic cycle, with a reduced volumes of 0.63 and 0.58, respectively [20]. Reduced volume is defined as the ratio of a cell volume to the volume of a sphere with the same surface area; thus a reduce volume of 1 indicates a complete round object [20]. As the parasites mature, the reduced volume increased up to 0.99 and 0.76 for HbAA- and HbAS-iRBCs at the schizont stage [20]. This indicates an increase of the cell sphericity for both groups at the end of the intraerythrocytic cycle, however not to the same extent. The characteristic sphericity observed for HbAA-iRBCs schizonts comes from a combination of the large stiff intracellular parasite and the erythrocyte swelling due to $NaCl^{-}$ influx accompanied by water via the new permeation pathways [251]. Our results showed that NPP were delayed in HbAS-iRBCs, which might contribute to the non-spherical schizonts [288]. Moreover, intracellular Ca^{2+} concentrations are elevated in HbS erythrocytes [277], consequently leading to activation of the Ca^{2+}

dependent Gardos channel. This event leads to the loss of K^+, Cl^- ions and accompanied water, provoking the red blood cell to dehydrate and shrink, thus impeding the cells from becoming spherical [280]. By not reaching a round shape and presenting reduced knob densities, HbAS-iRBCs prevent the smooth rolling behavior observed for infected wild type erythrocytes at the schizont stage.

Our experimental observations regarding the dynamic adhesion behavior for infected HbAS erythrocytes were similarly predicted by computational simulations using erythrocytes with decreased knob density and increased membrane bending rigidity [254]. These observations revealed the importance of knob density and cell rigidity in the iRBCs adhesion dynamics and predicted reduced contact areas and contact times for HbAS-iRBCs at both developmental stages [254]. This in turn might not only reduce the binding capabilities under flow conditions, but also decrease the probability of activating endothelial cells, since endothelial cell activation depends on the number of interactions and duration of the contact [289][166][290].

Moreover, the transition from trophozoite to schizont was accompanied by a reduced adhesive contact surface area of iRBCs to the substratum. Previous studies suggested that elasticity and shape at the trophozoites stage facilitates adhesion by enabling a larger contact area with the substratum, which leads to a greater binding strength required by *P. falciparum*-infected erythrocytes to resist shear stress encountered in the microvasculature [291]. On the contrary, more spherical and stiffer cells such as schizonts have reduced contact areas with the substratum, consequently leading to reduced binding strengths [291]. These assumptions are supported by simulations where larger contact areas were shown for trophozoites compared to schizonts, which may be critical since trophozoites are physiologically the parasitic stage that dynamically adhere and sequester within the deep microvasculature.

4.3. Strong binding population of infected HbAS erythrocytes

The binding strength of an infected erythrocyte to microvascular endothelial cells will determine the ability of these cells to resist shear stress encountered in the microvasculature and to remain adherent. A recent study, based on laser pulse detachment, compared the biding strength of infected HbAA and HbAS erythrocytes

to CD36 or ICAM-1 (Fröhlich B., 2018, personal communications). The results showed reduced adhesion strengths for infected hemoglobinopathic erythrocytes to both receptors at a population level when cells were bound under static conditions. This effect was probably the consequence of reduced PfEMP-1 expression levels, altered PfEMP-1 and reduced knob densities display on the infected hemoglobinopathic erythrocyte surface. Under static conditions all infected erythrocytes sediment by gravity and adhere to the endothelium in a weak or strong manner, depending on the adhesive and mechanical properties of the infected erythrocytes. Therefore, this technique allows quantifying the overall binding strength of infected erythrocytes present in a population.

Under flow conditions, fewer infected erythrocytes might adhere. Only those that present the optimal adhesive and mechanical properties will be able to firmly adhere. Therefore, infected erythrocytes that are able to remain adherent under flow conditions, might show stronger binding that those that were not capable of adhering. Our results showed that fewer infected hemoglobinopathic erythrocytes bound to microvascular endothelial cells under flow, but however they adhered with comparable strengths as infected wild-type erythrocytes. These results suggested the presence of a population of strong binding infected hemoglobinopathic erythrocytes and a population of weak binding infected erythrocytes. In agreement with our observations, earlier studies suggested the existence of different infected HbAS and HbAC erythrocyte populations based on knob density and PfEMP-1 surface expression levels [203][214]. Those studies revealed that a fraction of infected HbAS and HbAC showed similar knob densities which resembled those HbAA-iRBCs in terms of knob morphology and distribution. In contrast, the other remaining iRBCs fraction presented reduced amount of knobs with an abnormal morphology and distribution [203][214]. The differences between these subpopulations was attributed to the age of the hemoglobinopathic erythrocyte, since the knob density and morphology of older hemoglobinopathic cells were more affected [214]. Such strong binding subpopulations may contribute to chronic infection, since these parasitized erythrocytes are not cleared from the circulation by the spleen, unlike the non-adhering cells (weak binders). This observation helps explain the development of substantial parasite densities in HbAS and HbAC individuals infected with *P. falciparum*.

Nevertheless, future comparative studies are required in order to provide a deep insight in to the main differences between these two distinct populations. It is thought however, that even though infected HbAS erythrocytes adhered under flow and bound strong enough to prevent detachment from the endothelium, these cells still presented altered adhesive and mechanical properties which might impede the proper interaction with endothelial cell ligands, thus leading to reduced endothelial cell activation. Indeed, endothelial cell activation was reduced under static and flow conditions for infected HbAS erythrocytes, despite the binding of several iRBCs to a major proportion of the endothelial cell layer.

4.4. Reduced endothelial cell activation by infected HbAS erythrocytes

Endothelial cell activation has been associated with disease severity as a direct consequence of *P. falciparum* binding. Binding of infected erythrocytes to HUVEC can increase the levels of ICAM-1 cell surface expression and IL-6 secretion [165]. The induced prolonged increased expression of ICAM-1 can promote cytoadhesion of following parasite generations, thus inducing a state of hyperadhesiveness [165]. Our data support these previous observations and showed that both ICAM-1 surface expression and IL-6 secretion in HDMEC is induced by infected erythrocyte binding.

The activation of different signaling pathways in endothelial cells upon infected erythrocyte contact, seems to depend on the binding avidity of the PfEMP-1 to endothelial cell receptors [289][166] and has been shown to occur in a time and dose dependent manner [290][292]. It is thought that ICAM-1 binding induces ICAM-1 surface expression through the NF-κB pathway. ICAM-1 ligation by leukocytes or linking antibodies induced the upregulation of ICAM-1 cell surface expression [292]. Interestingly, NF-κB signaling was shown to be induced by *P. falciparum*-iRBCs, where the NF-κB p65 subunit almost completely translocates into the nucleus shortly after direct interaction between infected erythrocyte and endothelial cells [290].

Moreover, NF-κB p65 nuclear translocation as a consequence of parasite binding results in increased ICAM-1 surface expression [290], further suggesting that this signaling pathway might be involved in ICAM-1 expression. Similarly, IL-6 secreted

by endothelial cells after iRBC binding [165] might also be induced via NF-κB nuclear translocation [176][165][171].

Our results indeed showed an increase of ICAM-1 endothelial surface expression, IL-6 secretion and NF-κB nuclear translocation upon binding of iRBCs. Under static and flow conditions infected HbAS erythrocytes activated HDMEC to a lesser extent unlike infected wild-type erythrocytes. By displaying reduced PfEMP-1 levels these infected hemoglobinopathic erythrocytes could weaken the binding interactions to endothelial receptors [202] leading to a reduced receptor engagement and reduced probability of fully activating the endothelial cells. Furthermore, morphologically abnormal knobs might not present PfEMP-1 molecules in the ideal orientations, required for optimal binding to different receptors [202]. A reduced contact area and contact time predicted for HbAS-iRBCs might also impede full interaction and engagement to host cytoadherence receptors.

As previously suggested, the pathogenesis of severe malaria is likely to be a multi-factorial process involving microvascular sequestration and endothelial activation [189]. Through reduced and abnormal presentation of PfEMP-1, infected HbAS erythrocytes not only decrease the vascular lumen obstruction by reducing adhesion under flow, but also mitigate the inflammatory response. By reducing the activation of microvascular endothelial cells and the subsequent expression of endothelial adhesion receptors such as ICAM-1, hemoglobinopathic erythrocytes might prevent the development of a hyperadhesiveness state. Furthermore, reduced activation could also decrease the production of pro-inflammatory cytokines, such as IL-6, which is known to increase the binding strength to CD36 by promoting its ecto-domain dephosphorylation via AP activity on the endothelial cells [172]. However, other endothelial cell responses to the binding of infected erythrocytes should also further be investigated such as binding strengthening, endothelial dysfunction and loss of barrier integrity.

Our results lead us to propose a model for protection against severe malaria whereby reduced adhesiveness and altered mechanical properties interfere with infected hemoglobinopathic erythrocytes host interactions. This leads to irregular dynamic adhesion and a subsequent reduction in firm adhesion, which prevents the binding

and obstruction of microvessels in vital organs, by high numbers of infected erythrocytes. A fraction of infected erythrocytes can however bind under flow conditions and remains adherent, thus promoting the development of substantial parasite densities. In comparison to wild-type erythrocytes, this infected HbAS erythrocyte fraction has different adhesion and mechanical properties which affects host-pathogen interactions and leads to reduced endothelial cell activation. This in turn mitigates the life-threatening inflammatory response exerted by infected wild-type erythrocytes thereby avoiding the development of severe forms of the disease.

Overall, impaired adhesiveness, increased cell rigidity and morphological differences contribute to strong differences in the dynamic adhesion behavior of HbAS-iRBCs. The attenuation of parasite-host interactions during the *P. falciparum* intraerythrocytic stage not only attenuates microvascular obstruction, but also diminishes the activation of microvascular endothelial cells. These events might collaborate to prevent the development of severe malaria symptoms. Our results provide a further understanding of the complex mechanism of protection against severe malaria by sickle trait hemoglobin. Similar results observed for infected HbC erythrocytes regarding adhesive and erythrocyte mechanical properties suggests a common mechanism of protection against severe malaria by HbS and HbC variants. However, further studies on HbAC and HbCC erythrocytes should be performed to confirm this idea. Understanding the relevant pathophysiological processes leading to severe malaria will encourage the development of new strategies for future clinical interventions.

In summary, our data shows that differential dynamic behavior and firm adhesion of infected HbAS and HbAC erythrocytes results in reduced endothelial cell activation, supporting the model of HbAS and HbAC protecting against severe malaria by elucidating a milder inflammatory response and causing reduced microvascular obstruction.

5. Conclusions and Outlook

The present work shows significant differences in both firm and dynamic adhesion of infected hemoglobinopathic erythrocytes and the subsequent attenuation of endothelial cell activation. Our results further suggested the existence of two populations of infected hemoglobinopathic erythrocytes based on the adhesive capabilities. The fraction of strong binding infected erythrocytes which were able to adhere to microvascular endothelial cells under flow conditions, may contribute to chronic infection and permit sickle cell trait and hemoglobin C individuals to develop substantial parasitemia during a *P. falciparum* malaria episode. On the other hand, the weak binding infected erythrocytes might benefit the host by largely contributing to the decreasing vascular obstruction and endothelial activation.

The major challenge to study these two distinct iRBCs binding populations, is to separate them. Attempts to collect the strong binders by washing them off from the endothelial monolayer after initial binding were unsuccessful due to cell lysis and contamination of the cell pellet with cellular debris from both endothelial cells and infected erythrocytes. Therefore, a methodology that allows separating infected erythrocytes according to their binding capabilities is needed. Following previous publications [293], a microfluidic cell-sorting chamber is currently being developed in our group and will be used to separate the heterogeneous population of infected hemoglobinopathic erythrocytes, according to their binding capabilities. In this device, the adhesion receptors such as ICAM-1 or CD36, will be imprinted on a glass surface by micro-contact printing, creating an adhesion receptor pattern of periodic stripes inclined at specific angles intercalated with BSA-passivated non-adhesive zones. Infected erythrocytes might be able to roll on and follow the direction of receptor stripes, resulting in the adherent cell separation from the non-adherent group. Previous simulations have predicted that infected erythrocytes with high PfEMP-1 levels will have larger rolling displacement towards the upper channel, whereas, cells with low levels of PfEMP-1 will roll poorly, causing them to stay in the lower part of the channel [294]. After separation, infected erythrocyte populations can be characterized according to knob density, distribution and morphology, cell shape and mechanical properties. Moreover, the binding capabilities, binding strength and endothelial cell activation of these iRBCs populations can be investigated using

established techniques including AFM-SCFS to study iRBCs binding strength and adhesion strengthening at a single cell level.

References

[1] F. J. Walburn and D. J. Schneck, “A constitutive equation for whole human blood.,” *Biorheology*, vol. 13, no. 3, pp. 201–10, Jun. 1976.

[2] O. K. Baskurt and H. J. Meiselman, “Blood Rheology and Hemodynamics,” *Seminars in Thrombosis and Hemostasis*, vol. 29, no. 5. pp. 435–450, Oct-2003.

[3] S. Chien and L. A. Sung, “Physicochemical basis and clinical implications of red cell aggregation,” *Clin. Hemorheol. Microcirc.*, vol. 7, no. 1, pp. 71–91, Dec. 2016.

[4] V. V Tuchin, “Handbook of Optical Sensing of Glucose in Biological Fluids and Tissues,” *Handb. Opt. Sens. Glucose Biol. Fluids Tissues Ser. Med. Phys. Biomed. Eng.*, p. 419, 2009.

[5] Y. C. Fung, *Mechanical Properties of Living Tissues*. Springer-Verlag, 1981.

[6] Y. Kim, K. Kim, and Y. Park, “Measurement Techniques for Red Blood Cell Deformability: Recent Advances.”

[7] G. Tomaiuolo, “Biomechanical properties of red blood cells in health and disease towards microfluidics,” *Biomicrofluidics*, vol. 8, no. 5, p. 51501, Sep. 2014.

[8] A. Fridman and G. Friedman, *Plasma Medicine*. John Wiley & Sons, 2013.

[9] T. Kanias and J. P. Acker, “Biopreservation of red blood cells - The struggle with hemoglobin oxidation,” *FEBS Journal*, vol. 277, no. 2. Blackwell Publishing Ltd, pp. 343–356, 01-Jan-2010.

[10] G. A. Barabino, M. O. Platt, and D. K. Kaul, “Sickle Cell Biomechanics,” *Annu. Rev. Biomed. Eng.*, vol. 12, no. 1, pp. 345–367, Jul. 2010.

[11] M. Diez-Silva, M. Dao, J. Han, C.-T. Lim, and S. Suresh, “Shape and Biomechanical Characteristics of Human Red Blood Cells in Health and Disease,” *MRS Bull.*, vol. 35, no. 5, pp. 382–388, May 2010.

[12] B. M. Cooke, N. Mohandas, and R. L. Coppel, “The malaria-infected red blood cell: structural and functional changes.,” *Adv. Parasitol.*, vol. 50, pp. 1–86, 2001.

[13] I. W. Sherman, *Molecular approaches to malaria*, 1st ed. Washington, DC: American Society for Microbiology, 2005.

[14] A. Molina-Cruz *et al.*, “Some strains of {Plasmodium} falciparum, a human

malaria parasite, evade the complement-like system of {Anopheles} gambiae mosquitoes," *Proc. Natl. Acad. Sci. U. S. A.*, vol. 109, no. 28, pp. E1957--E1962, 2012.

[15] L. A. Cormier and P. E. (Pauline E. Jolly, *The primate zoonoses : culture change and emerging diseases*. 2018.

[16] "WHO | World Malaria Report 2016," *WHO*, 2017.

[17] D. Shahinas, A. Folefoc, and D. R. Pillai, "Targeting Plasmodium falciparum Hsp90: Towards Reversing Antimalarial Resistance.," *Pathog. (Basel, Switzerland)*, vol. 2, no. 1, pp. 33–54, Feb. 2013.

[18] J. Chernin, *Parasitology*. Taylor & Francis, 2000.

[19] A. F. Cowman, J. Healer, D. Marapana, and K. Marsh, "Malaria: Biology and Disease," *Cell*, vol. 167, no. 3, pp. 610–624, 2016.

[20] M. Waldecker *et al.*, "Differential time-dependent volumetric and surface area changes and delayed induction of new permeation pathways in *P. falciparum* -infected hemoglobinopathic erythrocytes," *Cell. Microbiol.*, vol. 19, no. 2, p. e12650, Feb. 2017.

[21] P. S. Gomes, J. Bhardwaj, J. Rivera-Correa, C. G. Freire-De-Lima, and A. Morrot, "Immune Escape Strategies of Malaria Parasites.," *Front. Microbiol.*, vol. 7, p. 1617, 2016.

[22] D. G. Bowen and C. M. Walker, "Mutational escape from CD8+ T cell immunity: HCV evolution, from chimpanzees to man.," *J. Exp. Med.*, vol. 201, no. 11, pp. 1709–1714, Jun. 2005.

[23] A. L. DeFranco, R. M. Locksley, and M. Robertson, *Immunity : the immune response in infectious and inflammatory disease*. New Science Press, 2007.

[24] B. Autino, Y. Corbett, F. Castelli, and D. Taramelli, "Pathogenesis of malaria in tissues and blood," *Mediterr. J. Hematol. Infect. Dis.*, vol. 4, no. 1, 2012.

[25] I. A. Clark and W. B. Cowden, "The pathophysiology of falciparum malaria," *Pharmacol. Ther.*, vol. 99, no. 2, pp. 221–260, Aug. 2003.

[26] L. H. Miller, D. I. Baruch, K. Marsh, and O. K. Doumbo, "The pathogenic basis of malaria," *Nature*, vol. 415, no. 6872, pp. 673–679, 2002.

[27] G. Krishnegowda *et al.*, "Induction of proinflammatory responses in macrophages by the glycosylphosphatidylinositols of Plasmodium falciparum: Cell signaling receptors, glycosylphosphatidylinositol (GPI) structural requirement, and regulation of GPI activity," *J. Biol. Chem.*, vol. 280, no. 9, pp. 8606–8616, Mar. 2005.

[28] W.-C. Teng, H. H. Kiat, R. Suwanarusk, and H. L. Koh, *Medicinal plants and malaria : applications, trends, and prospects*. 2016.

[29] L. H. Bannister and I. W. Sherman, “Plasmodium,” in *Encyclopedia of Life Sciences*, Chichester, UK: John Wiley & Sons, Ltd, 2009.

[30] M. C. Bruce, P. Alano, S. Duthie, and R. Carter, “Commitment of the malaria parasite Plasmodium falciparum to sexual and asexual development.,” *Parasitology*, vol. 100 Pt 2, pp. 191–200, Apr. 1990.

[31] U. Kishore, *Target pattern recognition in innate immunity*. Springer Science+Business Media, 2009.

[32] K. Marsh *et al.*, “Indicators of Life-Threatening Malaria in African Children,” *N. Engl. J. Med.*, vol. 332, no. 21, pp. 1399–1404, 1995.

[33] A. M. Dondorp *et al.*, “Direct In Vivo Assessment of Microcirculatory Dysfunction in Severe Falciparum Malaria,” *J. Infect. Dis.*, vol. 197, no. 1, pp. 79–84, 2008.

[34] M. E. Molyneux, T. E. Taylor, J. J. Wirimaf, and A. Borgsteinj, “Clinical Features and Prognostic Indicators in Paediatric Cerebral Malaria: A Study of 131 Comatose Malawian Children,” *Q. J. Med. New Ser.*, vol. 71, no. 265, pp. 441–459, 1989.

[35] D. Waller *et al.*, “Clinical features and outcome of severe malaria in Gambian children.,” *Clin. Infect. Dis.*, vol. 21, no. 3, pp. 577–87, Sep. 1995.

[36] E. Schmutzhard and F. Gerstenbrand, “Cerebral malaria in Tanzania. Its epidemiology, clinical symptoms and neurological long term sequelae’ in the light of 66 cases,” *Trans. R. Soc. Trop. Med. Hyg.*, vol. 78, pp. 351–353, 1984.

[37] D. R. Brewster, D. Kwiatkowski, and N. J. White, “Neurological sequelae of cerebral malaria in children.,” *Lancet (London, England)*, vol. 336, no. 8722, pp. 1039–43, Oct. 1990.

[38] L. A. Salako, A. Sowunmil, and F. S. Bondi, “Prognostic risk factors and post mortem findings in cerebral malaria in children,” *Trans. R. Soc. Trop. Med. Hyg.*, vol. 86, 1992.

[39] G. G. MacPherson, M. J. Warrell, N. J. White, S. Looareesuwan, and D. A. Warrell, “Human cerebral malaria. A quantitative ultrastructural analysis of parasitized erythrocyte sequestration.,” *Am. J. Pathol.*, vol. 119, no. 3, pp. 385–401, Jun. 1985.

[40] M. Fried and P. E. Duffy, “Adherence of Plasmodium falciparum to Chondroitin Sulfate A in the Human Placenta,” *Science (80-.).*, vol. 272, no. 5267, pp.

1502–1504, Jun. 1996.

[41] A. M. Dondorp, E. Pongponratn, and N. J. White, “Reduced microcirculatory flow in severe falciparum malaria: pathophysiology and electron-microscopic pathology.,” *Acta Trop.*, vol. 89, no. 3, pp. 309–17, Feb. 2004.

[42] D. I. Baruch, S. J. Rogerson, and B. M. Cooke, “Asexual blood stages of malaria antigens: cytoadherence.,” *Chem. Immunol.*, vol. 80, pp. 144–162, 2002.

[43] J. Connor, C. C. Pak, and A. J. Schroit, “Exposure of Phosphatidylserine in the Outer Leaflet of Human Red Blood Cells: Relationship to Cell Density, Cell Age, and Clearance by Mononuclear Cells,” *J. Biol. Chem.*, vol. 269, no. 4, pp. 2399–2404, Jan. 1994.

[44] R. E. Mebius and G. Kraal, “Structure and function of the spleen,” *Nat. Rev. Immunol.*, vol. 5, no. 8, pp. 606–616, Aug. 2005.

[45] J. A. Rowe, A. Claessens, R. A. Corrigan, and M. Arman, “Adhesion of Plasmodium falciparum-infected erythrocytes to human cells: molecular mechanisms and therapeutic implications,” *Expert Rev. Mol. Med.*, vol. 11, no. May, p. e16, 2009.

[46] K. Mohan, M. L. Dubey, N. K. Ganguly, and R. C. Mahajan, “Plasmodium falciparum: Role of Activated Blood Monocytes in Erythrocyte Membrane Damage and Red Cell Loss during Malaria,” *Exp. Parasitol.*, vol. 80, no. 1, pp. 54–63, Feb. 1995.

[47] A. M. Dondorp, F. Omodeo-Salè, K. Chotivanich, D. Taramelli, and N. J. White, “Oxidative stress and rheology in severe malaria.,” *Redox Rep.*, vol. 8, no. 5, pp. 292–4, Oct. 2003.

[48] A. M. Dondorp *et al.*, “Prognostic significance of reduced red blood cell deformability in severe falciparum malaria.,” *Am. J. Trop. Med. Hyg.*, vol. 57, no. 5, pp. 507–11, Nov. 1997.

[49] A. P. Gomes, R. Vitorino, A. Pina Costa, E. G. Mendonça, M. G. de A. Oliveira, and R. Siqueira-Batista, “Malária grave por Plasmodium falciparum,” *Rev Bras Ter Intensiva*, vol. 23, no. 3, pp. 358–369, Sep. 2011.

[50] T. Planche, A. Dzeing, E. Ngou-Milama, M. Kombila, and P. W. Stacpoole, “Metabolic complications of severe malaria.,” *Curr. Top. Microbiol. Immunol.*, vol. 295, pp. 105–36, 2005.

[51] M. J. B. John E. Bennett, Raphael Dolin, “Principles and Practice of Infectious Diseases,” *Elsevier Saunders*, p. 19103, 2015.

[52] N. Kilian *et al.*, “Hemoglobin S and C affect protein export in Plasmodium falciparum-infected erythrocytes.,” *Biol. Open*, vol. 4, no. 3, pp. 400–10, Feb. 2015.

[53] P. H. David, S. M. Handunnetti, J. H. Leech, P. Gamage, and K. N. Mendis, “Rosetting: A new cytoadherence property of malaria-infected erythrocytes,” *Am. J. Trop. Med. Hyg.*, vol. 38, no. 2, pp. 289–297, Mar. 1988.

[54] K. W. Deitsch and L. Hviid, “Variant surface antigens, virulence genes and the pathogenesis of malaria,” *Trends in Parasitology*, vol. 20, no. 12. pp. 562–566, Dec-2004.

[55] N. D. Pasternak and R. Dzikowski, “PfEMP1: An antigen that plays a key role in the pathogenicity and immune evasion of the malaria parasite Plasmodium falciparum,” *Int. J. Biochem. Cell Biol.*, vol. 41, no. 7, pp. 1463–1466, 2009.

[56] H. M. Taylor, S. A. Kyes, and C. I. Newbold, “Var gene diversity in Plasmodium falciparum is generated by frequent recombination events,” *Mol. Biochem. Parasitol.*, vol. 110, no. 2, pp. 391–397, Oct. 2000.

[57] N. Rasti, M. Wahlgren, and Q. Chen, “Molecular aspects of malaria pathogenesis,” *FEMS Immunology and Medical Microbiology*, vol. 41, no. 1. pp. 9–26, 01-May-2004.

[58] S. S. Oh *et al.*, “Plasmodium falciparum erythrocyte membrane protein 1 is anchored to the actin-spectrin junction and knob-associated histidine-rich protein in the erythrocyte skeleton,” *Mol. Biochem. Parasitol.*, vol. 108, no. 2, pp. 237–247, May 2000.

[59] J. D. Smith, G. Subramanian, B. Gamain, D. I. Baruch, and L. H. Miller, “Classification of adhesive domains in the Plasmodium falciparum Erythrocyte Membrane Protein 1 family,” *Mol. Biochem. Parasitol.*, vol. 110, no. 2, pp. 293–310, Oct. 2000.

[60] D. I. Baruch, J. A. Gormely, C. Ma, R. J. Howard, and B. L. Pasloske, “Plasmodium falciparum erythrocyte membrane protein 1 is a parasitized erythrocyte receptor for adherence to CD36, thrombospondin, and intercellular adhesion molecule 1.,” *Proc. Natl. Acad. Sci. U. S. A.*, vol. 93, no. 8, pp. 3497–502, 1996.

[61] J. G. Beeson and G. V. Brown, “Pathogenesis of Plasmodium falciparum malaria: The roles of parasite adhesion and antigenic variation,” *Cell. Mol. Life Sci.*, vol. 59, no. 2, pp. 258–271, 2002.

[62] A. Craig and A. Scherf, “Molecules on the surface of the Plasmodium

falciparum infected erythrocyte and their role in malaria pathogenesis and immune evasion," *Mol. Biochem. Parasitol.*, vol. 115, no. 2, pp. 129–143, 2001.

[63] L. Turner *et al.*, "Severe malaria is associated with parasite binding to endothelial protein C receptor," *Nature*, vol. 498, no. 7455, pp. 502–505, Jun. 2013.

[64] A. M. Senczuk, J. C. Reeder, M. M. Kosmala, and M. Ho, "Plasmodium falciparum erythrocyte membrane protein 1 functions as a ligand for P-selectin," *Blood*, vol. 98, no. 10, pp. 3132–3135, Nov. 2001.

[65] Q. Chen *et al.*, "Developmental selection of var gene expression in Plasmodium falciparum," *Nature*, vol. 394, no. 6691, pp. 392–395, Jul. 1998.

[66] A. Scherf *et al.*, "Antigenic variation in malaria: In situ switching, relaxed and mutually exclusive transcription of var genes during intra-erythrocytic development in Plasmodium falciparum," *EMBO J.*, vol. 17, no. 18, pp. 5418–5426, Sep. 1998.

[67] D. J. Roberts *et al.*, "Rapid switching to multiple antigenic and adhesive phenotypes in malaria," *Nature*, vol. 357, no. 6380, pp. 689–692, Jun. 1992.

[68] K. W. Deitsch, E. R. Moxon, and T. E. Wellems, "Shared themes of antigenic variation and virulence in bacterial, protozoal, and fungal infections.," *Microbiol. Mol. Biol. Rev.*, vol. 61, no. 3, pp. 281–293, Sep. 1997.

[69] S. a Frank, "Immunology and Evolution of Infectious Disease," *Heal. San Fr.*, vol. 300, no. 5617, p. 358, 2002.

[70] J. D. Smith *et al.*, "Analysis of adhesive domains from the A4VAR Plasmodium falciparum erythrocyte membrane protein-1 identifies a CD36 binding domain," *Mol. Biochem. Parasitol.*, vol. 97, no. 1–2, pp. 133–148, Nov. 1998.

[71] D. I. Baruch, X. C. Ma, H. B. Singh, X. Bi, B. L. Pasloske, and R. J. Howard, "Identification of a region of PfEMP1 that mediates adherence of Plasmodium falciparum infected erythrocytes to CD36: conserved function with variant sequence.," *Blood*, vol. 90, no. 9, pp. 3766–75, Nov. 1997.

[72] B. A. Robinson, T. L. Welch, and J. D. Smith, "Widespread functional specialization of Plasmodium falciparum erythrocyte membrane protein 1 family members to bind CD36 analysed across a parasite genome," *Mol. Microbiol.*, vol. 47, no. 5, pp. 1265–1278, Mar. 2003.

[73] J. D. Smith, J. A. Rowe, M. K. Higgins, and T. Lavstsen, "Malaria's deadly grip: Cytoadhesion of Plasmodium falciparum-infected erythrocytes," *Cell. Microbiol.*, vol. 15, no. 12, pp. 1976–1983, 2013.

[74] A. Mayor *et al.*, “Receptor-binding residues lie in central regions of Duffy-binding-like domains involved in red cell invasion and cytoadherence by malaria parasites,” *Blood*, vol. 105, no. 6, pp. 2557–2563, Mar. 2005.

[75] P. A. Buffet *et al.*, “Plasmodium falciparum domain mediating adhesion to chondroitin sulfate A: A receptor for human placental infection,” *Proc. Natl. Acad. Sci.*, vol. 96, no. 22, pp. 12743–12748, Oct. 1999.

[76] B. Gamain *et al.*, “Identification of a 67-amino-acid region of the Plasmodium falciparum variant surface antigen that binds chondroitin sulphate A and elicits antibodies reactive with the surface of placental isolates,” *Mol. Microbiol.*, vol. 53, no. 2, pp. 445–455, Jun. 2004.

[77] I. Udeinya, J. Schmidt, M. Aikawa, L. Miller, and I. Green, “Falciparum malaria-infected erythrocytes specifically bind to cultured human endothelial cells,” *Science (80-.).*, vol. 213, no. 4507, pp. 555–557, Jul. 1981.

[78] R. S. Bray and R. E. Sinden, “The sequestration of plasmodium falciparum infected erythrocytes in the placenta,” *Trans. R. Soc. Trop. Med. Hyg.*, vol. 73, no. 6, pp. 716–719, 1979.

[79] M. Wahlgren, J. Carlson, R. Udomsangpetch, and P. Perlmann, “Why do Plasmodium falciparumm-infected erythrocytes form spontaneous erythrocyte rosettes?,” *Parasitol. Today*, vol. 5, no. 6, pp. 183–185, May 1989.

[80] A. Pain *et al.*, “Platelet-mediated clumping of Plasmodium falciparum-infected erythrocytes is a common adhesive phenotype and is associated with severe malaria,” *Proc. Natl. Acad. Sci.*, vol. 98, no. 4, pp. 1805–1810, Feb. 2001.

[81] R. L. Silverstein and M. Febbraio, “CD36, a scavenger receptor involved in immunity, metabolism, angiogenesis, and behavior,” *Science Signaling*, vol. 2, no. 72. NIH Public Access, p. re3, 26-May-2009.

[82] D. E. Greenwalt, R. H. Lipsky, C. F. Ockenhouse, H. Ikeda, N. N. Tandon, and G. a Jamieson, “Membrane glycoprotein CD36: a review of its roles in adherence, signal transduction, and transfusion medicine.,” *Blood*, vol. 80, no. 5, pp. 1105–1115, 1992.

[83] D. I. Baruch, X. C. Ma, B. Pasloske, R. J. Howard, and L. H. Miller, “CD36 peptides that block cytoadherence define the CD36 binding region for Plasmodium falciparum-infected erythrocytes.,” *Blood*, vol. 94, no. 6, pp. 2121–2127, Sep. 1999.

[84] C. Newbold *et al.*, “Receptor-specific adhesion and clinical disease in Plasmodium falciparum,” *Am. J. Trop. Med. Hyg.*, vol. 57, no. 4, pp. 389–398,

Oct. 1997.

[85] J. D. Chulay, H. K. Webster, and N. N. Tandon, “Molecular basis of sequestration in severe and uncomplicated plasmodium falciparum malaria: Differential adhesion of infected erythrocytes to cd36 and icam-1,” *J. Infect. Dis.*, vol. 164, no. 1, pp. 163–169, Jul. 1991.

[86] M. Ho, B. Singh, S. Looareesuwan, T. M. E. Davis, D. Bunnag, and N. J. White, “Clinical correlates of in vitro Plasmodium falciparum cytoadherence,” *Infect. Immun.*, vol. 59, no. 3, pp. 873–878, 1991.

[87] A. Pain *et al.*, “A non-sense mutation in Cd36 gene is associated with protection from severe malaria,” *Lancet*, vol. 357, no. 9267, pp. 1502–1503, May 2001.

[88] K. Omi *et al.*, “CD36 polymorphism is associated with protection from cerebral malaria.,” *Am. J. Hum. Genet.*, vol. 72, no. 2, pp. 364–374, Feb. 2003.

[89] R. Rothlein, M. L. Dustin, S. D. Marlin, and T. A. Springer, “A human intercellular adhesion molecule (ICAM-1) distinct from LFA-1.,” *J. Immunol.*, vol. 137, no. 4, pp. 1270–1274, Aug. 1986.

[90] S. Moncada and A. Higgs, *The vascular endothelium. I*. Springer, 2006.

[91] D. C. Hess, T. Bhutwala, J. C. Sheppard, W. Zhao, and J. Smith, “ICAM-1 expression on human brain microvascular endothelial cells.,” *Neurosci. Lett.*, vol. 168, no. 1–2, pp. 201–4, Feb. 1994.

[92] V. R. Preedy, *Adhesion molecules*. Science Publishers, 2010.

[93] A. R. Berendt *et al.*, “The binding site on ICAM-1 for Plasmodium falciparum-infected erythrocytes overlaps, but is distinct from, the LFA-1-binding site.,” *Cell*, vol. 68, no. 1, pp. 71–81, Jan. 1992.

[94] L. B. Ochola *et al.*, “Specific Receptor Usage in Plasmodium falciparum Cytoadherence Is Associated with Disease Outcome,” *PLoS One*, vol. 6, no. 3, p. e14741, Mar. 2011.

[95] K. Silamut *et al.*, “A quantitative analysis of the microvascular sequestration of malaria parasites in the human brain,” *Am. J. Pathol.*, vol. 155, no. 2, pp. 395–410, Aug. 1999.

[96] G. D. Turner *et al.*, “An immunohistochemical study of the pathology of fatal malaria. Evidence for widespread endothelial activation and a potential role for intercellular adhesion molecule-1 in cerebral sequestration.,” *Am. J. Pathol.*, vol. 145, no. 5, pp. 1057–69, Nov. 1994.

[97] J. G. Beeson, G. V. Brown, M. E. Molyneux, C. Mhango, F. Dzinjalamala, and

S. J. Rogerson, “Plasmodium falciparum isolates from infected pregnant women and children are associated with distinct adhesive and antigenic properties.,” *J. Infect. Dis.*, vol. 180, no. 2, pp. 464–72, Aug. 1999.

[98] C. Menendez, “Malaria during pregnancy: a priority area of malaria research and control.,” *Parasitol. Today*, vol. 11, no. 5, pp. 178–83, May 1995.

[99] J. G. Beeson *et al.*, “Adhesion of Plasmodium falciparum-infected erythrocytes to hyaluronic acid in placental malaria,” *Nat. Med.*, vol. 6, no. 1, pp. 86–90, Dec. 2000.

[100] N. K. Viebig *et al.*, “Disruption of Var2CSA gene impairs placental malaria associated adhesion phenotype,” *PLoS One*, vol. 2, no. 9, p. e910, Sep. 2007.

[101] B. J. Brabin, “An analysis of malaria in pregnancy in Africa.,” *Bull. World Health Organ.*, vol. 61, no. 6, pp. 1005–16, 1983.

[102] S. J. Rogerson, L. Hviid, P. E. Duffy, R. F. Leke, and D. W. Taylor, “Malaria in pregnancy: pathogenesis and immunity,” *Lancet Infectious Diseases*, vol. 7, no. 2. pp. 105–117, Feb-2007.

[103] J. G. Beeson *et al.*, “Adhesion of Plasmodium falciparum-infected erythrocytes to hyaluronic acid in placental malaria.,” *Nat. Med.*, vol. 6, no. 1, pp. 86–90, Jan. 2000.

[104] Z. Bian, G. Wang, X. Tian, and J. Fan, “Expression of Plasmodium falciparum-infected erythrocyte membrane protein from cerebral malaria patients.,” *Zhongguo Ji Sheng Chong Xue Yu Ji Sheng Chong Bing Za Zhi*, vol. 17, no. 6, pp. 359–362, 1999.

[105] R. Daneman, “The blood-brain barrier in health and disease,” *Ann. Neurol.*, vol. 72, no. 5, pp. 648–672, 2012.

[106] J. Alexandra Rowe, J. M. Moulds, C. I. Newbold, and L. H. Miller, “P. falciparum rosetting mediated by a parasite-variant erythrocyte membrane protein and complement-receptor 1,” *Nature*, vol. 388, no. 6639, pp. 292–295, Jul. 1997.

[107] C. W. Wang and L. Hviid, “Rifins, rosetting, and red blood cells,” *Trends in Parasitology*, vol. 31, no. 7. pp. 285–286, Jul-2015.

[108] I. A. Cockburn *et al.*, “A human complement receptor 1 polymorphism that reduces Plasmodium falciparum rosetting confers protection against severe malaria.,” *Proc. Natl. Acad. Sci. U. S. A.*, vol. 101, no. 1, pp. 272–7, Jan. 2004.

[109] A. Mayor *et al.*, “Association of severe malaria outcomes with platelet-mediated clumping and adhesion to a novel host receptor.,” *PLoS One*, vol. 6, no. 4, p.

e19422, Apr. 2011.

[110] D. J. Bridges *et al.*, “Rapid activation of endothelial cells enables Plasmodium falciparum adhesion to platelet-decorated von Willebrand factor strings,” *Blood*, vol. 115, no. 7, pp. 1472–1474, Feb. 2010.

[111] B. S. Crabb *et al.*, “Targeted Gene Disruption Shows That Knobs Enable Malaria-Infected Red Cells to Cytoadhere under Physiological Shear Stress,” *Cell*, vol. 89, no. 2, pp. 287–296, 1997.

[112] M. Aikawa *et al.*, “Membrane knobs of unfixed Plasmodium falciparum infected erythrocytes: New findings as revealed by atomic force microscopy and surface potential spectroscopy,” *Exp. Parasitol.*, vol. 84, no. 3, pp. 339–343, Dec. 1996.

[113] S. M. Marchenko and S. O. Sage, “Electrical properties of resting and acetylcholine-stimulated endothelium in intact rat aorta.,” *J. Physiol.*, vol. 462, pp. 735–51, Mar. 1993.

[114] M. Rug, S. W. Prescott, K. M. Fernandez, B. M. Cooke, and A. F. Cowman, “The role of KAHRP domains in knob formation and cytoadherence of P falciparum-infected human erythrocytes,” *Blood*, vol. 108, no. 1, pp. 370–378, 2006.

[115] K. A. Quadt *et al.*, “The Density of Knobs on Plasmodium falciparum-Infected Erythrocytes Depends on Developmental Age and Varies among Isolates,” *PLoS One*, vol. 7, no. 9, p. e45658, Sep. 2012.

[116] R. Subramani *et al.*, “Plasmodium falciparum-infected erythrocyte knob density is linked to the PfEMP1 variant expressed.,” *MBio*, vol. 6, no. 5, pp. e01456-15, Oct. 2015.

[117] J. Gruenberg, D. R. Allred, and I. W. Sherman, “Scanning electron microscope-analysis of the protrusions (knobs) present on the surface of Plasmodium falciparum-infected erythrocytes,” *J. Cell Biol.*, vol. 97, no. 3, pp. 795–802, Sep. 1983.

[118] N. Kriek *et al.*, “Characterization of the pathway for transport of the cytoadhereince- mediating protein, PfEMP1, to the host cell surface in malaria parasite-infected erythrocytes,” *Mol. Microbiol.*, vol. 50, no. 4, pp. 1215–1227, Nov. 2003.

[119] M. Lanzer, H. Wickert, G. Krohne, L. Vincensini, and C. Braun Breton, “Maurer’s clefts: A novel multi-functional organelle in the cytoplasm of Plasmodium falciparum-infected erythrocytes,” *Int. J. Parasitol.*, vol. 36, no. 1, pp. 23–36, 2006.

[120] M. Cyrklaff *et al.*, “Hemoglobins S and C Interfere with Actin Remodeling in Plasmodium falciparum-Infected Erythrocytes,” *Science (80-.).*, vol. 334, no. 6060, pp. 1283–1286, Dec. 2011.

[121] M. Cyrklaff, C. P. Sanchez, F. Frischknecht, and M. Lanzer, “Host actin remodeling and protection from malaria by hemoglobinopathies,” *Trends Parasitol.*, vol. 28, no. 11, pp. 479–485, Nov. 2012.

[122] J. M. Przyborski, H. Wickert, G. Krohne, and M. Lanzer, “Maurer’s clefts - A novel secretory organelle?,” *Mol. Biochem. Parasitol.*, vol. 132, no. 1, pp. 17–26, 2003.

[123] E. Mundwiler-Pachlatko and H.-P. Beck, “Maurer’s clefts, the enigma of Plasmodium falciparum,” *Proc. Natl. Acad. Sci.*, vol. 110, no. 50, pp. 19987–19994, 2013.

[124] G. Helms, A. K. Dasanna, U. S. Schwarz, and M. Lanzer, “Modeling cytoadhesion of Plasmodium falciparum-infected erythrocytes and leukocytes—common principles and distinctive features,” *FEBS Letters*, vol. 590, no. 13. pp. 1955–1971, Jul-2016.

[125] L. G. Pologe, A. Pavlovec, H. Shio, and J. V Ravetch, “Primary structure and subcellular localization of the knob-associated histidine-rich protein of Plasmodium falciparum.,” *Proc. Natl. Acad. Sci. U. S. A.*, vol. 84, no. 20, pp. 7139–7143, Oct. 1987.

[126] J.-P. Vernot-Hernandez and H.-G. Heidrich, “Time-course of synthesis, transport and incorporation of a protein identified in purified membranes of host erythrocytes infected with a knob-forming strain of Plasmodium falciparum,” *Mol. Biochem. Parasitol.*, vol. 12, no. 3, pp. 337–350, Jul. 1984.

[127] B. M. Cooke, F. K. Glenister, N. Mohandas, and R. L. Coppel, “Assignment of functional roles to parasite proteins in malaria-infected red blood cells by competitive flow-based adhesion assay,” *Br. J. Haematol.*, vol. 117, no. 1, pp. 203–211, Apr. 2002.

[128] P. Horrocks *et al.*, “PfEMP1 expression is reduced on the surface of knobless Plasmodium falciparum infected erythrocytes,” *J Cell Sci*, vol. 118, no. Pt 11, pp. 2507–2518, Jun. 2005.

[129] X. Pei, X. An, X. Guo, M. Tarnawski, R. Coppel, and N. Mohandas, “Structural and functional studies of interaction between Plasmodium falciparum knob-associated histidine-rich protein (KAHRP) and erythrocyte spectrin,” *J. Biol. Chem.*, vol. 280, no. 35, pp. 31166–31171, Sep. 2005.

[130] E. E. Cutts *et al.*, “Structural analysis of P. falciparum KAHRP and PfEMP1 complexes with host erythrocyte spectrin suggests a model for cytoadherent knob protrusions,” *PLoS Pathog.*, vol. 13, no. 8, p. e1006552, Aug. 2017.

[131] H. Weng *et al.*, “Interaction of Plasmodium falciparum knob-associated histidine-rich protein (KAHRP) with erythrocyte ankyrin R is required for its attachment to the erythrocyte membrane,” *Biochim. Biophys. Acta - Biomembr.*, vol. 1838, no. 1 PARTB, pp. 185–192, Jan. 2014.

[132] L. J. Bruce *et al.*, “A band 3-based macrocomplex of integral and peripheral proteins in the RBC membrane,” *Blood*, vol. 101, no. 10, pp. 4180–4188, May 2003.

[133] V. Bennett, “Ankyrins: Adaptors between diverse plasma membrane proteins and the cytoplasm,” *Journal of Biological Chemistry*, vol. 267, no. 13. pp. 8703–8706, 05-May-1992.

[134] K. L. Waller, B. M. Cooke, W. Nunomura, N. Mohandas, and R. L. Coppel, “Mapping the binding domains involved in the interaction between the Plasmodium falciparum knob-associated histidine-rich protein (KAHRP) and the cytoadherence ligand P. falciparum erythrocyte membrane protein 1 (PfEMP1),” *J. Biol. Chem.*, vol. 274, no. 34, pp. 23808–23813, Aug. 1999.

[135] A. Oberli *et al.*, “A Plasmodium falciparum PHIST protein binds the virulence factor PfEMP1 and comigrates to knobs on the host cell surface,” *FASEB J.*, vol. 28, no. 10, pp. 4420–4433, Oct. 2014.

[136] A. Oberli *et al.*, “Plasmodium falciparum Plasmodium helical interspersed subtelomeric proteins contribute to cytoadherence and anchor P. falciparum erythrocyte membrane protein 1 to the host cell cytoskeleton,” *Cell. Microbiol.*, vol. 18, no. 10, pp. 1415–1428, Oct. 2016.

[137] C. Magowan *et al.*, “Plasmodium falciparum histidine-rich protein 1 associates with the band 3 binding domain of ankyrin in the infected red cell membrane,” *Biochim. Biophys. Acta - Mol. Basis Dis.*, vol. 1502, no. 3, pp. 461–470, Nov. 2000.

[138] J. M. Watermeyer *et al.*, “A spiral scaffold underlies cytoadherent knobs in Plasmodium falciparum-infected erythrocytes,” *Blood*, vol. 127, no. 3, pp. 343–351, Jan. 2016.

[139] Y. Zhang *et al.*, “Multiple stiffening effects of nanoscale knobs on human red blood cells infected with *Plasmodium falciparum* malaria parasite,” *Proc. Natl. Acad. Sci.*, vol. 112, no. 19, pp. 6068–6073, May 2015.

[140] M. Paulitschke and G. B. Nash, “Membrane rigidity of red blood cells parasitized by different strains of Plasmodium falciparum.,” *J. Lab. Clin. Med.*, vol. 122, no. 5, pp. 581–9, Nov. 1993.

[141] F. K. Glenister, R. L. Coppel, A. F. Cowman, N. Mohandas, and B. M. Cooke, “Contribution of parasite proteins to altered mechanical properties of malaria-infected red blood cells,” *Blood*, vol. 99, no. 3, pp. 1060–1063, Feb. 2002.

[142] K. L. Waller *et al.*, “Interactions of Plasmodium falciparum erythrocyte membrane protein 3 with the red blood cell membrane skeleton.,” *Biochim. Biophys. Acta*, vol. 1768, no. 9, pp. 2145–56, Sep. 2007.

[143] M. Diez-Silva *et al.*, “Pf155/RESA protein influences the dynamic microcirculatory behavior of ring-stage Plasmodium falciparum infected red blood cells,” *Sci. Rep.*, vol. 2, p. 614, 2012.

[144] D. I. Baruch *et al.*, “Cloning the P. falciparum gene encoding PfEMP1, a malarial variant antigen and adherence receptor on the surface of parasitized human erythrocytes,” *Cell*, vol. 82, no. 1, pp. 77–87, Jul. 1995.

[145] X. zhuan Su *et al.*, “The large diverse gene family var encodes proteins involved in cytoadherence and antigenic variation of plasmodium falciparum-infected erythrocytes,” *Cell*, vol. 82, no. 1, pp. 89–100, Jul. 1995.

[146] G. B. Nash, E. O’Brien, E. C. Gordon-Smith, and J. A. Dormandy, “Abnormalities in the mechanical properties of red blood cells caused by Plasmodium falciparum.,” *Blood*, vol. 74, no. 2, pp. 855–61, 1989.

[147] G. W. Schmid-Schönbein, S. Usami, R. Skalak, and S. Chien, “The interaction of leukocytes and erythrocytes in capillary and postcapillary vessels,” *Microvasc. Res.*, vol. 19, no. 1, pp. 45–70, Jan. 1980.

[148] H. L. Goldsmith and S. Spain, “Margination of leukocytes in blood flow through small tubes,” *Microvasc. Res.*, vol. 27, no. 2, pp. 204–222, Mar. 1984.

[149] K. Ley, “Molecular mechanisms of leukocyte recruitment in the inflammatory process,” *Cardiovasc Res*, vol. 32, no. 4, pp. 733–742, Oct. 1996.

[150] H. W. Hou *et al.*, “Deformability based cell margination—A simple microfluidic design for malaria-infected erythrocyte separation,” *Lab Chip*, vol. 10, no. 19, p. 2605, Oct. 2010.

[151] D. N. Granger and E. Senchenkova, *Inflammation and the microcirculation*. Morgan & Claypool Life Sciences Publishers, 2010.

[152] K. L. Moore *et al.*, “P-selectin glycoprotein ligand-1 mediates rolling of human neutrophils on P-selectin.,” *J. Cell Biol.*, vol. 128, no. 4, pp. 661–71, Feb. 1995.

[153] P. Mehta, R. D. Cummings, and R. P. McEver, “Affinity and kinetic analysis of P-selectin binding to P-selectin glycoprotein ligand-1.,” *J. Biol. Chem.*, vol. 273, no. 49, pp. 32506–13, Dec. 1998.

[154] N. A. Raffler, J. Rivera-Nieves, and K. Ley, “L-selectin in inflammation, infection and immunity.”

[155] A. D. Luster, R. Alon, and U. H. von Andrian, “Immune cell migration in inflammation: present and future therapeutic targets,” *Nat. Immunol.*, vol. 6, no. 12, pp. 1182–1190, Dec. 2005.

[156] T. A. Springer, “Traffic signals for lymphocyte recirculation and leukocyte emigration: the multistep paradigm.,” *Cell*, vol. 76, no. 2, pp. 301–14, Jan. 1994.

[157] I. Mitroulis, V. I. Alexaki, I. Kourtzelis, A. Ziogas, G. Hajishengallis, and T. Chavakis, “Leukocyte integrins: role in leukocyte recruitment and as therapeutic targets in inflammatory disease.,” *Pharmacol. Ther.*, vol. 147, pp. 123–135, Mar. 2015.

[158] A. Zarbock, T. L. Deem, T. L. Burcin, and K. Ley, “Galphai2 is required for chemokine-induced neutrophil arrest.,” *Blood*, vol. 110, no. 10, pp. 3773–9, Nov. 2007.

[159] S. J. Rogerson, S. Novakovic, B. M. Cooke, and G. V. Brown, “Plasmodium falciparum-infected erythrocytes adhere to the proteoglyean thrombomodulin in static and flow-based systems,” *Exp. Parasitol.*, vol. 86, no. 1, pp. 8–18, May 1997.

[160] B. G. Yipp *et al.*, “Differential Roles of CD36, ICAM-1, and P-selectin in *Plasmodium falciparum* Cytoadherence In Vivo,” *Microcirculation*, vol. 14, no. 6, pp. 593–602, Jan. 2007.

[161] C. J. McCormick, A. Craig, D. Roberts, C. I. Newbold, and A. R. Berendt, “Intercellular adhesion molecule-1 and CD36 synergize to mediate adherence of Plasmodium falciparum-infected erythrocytes to cultured human microvascular endothelial cells.,” *J. Clin. Invest.*, vol. 100, no. 10, pp. 2521–9, Nov. 1997.

[162] S. P. Davis, M. Amrein, M. R. Gillrie, K. Lee, D. A. Muruve, and M. Ho, “Plasmodium falciparum-induced CD36 clustering rapidly strengthens cytoadherence via p130CAS-mediated actin cytoskeletal rearrangement.,” *FASEB J.*, vol. 26, no. 3, pp. 1119–30, Mar. 2012.

[163] B. G. Yipp, S. M. Robbins, M. E. Resek, D. I. Baruch, S. Looareesuwan, and

M. Ho, “Src-family kinase signaling modulates the adhesion of Plasmodium falciparum on human microvascular endothelium under flow,” *Blood*, vol. 101, no. 7, pp. 2850–2857, 2003.

[164] S. P. Davis, K. Lee, M. R. Gillrie, L. Roa, M. Amrein, and M. Ho, “CD36 Recruits a 5 b 1 Integrin to Promote Cytoadherence of P. falciparum-Infected Erythrocytes,” 2013.

[165] N. K. Viebig *et al.*, “Direct Activation of Human Endothelial Cells by Plasmodium falciparum -Infected Erythrocytes,” *Infect Immun*, vol. 73, no. 6, pp. 3271–3277, 2005.

[166] S. J. Chakravorty, K. R. Hughes, and A. G. Craig, “Host response to cytoadherence in Plasmodium falciparum.,” *Biochem. Soc. Trans.*, vol. 36, no. Pt 2, pp. 221–8, Apr. 2008.

[167] L. N. Cruz, Y. Wu, A. G. Craig, and C. R. S. Garcia, “Signal transduction in Plasmodium-Red Blood Cells interactions and in cytoadherence,” *An Acad Bras Cienc*, vol. 84, no. 2, 2012.

[168] J. Porta *et al.*, “Immunopathological changes in human cerebral malaria.,” *Clin. Neuropathol.*, vol. 12, no. 3, pp. 142–146, 1993.

[169] A. K. Tripathi, D. J. Sullivan, and M. F. Stins, “Plasmodium falciparum-Infected Erythrocytes Increase Intercellular Adhesion Molecule 1 Expression on Brain Endothelium through NF- B,” *Infect. Immun.*, vol. 74, no. 6, pp. 3262–3270, Jun. 2006.

[170] J. I. Lee and G. J. Burckart, “Nuclear factor kappa B: important transcription factor and therapeutic target.,” *J. Clin. Pharmacol.*, vol. 38, no. 11, pp. 981–993, Nov. 1998.

[171] A. K. Tripathi, W. Sha, V. Shulaev, M. F. Stins, and D. J. Sullivan, “Plasmodium falciparum–infected erythrocytes induce NF-kB regulated inflammatory pathways in human cerebral endothelium.”

[172] M. Ho *et al.*, “Ectophosphorylation of CD36 regulates cytoadherence of Plasmodium falciparum to microvascular endothelium under flow conditions.,” *Infect. Immun.*, vol. 73, no. 12, pp. 8179–87, Dec. 2005.

[173] P. Kern, C. J. Hemmer, J. Van Damme, H. J. Gruss, and M. Dietrich, “Elevated tumor necrosis factor alpha and interleukin-6 serum levels as markers for complicated Plasmodium falciparum malaria.,” *Am. J. Med.*, vol. 87, no. 2, pp. 139–43, Aug. 1989.

[174] N. P. Day *et al.*, “The prognostic and pathophysiologic role of pro- and

antiinflammatory cytokines in severe malaria," *J. Infect. Dis.*, vol. 180, no. 4, pp. 1288–1297, 1999.

[175] R. K. Oldham and R. O. Dillman, *Principles of cancer biotherapy*. Springer, 2009.

[176] A. R. Brasier, "The nuclear factor-B-interleukin-6 signalling pathway mediating vascular inflammation," *Cardiovascular Research*, vol. 86, no. 2. Oxford University Press, pp. 211–218, 01-May-2010.

[177] Y. Wallez and P. Huber, "Endothelial adherens and tight junctions in vascular homeostasis, inflammation and angiogenesis," *Biochim. Biophys. Acta - Biomembr.*, vol. 1778, no. 3, pp. 794–809, Mar. 2008.

[178] H. Brown *et al.*, "Evidence of blood-brain barrier dysfunction in human cerebral malaria.," *Neuropathol. Appl. Neurobiol.*, vol. 25, no. 4, pp. 331–40, Aug. 1999.

[179] H. Brown *et al.*, "Blood-brain barrier function in cerebral malaria in Malawian children.," *Am. J. Trop. Med. Hyg.*, vol. 64, no. 3–4, pp. 207–13.

[180] H. C. Brown *et al.*, "Blood-brain barrier function in cerebral malaria and CNS infections in Vietnam.," *Neurology*, vol. 55, no. 1, pp. 104–11, Jul. 2000.

[181] A. K. Tripathi, D. J. Sullivan, and M. F. Stins, "*Plasmodium falciparum* –Infected Erythrocytes Decrease the Integrity of Human Blood-Brain Barrier Endothelial Cell Monolayers," *J. Infect. Dis.*, vol. 195, no. 7, pp. 942–950, 2007.

[182] M. Bernabeu and J. D. Smith, "EPCR and Malaria Severity: The Center of a Perfect Storm," *Trends Parasitol.*, vol. 33, no. 4, pp. 295–308, Apr. 2017.

[183] W. C. Aird, L. O. Mosnier, and R. M. Fairhurst, "Plasmodium falciparum picks (on) EPCR.," *Blood*, vol. 123, no. 2, pp. 163–7, Jan. 2014.

[184] L. C. Paul and T. B. Issekutz, *Adhesion molecules in health and disease*. Marcel Dekker, Inc, 1997.

[185] D. Kwiatkowski *et al.*, "TNF concentration in fatal cerebral, non-fatal cerebral, and uncomplicated Plasmodium falciparum malaria.," *Lancet (London, England)*, vol. 336, no. 8725, pp. 1201–4, Nov. 1990.

[186] M. R. Gillrie *et al.*, "Src-family kinase-dependent disruption of endothelial barrier function by Plasmodium falciparum merozoite proteins," *Blood*, vol. 110, no. 9, pp. 3426–3435, 2007.

[187] L. H. Miller, H. C. Ackerman, X. Su, and T. E. Wellems, "Malaria biology and disease pathogenesis: insights for new treatments," *Nat. Med.*, vol. 19, no. 2, pp. 156–167, Feb. 2013.

[188] B. K. Lopansri *et al.*, "Low plasma arginine concentrations in children with

cerebral malaria and decreased nitric oxide production," *Lancet*, vol. 361, no. 9358, pp. 676–678, Feb. 2003.

[189] J. Storm and A. G. Craig, "Pathogenesis of cerebral malaria--inflammation and cytoadherence.," *Front. Cell. Infect. Microbiol.*, vol. 4, no. July, p. 100, 2014.

[190] N. M. Anstey *et al.*, "Nitric oxide in Tanzanian children with malaria: inverse relationship between malaria severity and nitric oxide production/nitric oxide synthase type 2 expression.," *J. Exp. Med.*, vol. 184, no. 2, pp. 557–67, Aug. 1996.

[191] C. S. Thom, C. F. Dickson, D. A. Gell, and M. J. Weiss, "Hemoglobin Variants: Biochemical Properties and Clinical Correlates."

[192] L. B. Jorde, J. C. Carey, and M. J. Bamshad, *Medical genetics*. Mosby/Elsevier, 2010.

[193] T. G. Kimman, *Genetics of infectious disease susceptibility*. Kluwer Academic Publishers, 2001.

[194] A. P. Patil *et al.*, "Global distribution of the sickle cell gene and geographical confirmation of the malaria hypothesis," *Nat. Commun.*, vol. 1, 2010.

[195] T. Wu, X. S. Wang, B. Cohen, and H. Ge, "Molecular Modeling of Normal and Sickle Hemoglobins," *Int. J. Multiscale Comput. Eng.*, vol. 8, no. 2, pp. 237–244, 2010.

[196] P. Naik, *Essentials of biochemistry*. 2012.

[197] F. Bauduer, "Red cell polymorphisms and malaria: an evolutionary approach," *Bull. Mem. Soc. Anthropol. Paris*, vol. 25, no. 1–2, pp. 55–64, Apr. 2013.

[198] D. J. Roberts and T. N. Williams, "Haemoglobinopathies and resistance to malaria," *Redox Rep.*, vol. 8, no. 5, pp. 304–310, Oct. 2003.

[199] M. Aidoo *et al.*, "Protective effects of the sickle cell gene against malaria morbidity and mortality," *Lancet*, vol. 359, no. 9314, pp. 1311–1312, Apr. 2002.

[200] P. J. Russell, P. E. Hertz, and B. McMillan, *Biology: The Dynamic Science*, vol. 3. Thomson Brooks/Cole, 2013.

[201] K. Ayi, F. Turrini, A. Piga, and P. Arese, "Enhanced phagocytosis of ring-parasitized mutant erythrocytes: a common mechanism that may explain protection against falciparum malaria in sickle trait and beta-thalassemia trait.," *Blood*, vol. 104, no. 10, pp. 3364–71, Nov. 2004.

[202] R. M. Fairhurst, C. D. Bess, and M. A. Krause, "Abnormal PfEMP1/knob display on Plasmodium falciparum-infected erythrocytes containing hemoglobin variants: fresh insights into malaria pathogenesis and protection," *Microbes*

Infect., vol. 14, no. 10, pp. 851–862, Aug. 2012.

[203] R. Cholera *et al.*, “Impaired cytoadherence of Plasmodium falciparum-infected erythrocytes containing sickle hemoglobin.,” *Proc. Natl. Acad. Sci. U. S. A.*, vol. 105, no. 3, pp. 991–6, Jan. 2008.

[204] J. Carlson, G. B. Nash, V. Gabutti, F. Al-Yaman, and M. Wahlgren, “Natural protection against severe Plasmodium falciparum malaria due to impaired rosette formation.,” *Blood*, vol. 84, no. 11, pp. 3909–14, 1994.

[205] J. Flint, R. M. Harding, A. J. Boyce, and J. B. Clegg, “The population genetics of the haemoglobinopathies.,” *Baillieres. Clin. Haematol.*, vol. 6, no. 1, pp. 215–62, Mar. 1993.

[206] R. Hutagalung, P. Wilairatana, S. Looareesuwan, G. M. Brittenham, M. Aikawa, and V. R. Gordeuk, “Influence of Hemoglobin E Trait on the Severity of Falciparum Malaria,” *J. Infect. Dis.*, vol. 179, no. 1, pp. 283–286, Jan. 1999.

[207] K. Chotivanich *et al.*, “Hemoglobin E: a balanced polymorphism protective against high parasitemias and thus severe P falciparum malaria.,” *Blood*, vol. 100, no. 4, pp. 1172–6, Aug. 2002.

[208] F. B. Piel *et al.*, “The distribution of haemoglobin C and its prevalence in newborns in Africa,” *Sci. Rep.*, vol. 3, p. 1671, 2013.

[209] E. Gilbert-Barness, L. A. Barness, and P. M. Farrell, *Metabolic diseases : foundations of clinical management, genetics, and pathology*. .

[210] A. Agarwal *et al.*, “Hemoglobin C associated with protection from severe malaria in the Dogon of Mali, a West African population with a low prevalence of hemoglobin S.,” *Blood*, vol. 96, no. 7, pp. 2358–63, Oct. 2000.

[211] D. Modiano *et al.*, “Haemoglobin C protects against clinical Plasmodium falciparum malaria,” *Nature*, vol. 414, no. 6861, pp. 305–308, Nov. 2001.

[212] R. M. Fairhurst, H. Fujioka, K. Hayton, K. F. Collins, and T. E. Wellems, “Aberrant development of Plasmodium falciparum in hemoglobin CC red cells: implications for the malaria protective effect of the homozygous state,” *Blood*, vol. 101, no. 8, pp. 3309–3315, Apr. 2003.

[213] M. J. Friedman, E. F. Roth, R. L. Nagel, and W. Trager, “The role of hemoglobins C, S, and Nbalt in the inhibition of malaria parasite development in vitro.,” *Am. J. Trop. Med. Hyg.*, vol. 28, no. 5, pp. 777–80, Sep. 1979.

[214] R. M. Fairhurst *et al.*, “Abnormal display of PfEMP-1 on erythrocytes carrying haemoglobin C may protect against malaria,” *Nature*, vol. 435, no. 7045, pp. 1117–1121, 2005.

[215] R. P. Hebbel, “Beyond hemoglobin polymerization: the red blood cell membrane and sickle disease pathophysiology.,” *Blood*, vol. 77, no. 2, pp. 214–37, Jan. 1991.

[216] M. A. F. Chaves, M. S. S. Leonart, and A. J. do Nascimento, “Oxidative process in erythrocytes of individuals with hemoglobin S,” *Hematology*, vol. 13, no. 3, pp. 187–192, Jun. 2008.

[217] P. Jarolim, M. Lahav, S. C. Liu, and J. Palek, “Effect of hemoglobin oxidation products on the stability of red cell membrane skeletons and the associations of skeletal proteins: correlation with a release of hemin.,” *Blood*, vol. 76, no. 10, pp. 2125–31, Nov. 1990.

[218] M. E. Farah, V. Sirotkin, B. Haarer, D. Kakhniashvili, and D. C. Amberg, “Diverse protective roles of the actin cytoskeleton during oxidative stress,” *Cytoskeleton*, vol. 68, no. 6, pp. 340–354, Jun. 2011.

[219] M. Cyrklaff *et al.*, “Oxidative insult can induce malaria-protective trait of sickle and fetal erythrocytes,” *Nat. Commun.*, vol. 7, p. 13401, Nov. 2016.

[220] W. Trager and J. B. Jenson, “Cultivation of malarial parasites,” *Nature*, vol. 273, no. 5664, pp. 621–622, Jun. 1978.

[221] W. Trager and J. B. Jensen, “Human Malaria Parasites in Continuous Culture,” *Science (80-.).*, vol. 193, no. 4254, pp. 673–675, 1976.

[222] H. Ginsburg, M. Krugliak, O. Eidelman, and Z. Ioav Cabantchik, “New permeability pathways induced in membranes of Plasmodium falciparum infected erythrocytes,” *Mol. Biochem. Parasitol.*, vol. 8, no. 2, pp. 177–190, 1983.

[223] J. B. Jensen, “Concentration from continuous culture of erythrocytes infected with trophozoites and schizonts of Plasmodium falciparum,” *Am. J. Trop. Med. Hyg.*, vol. 27, no. 6, p. 1274—1276, Nov. 1978.

[224] a L. Tappel, “The mechanism of the oxidation of unsaturated fatty acids catalyzed by hematin compounds.,” *Arch. Biochem. Biophys.*, vol. 44, no. 2, pp. 378–395, 1953.

[225] M. A. RUDZINSKA, W. TRAGER, and R. S. BRAY, “Pinocytotic Uptake and the Digestion of Hemoglobin in Malaria Parasites,” *J. Protozool.*, vol. 12, no. 4, pp. 563–576, 1965.

[226] A. Sienkiewicz *et al.*, “HIGH FIELD ESR INVESTIGATION OF IRON FeIII CENTER IN MALARIAL PIGMENT AND ITS SYNTHETIC SUBSTITUTE BETA-HEMATIN,” no. May 2014, pp. 2–3, 2014.

[227] L. Mata-Cantero, M. J. Lafuente, L. Sanz, and M. S. Rodriguez, “Magnetic isolation of Plasmodium falciparum schizonts iRBCs to generate a high parasitaemia and synchronized in vitro culture,” *Malar. J.*, vol. 13, no. 1, p. 112, 2014.

[228] K. Chotivanich *et al.*, “Parasite multiplication potential and the severity of falciparum malaria.,” *J. Infect. Dis.*, vol. 181, no. 3, pp. 1206–9, 2000.

[229] A. Claessens and J. A. Rowe, “Selection of Plasmodium falciparum Parasites for Cytoadhesion to Human Brain Endothelial Cells,” *J. Vis. Exp.*, no. 59, pp. 1–7, 2012.

[230] B. G. Yipp, S. Anand, T. Schollaardt, K. D. Patel, S. Looareesuwan, and M. Ho, “Synergism of multiple adhesion molecules in mediating cytoadherence of Plasmodium falciparum-infected erythrocytes to microvascular endothelial cells under flow.,” *Blood*, vol. 96, no. 6, pp. 2292–2298, 2000.

[231] S. Chien, “Present state of blood rheology. Hemodilution, theoretical basis and clinical application,” 1971.

[232] A. K. Dasanna, C. Lansche, M. Lanzer, and U. S. Schwarz, “Rolling Adhesion of Schizont Stage Malaria-Infected Red Blood Cells in Shear Flow,” *Biophys. J.*, vol. 112, no. 9, pp. 1908–1919, 2017.

[233] C. Janeway, *Immunobiology : the immune system in health and disease*. Garland Science, 2005.

[234] W. B. Storch, *Immunofluorescence in Clinical Immunology : a Primer and Atlas*. Birkhäuser Basel, 2000.

[235] S. Vora *et al.*, “Nuclear factor-kappa B localization and function within intrauterine tissues from term and preterm labor and cultured fetal membranes,” *Reprod. Biol. Endocrinol.*, vol. 8, no. 1, p. 8, Jan. 2010.

[236] N. Yeow, R. F. Tabor, and G. Garnier, “Atomic force microscopy: From red blood cells to immunohaematology,” *Adv. Colloid Interface Sci.*, vol. 249, pp. 149–162, Nov. 2017.

[237] T. S. Rask, D. A. Hansen, T. G. Theander, A. Gorm Pedersen, and T. Lavstsen, “Plasmodium falciparum Erythrocyte Membrane Protein 1 Diversity in Seven Genomes – Divide and Conquer,” *PLoS Comput. Biol.*, vol. 6, no. 9, p. e1000933, Sep. 2010.

[238] A. R. Berendt, D. L. Simmons, J. Tansey, C. I. Newbold, and K. Marsh, “Intercellular adhesion molecule-1 is an endothelial cell adhesion receptor for Plasmodium falciparum,” *Nature*, vol. 341, no. 6237, pp. 57–59, 1989.

[239] N. J. Rogers, O. Daramola, G. A. T. Targett, and B. S. Hall, “CD36 and Intercellular Adhesion Molecule 1 Mediate Adhesion of Developing Plasmodium falciparum Gametocytes,” *Infect. Immun.*, vol. 64, no. 4, pp. 1480–1483, 1996.

[240] L. Daviet, M. C. Morel-Kopp, C. Kaplan, and J. L. McGregor, “A structural/functional domain on human CD36 is involved in the binding of anti-Nak(a) antibodies.,” *Thromb. Haemost.*, vol. 73, no. 3, pp. 543–5, Mar. 1995.

[241] J. H. Janes *et al.*, “Investigating the Host Binding Signature on the Plasmodium falciparum PfEMP1 Protein Family,” *PLoS Pathog*, vol. 7, no. 5, 2011.

[242] A. Brown *et al.*, “Molecular architecture of a complex between an adhesion protein from the malaria parasite and intracellular adhesion molecule 1.,” *J. Biol. Chem.*, vol. 288, no. 8, pp. 5992–6003, Feb. 2013.

[243] M. Avril *et al.*, “A restricted subset of var genes mediates adherence of Plasmodium falciparum-infected erythrocytes to brain endothelial cells.,” *Proc. Natl. Acad. Sci. U. S. A.*, vol. 109, no. 26, pp. E1782-90, Jun. 2012.

[244] S. M. Kraemer and J. D. Smith, “A family affair: var genes, PfEMP1 binding, and malaria disease,” *Curr. Opin. Microbiol.*, vol. 9, no. 4, pp. 374–380, Aug. 2006.

[245] A. U. Orjih, “Maturation of Plasmodium falciparum in multiply infected erythrocytes and the potential role in malaria pathogenesis,” *Parasitol. Res.*, vol. 113, no. 11, pp. 4045–4056, Nov. 2014.

[246] A. A. Khalili and M. R. Ahmad, “A Review of Cell Adhesion Studies for Biomedical and Biological Applications.,” *Int. J. Mol. Sci.*, vol. 16, no. 8, pp. 18149–84, Aug. 2015.

[247] F. Joanny, J. Held, and B. Mordmüller, “In Vitro activity of fluorescent dyes against asexual blood stages of Plasmodium falciparum,” *Antimicrob. Agents Chemother.*, vol. 56, no. 11, pp. 5982–5985, 2012.

[248] J. Gruenberg, D. R. Allred, and I. W. Sherman, “Scanning Electron Microscope-Analysis of the Protrusions (Knobs) Present on the Surface Plasmodium falciparum-infected Erythrocytes of.”

[249] S. Suresh *et al.*, “Connections between single-cell biomechanics and human disease states: gastrointestinal cancer and malaria.,” *Acta Biomater.*, vol. 1, no. 1, pp. 15–30, Jan. 2005.

[250] H. Ginsburg and W. D. Stein, “The New Permeability Pathways Induced by the Malaria Parasite in the Membrane of the Infected Erythrocyte: Comparison of

Results Using Different Experimental Techniques," *J. Membr. Biol.*, vol. 197, no. 2, pp. 113–122, Feb. 2004.

[251] J. M. A. Mauritz, A. Esposito, H. Ginsburg, C. F. Kaminski, T. Tiffert, and V. L. Lew, "The Homeostasis of Plasmodium falciparum-Infected Red Blood Cells," *PLoS Comput. Biol.*, vol. 5, no. 4, p. e1000339, Apr. 2009.

[252] H. M. Staines, J. C. Ellory, and K. Kirk, "Perturbation of the pump-leak balance for Na(+) and K(+) in malaria-infected erythrocytes.," *Am. J. Physiol. Cell Physiol.*, vol. 280, no. 6, pp. C1576-87, Jun. 2001.

[253] B. Fröhlich *et al.*, "Hemoglobinopathy Modulates Temporal Evolution of Erythrocyte Mechanics Caused by P. falciparum Infection," *Prep.*, 2018.

[254] C. Lansche *et al.*, "Altered cell mechanics leads to differential adhesion dynamics and reduced endothelial cell activation by heterozygous sickle cell erythrocytes infected with Plasmodium falciparum," *Prep.*, 2018.

[255] C. Volanti, G. Gloire, A. Vanderplasschen, N. Jacobs, Y. Habraken, and J. Piette, "Downregulation of ICAM-1 and VCAM-1 expression in endothelial cells treated by photodynamic therapy," *Oncogene*, vol. 23, no. 53, pp. 8649–8658, Nov. 2004.

[256] J. May *et al.*, "Hemoglobin Variants and Disease Manifestations in Severe Falciparum Malaria," *JAMA*, vol. 297, no. 20, p. 2220, May 2007.

[257] A. . Allison, "The distribution of the sickle-cell trait in East Africa and elsewhere, and its apparent relationship to the incidence of subtertian malaria," *Trans. R. Soc. Trop. Med. Hyg.*, vol. 48, no. 4, pp. 312–318, Jul. 1954.

[258] F. Verra, G. Bancone, P. Avellino, I. Blot, J. Simporé, and D. Modiano, "Haemoglobin C and S in natural selection against Plasmodium falciparum malaria: a plethora or a single shared adaptive mechanism?," *Parassitologia*, vol. 49, no. 4, pp. 209–13, Dec. 2007.

[259] B. M. Cooke, N. Mohandas, and R. L. Coppel, "Malaria and the red blood cell membrane.," *Semin. Hematol.*, vol. 41, no. 2, pp. 173–88, Apr. 2004.

[260] D. A. Hassan, A. P. Arez, H. S. Mohamed, A. M. Elhussein, M. E. Ibrahim, and N. H. Abdulhadi, "The reduced sequestration of *Plasmodium-falciparum* - infected erythrocytes among malaria cases with sickle-cell trait: in-vivo evidence from Sudan," *Ann. Trop. Med. Parasitol.*, vol. 102, no. 8, pp. 743–748, Dec. 2008.

[261] O. Awotua-Efebo, E. A. D. Alikor, and K. E. O. Nkanginieme, "Malaria parasite density and splenic status by ultrasonography in stable sickle-cell anaemia

(HbSS) children.," *Niger. J. Med.*, vol. 13, no. 1, pp. 40–3, 2004.

[262] F. P. Mockenhaupt *et al.*, "Limited influence of haemoglobin variants on Plasmodium falciparum msp1 and msp2 alleles in symptomatic malaria," *Trans. R. Soc. Trop. Med. Hyg.*, vol. 98, no. 5, pp. 302–310, May 2004.

[263] P. A. Buffet *et al.*, "The pathogenesis of Plasmodium falciparum malaria in humans: insights from splenic physiology.," *Blood*, vol. 117, no. 2, pp. 381–92, Jan. 2011.

[264] L. Gong, S. Parikh, P. J. Rosenthal, and B. Greenhouse, "Biochemical and immunological mechanisms by which sickle cell trait protects against malaria," *Malar. J.*, vol. 12, no. 1, p. 317, Sep. 2013.

[265] F. Verra *et al.*, "Haemoglobin C and S role in acquired immunity against Plasmodium falciparum malaria.," *PLoS One*, vol. 2, no. 10, p. e978, Oct. 2007.

[266] T. N. Williams *et al.*, "An immune basis for malaria protection by the sickle cell trait," *PLoS Med.*, vol. 2, no. 5, pp. 0441–0445, 2005.

[267] Y. B. Lim, J. Thingna, J. Cao, and C. T. Lim, "Single molecule and multiple bond characterization of catch bond associated cytoadhesion in malaria," *Sci. Rep.*, vol. 7, no. 1, p. 4208, Dec. 2017.

[268] X. Xu *et al.*, "Probing the Cytoadherence of Malaria Infected Red Blood Cells under Flow," 2013.

[269] A. Li *et al.*, "Molecular Mechanistic Insights into the Endothelial Receptor Mediated Cytoadherence of Plasmodium falciparum-Infected Erythrocytes," *PLoS One*, vol. 6, no. 3, p. e16929, Mar. 2011.

[270] W. Thomas, "Catch Bonds in Adhesion," *Annu. Rev. Biomed. Eng.*, vol. 10, no. 1, pp. 39–57, Aug. 2008.

[271] B. M. Cooke, A. R. Berendt, A. G. Craig, J. MacGregor, C. I. Newbold, and G. B. Nash, "Rolling and stationary cytoadhesion of red blood cells parasitized by Plasmodium falciparum: Separate roles for ICAM-1, CD36 and thrombospondin," *Br. J. Haematol.*, vol. 87, no. 1, pp. 162–170, May 1994.

[272] A. K. Dasanna, C. Lansche, M. Lanzer, and U. S. Schwarz, "Rolling Adhesion of Schizont Stage Malaria-Infected Red Blood Cells in Shear Flow," *Biophys. J.*, vol. 112, no. 9, pp. 1908–1919, May 2017.

[273] H. Rieger *et al.*, "Cytoadhesion of Plasmodium falciparum - Infected erythrocytes to chondroitin-4-sulfate is cooperative and shear enhanced," *Blood*, vol. 125, no. 2, pp. 383–391, 2015.

[274] A.-K. Tilly *et al.*, "Type of in vitro cultivation influences cytoadhesion, knob

structure, protein localization and transcriptome profile of Plasmodium falciparum.," *Sci. Rep.*, vol. 5, p. 16766, Nov. 2015.

[275] D. A. Fedosov, B. Caswell, and G. E. Karniadakis, "Wall shear stress-based model for adhesive dynamics of red blood cells in malaria," *Biophys. J.*, vol. 100, no. 9, pp. 2084–2093, 2011.

[276] J. L. Maciaszek and G. Lykotrafitis, "Sickle cell trait human erythrocytes are significantly stiffer than normal," *J. Biomech.*, vol. 44, no. 4, pp. 657–661, 2011.

[277] T. Tiffert, R. M. Bookchin, and V. L. Lew, "Calcium Homeostasis in Normal and Abnormal Human Red Cells," in *Red Cell Membrane Transport in Health and Disease*, Berlin, Heidelberg: Springer Berlin Heidelberg, 2003, pp. 373–405.

[278] F. Liu, H. Mizukami, S. Sarnaik, and A. Ostafin, "Calcium-dependent human erythrocyte cytoskeleton stability analysis through atomic force microscopy," *J. Struct. Biol.*, vol. 150, no. 2, pp. 200–210, May 2005.

[279] Y. Takakuwa and N. Mohandas, "Modulation of erythrocyte membrane material properties by Ca2+ and calmodulin. Implications for their role in regulation of skeletal protein interactions.," *J. Clin. Invest.*, vol. 82, no. 2, pp. 394–400, Aug. 1988.

[280] O. P. Hamill, "Potassium and Chloride Channels in Red Blood Cells," in *Single-Channel Recording*, Boston, MA: Springer US, 1983, pp. 451–471.

[281] J. W. Stocker, L. De Franceschi, G. A. McNaughton-Smith, R. Corrocher, Y. Beuzard, and C. Brugnara, "ICA-17043, a novel Gardos channel blocker, prevents sickled red blood cell dehydration in vitro and in vivo in SAD mice," *Blood*, vol. 101, no. 6, pp. 2412–2418, Mar. 2003.

[282] E. Evans, N. Mohandas, and A. Leung, "Static and Dynamic Rigidities of Normal and Sickle Erythrocytes Major Influence of Cell Hemoglobin Concentration."

[283] E. A. Evans and N. Mohandas, "Membrane-Associated Sickle Hemoglobin: A Major Determinant of Sickle Erythrocyte Rigidity," *Blood. Vol*, vol. 70, no. 5, pp. 1443–1449, 1987.

[284] H. Byun *et al.*, "Optical measurement of biomechanical properties of individual erythrocytes from a sickle cell patient.," *Acta Biomater.*, vol. 8, no. 11, pp. 4130–8, Nov. 2012.

[285] J. A. Walder *et al.*, "The interaction of hemoglobin with the cytoplasmic domain of band 3 of the human erythrocyte membrane.," *J. Biol. Chem.*, vol. 259, no. 16, pp. 10238–46, Aug. 1984.

[286] M. H. Steinberg, *Disorders of hemoglobin : genetics, pathophysiology, and clinical management*. Cambridge University Press, 2009.

[287] M. I. Spengler, M. J. Svetaz, M. B. Leroux, S. M. Bertoluzzo, F. M. Parente, and P. Bosch, “Lipid peroxidation affects red blood cells membrane properties in patients with systemic lupus erythematosus.,” *Clin. Hemorheol. Microcirc.*, vol. 58, no. 4, pp. 489–95, 2014.

[288] A. K. Dasanna, C. Lansche, M. Lanzer, and U. S. Schwarz, “Rolling Adhesion of Schizont Stage Malaria-Infected Red Blood Cells in Shear Flow,” *Biophys. J.*, vol. 112, no. 9, pp. 1908–1919, May 2017.

[289] N. Jenkins, Y. Wu, S. Chakravorty, O. Kai, K. Marsh, and A. Craig, “Plasmodium Falciparum Intercellular Adhesion Molecule-1- Based Cytoadherence-Related Signaling in Human Endothelial Cells.”

[290] A. K. Tripathi, D. J. Sullivan, and M. F. Stins, “Plasmodium falciparum-infected erythrocytes increase intercellular adhesion molecule 1 expression on brain endothelium through NF-??B,” *Infect. Immun.*, vol. 74, no. 6, pp. 3262–3270, 2006.

[291] X. Xu *et al.*, “Probing the Cytoadherence of Malaria Infected Red Blood Cells under Flow,” *PLoS One*, vol. 8, no. 5, pp. 2–9, 2013.

[292] A. Clayton, R. A. Evans, E. Pettit, M. Hallett, J. D. Williams, and R. Steadman, “Cellular activation through the ligation of intercellular adhesion molecule-I.,” *J.Cell Sci.*, vol. 111, pp. 443–453, 1998.

[293] C.-H. Lee, S. Bose, K. J. Van Vliet, J. M. Karp, and R. Karnik, “Examining the Lateral Displacement of HL60 Cells Rolling on Asymmetric P-Selectin Patterns,” *Langmuir*, vol. 27, no. 1, pp. 240–249, Jan. 2011.

[294] A. K. Dasanna and U. S. Schwarz, “Adhesion-based sorting of blood cells: an adhesive dynamics simulation study,” *Prep.*, 2018.

Publications and Conference Presentations

The following publications resulted from this work:

C. Lansche, A. K. Dasanna, B. Frölich, K. Quadt, D. Missirilis, M. Tétard, B. Gamain, B. Buchholz, M. Tanaka, U. S. Schwarz, and M. Lanzer, "Altered cell mechanics leads to differential adhesion dynamics and reduced endothelial cell activation by heterozygous sickle cell erythrocytes infected with *Plasmodium falciparum*". **Manuscript in preparation for *Nature Communications***

A. K. Dasanna, **C. Lansche**, M. Lanzer, and U. S. Schwarz, "Rolling Adhesion of Schizont Stage Malaria-Infected Red Blood Cells in Shear Flow," ***Biophys. J.***, vol. 112, no. 9, pp. 1908–1919, 2017.

M. Waldecker, A. K. Dasanna, **C. Lansche**, M. Linke, S. Sirismith, M. Cyrklaff, C. Sanchez, U. S. Schwarz, and M. Lanzer, "Differential time-dependent volumetric and surface area changes and delayed induction of new permeation pathways in *P. falciparum* -infected hemoglobinopathic erythrocytes," ***Cell. Microbiol.***, vol. 19, no. 2, p. e12650, 2017.

The results of this work were presented at the following scientific conferences:

Molecular Parasitology Meeting 2017. Organized by the Marine Biological Laboratory, Woods Hole, MA, USA. Poster presentation. September 2017.

BioMalPar XII: Biology and Pathology of the Malaria Parasite. Organized by EMBL Heidelberg, Germany. Poster presentation. May 2016.

Acknowledgements

I cordially thank my thesis supervisor Prof. Dr. Michael Lanzer for the interesting research project that I thoroughly enjoyed working on. This experience along with the possibility to work in an excellent research environment will have a great impact on my future scientific career. Thank you so much for all your support along the course of my thesis, for your guidance, suggestions, encouragement and amiability. I greatly appreciate your mentoring, all the time you spend advising me and for sharing your knowledge with me.

I like to thank the members of my TAC committee Dr. Ann-Kristin Müller and Prof. Alexander Dalpke for their participation and discussions. Additionally, I thank Dr. Silvia Portugal for her participation as examiner in my Thesis defense.

My profound gratitude also goes to my project collaborators Anil Dasanna, Benjamin Fröhlich, Dimitris Misirilis, Katharina Quadt, Marilou Tétard and Benoît Gamain for all your help during my thesis project. Especially, thanks to Benjamin for teaching me the main techniques I required, and for being there every time I needed technical help, an advice or a hug. My sincere gratitude and appreciation goes to Anil, thanks you for all your help and for sharing your knowledge and extraordinary scientific ideas with me. I greatly enjoy working with you.

Big thanks go to my current and former colleagues Nick Sirismith, Marina Müller, Maillin Waldecker, Hanni Kartini, Sonia Molliner, Stephan Prior, Monika Jankowska, Maelle Duffey, Sebastiano Bellanca, Marvin Haag, Costanza Tacolli, Harden Rieger, María Hernandez, Priyanka Fernandes, Britta Nyboer, Lena Baron, Miriam Griesheimer and Sandra Niebel for all their help and advices during my time here, thank you for providing a friendly atmosphere in the lab and for giving me your support all the time.

I thank Marek Cyrklaff for introducing me to SEM and for our discussions; I fully enjoyed our brain storming. Special thanks go to Filomena Carvalho, for introducing me to AFM-SCFS technique, I really enjoyed my time there in you Lab. I thank Nicola Viebig for all the time you spend giving me explanations, ideas and suggestions

during my thesis. I thank Cecilia Sanchez for her help with different techniques and for our discussions.

I fully thank my friend Johanna Eberhard, without you I wouldn´t be here, thanks for your unconditional help and friendship. I also thank my dear friends “Los pingüinitos”, especially Alda, you made my time in Heidelberg spectacular.

I specifically thank my parents, Manuela and Karl Lansche, for providing the foundation on which my personal life and career is built. Foremost, I am grateful for all your support during this period. I also thank my brother and sister, Alan and Andrea Lansche, for being always there for me.

Last, but not least, I thank my beloved husband Santiago Casas for his patience, understanding and support during this time. Thank you for taking such a good care of me.